Distribution Agreement

In presenting this thesis or dissertation as a partial fulfillment of the requirements for an advanced degree from Emory University, I hereby grant to Emory University and its agents the non-exclusive license to archive, make accessible, and display my thesis or dissertation in whole or in part in all forms of media, now or hereafter known, including display on the world wide web. I understand that I may select some access restrictions as part of the online submission of this thesis or dissertation. I retain all ownership rights to the copyright of the thesis or dissertation. I also retain the right to use in future works (such as articles or books) all or part of this thesis or dissertation.

Signature:

_____ _____

Yixuan Han Date

Developing Experimental Methods to Investigate Local Changes in Density and Dynamics of Thin Polymer Films

By

Yixuan Han
Doctor of Philosophy

Physics

Connie B. Roth, Ph.D.
Advisor

Justin C. Burton, Ph.D.
Committee Member

Laura Finzi, Ph.D.
Committee Member

James T. Kindt, Ph.D.
Committee Member

Daniel M. Sussman, Ph.D.
Committee Member

Accepted:

Kimberly J. Arriola, Ph.D, MPH
Dean of the James T. Laney School of Graduate Studies

Date

Developing Experimental Methods to Investigate Local Changes in Density and Dynamics of Thin Polymer Films

By

Yixuan Han
B.S., Nankai Univerisity, Tianjin, China, 2016

Advisor: Connie B. Roth, Ph.D.

An abstract of
A dissertation submitted to the Faculty of the
James T. Laney School of Graduate Studies of Emory University
in partial fulfillment of the requirements for the degree of
Doctor of Philosophy
in Physics
2022

Abstract

Developing Experimental Methods to Investigate Local Changes in Density and Dynamics of Thin Polymer Films
By Yixuan Han

In this dissertation, I address changes to local material properties in polymer thin films (density and dynamics) perturbed by interfacial effects under nanoconfinement. I measured the refractive index with ellipsometry to infer density changes in polymer thin films under confinement. I have found similar apparent increases in the thickness-dependent refractive index trend $n(h)$ for three different polymers, polystyrene (PS), poly(methyl methacrylate) (PMMA), and poly(2-vinyl pyridine) (P2VP), despite the differences in polymer-silica substrate interactions. I tested for possible sources of non-uniform polarizability by varying the molecular weight, polydispersity, forming a film from bilayers with different interfaicial widths, and altering the surface chemistry of the substrate. However, the large unphysical apparent increase cannot be explained by any of these tests. I concluded that the use of homogeneous (uniform and isotropic) layer approximations can lead to unphysical results when film inhomogeneities and local property changes are frequently present in polymer thin films. I then developed an ellipsometric optical layer model with a depth-dependent refractive index gradient to model thin polymer films of PS, PMMA and P2VP. In the optical layer model, I proposed a linear gradient in the magnitude of refractive index, Cauchy parameter $A(z)$, with depth dependent position z. I demonstrated the presence of a strong positive gradient in the magnitude of the refractive index (%grade) for PMMA and PS thin films, while P2VP films show a refractive index gradient that primarily fluctuates around zero for all film thicknesses. This positive gradient in refractive index indicates a higher density near the free surface, counter to common expectations of a simple free volume correlation between density and dynamics. I rationalize this denser than bulk region near the free surface based on the vapor deposited stable glasses with optimized denser molecular packings caused by the presence of the observed faster dynamics at the free surface.

In addition to probing the local density changes in polymer thin films, I developed a new experimental method using the fluorophore perylene to probe dynamics via fluorescence spectroscopy. I measured the temperature dependence of perylene doped in bulk PS, PMMA, P2VP, and polycarbonate (PC) films, defining a fluorescence intensity "shift factor" $\log(a_T)$ based on the intensity ratio between the intensity of the first peak and the intensity of temperature invariant self-reference region (SRR). I found that the temperature dependence of $\log(a_T)$ associated with the nonradiative decay process reflects the local polymer dynamics transitioning from the liquid to glassy regimes, where the rate of nonradiative decay is influenced by cooperative α-relaxation in the supercooled liquid regime, and the local β-relaxation in the glassy regime.

Developing Experimental Methods to Investigate Local Changes in Density and Dynamics of Thin Polymer Films

By

Yixuan Han
B.S., Nankai Univerisity, Tianjin, China, 2016

Advisor: Connie B. Roth, Ph.D.

A dissertation submitted to the Faculty of the
James T. Laney School of Graduate Studies of Emory University
in partial fulfillment of the requirements for the degree of
Doctor of Philosophy
in Physics
2022

Acknowledgments

At the very beginning, I would like to thank my advisor, Connie Roth, who is the greatest mentor I have ever met. It is hard to memorize how much experience and wisdom she shared with me. But without the inspiration and support from her, I would not be who I am today. I have been appreciating her high standards for making me into a better person, both in academia and in life.

I would like to thank my committee members, Justin Burton, Laura Finzi, James Kindt and Daniel Sussman, for their valuable discussion and feedback over the years. Their knowledge and unique perspectives have brought this dissertation to a higher level. I appreciated those thoughts and ideas we shared together which become a significant part of this dissertation.

I have received a lot of help from staffs in the physics department during my several years here. Without their contribution, a lot of wonderful things would not happen. I would like to thank the machine shop staffs, Horace Dale and Alan Fannin, for helping me building the pressure heater, as well as providing assistance when I encountered problems. Additional thanks go to Lowell Ramsey, who saved me a lot of times from the weeds of electronic problems. I would like to thank Jason Boss and Tom Pierce for assisting all the computer problems. Last but not the least, I must thank all the administrative staffs in the department for organizing fantastic events and taking care of miscellaneous stuff, with special thanks to Barbara Conner and Susan Cook.

I enjoyed the time I spent with the Roth lab members. Big thanks go to Xinru Huang and Michael Thees, for guiding me through the first few years in the lab and providing generous help. I would also like to thank my colleagues, Yannic Gagnon, James Merrill, Alex Couturier, Alan Rohrbach, Olivia Boyd, Jennifer McGuire, and Benjamin Kasavan for the inspirations and joys we had together, especially the “happy hour” after group discussions.

Finally, I would like to say thank you to my wife, Jiaying, who has always been the strongest support behind me when I was trapped in frustrations. I am so grateful to have you as a part of my life.

Funding from the National Science Foundation (NSF) Polymers program (DMR-1905782 and DMR-1709132), as well as Emory University is gratefully acknowledged.

Contents

List of Figures

Chapter 1

Introduction

1.1 Synopsis

This dissertation is about studying changes in material properties (density and modulus) of polymer thin films and contributing to the understanding of how density and modulus are related to the glass transition and dynamics. The glass transition, a long-standing open question in the field, is associated with dramatic slowing down of the dynamics over a short temperature range. The true mechanism that drives this slowing down in dynamics is still unclear. Polymer thin films, a ubiquitous geometry that is confined in the thickness dimension, have shown shifts in material properties with respect to the bulk values. Such changes in material properties are often used to infer changes in the dynamics, and are a significant avenue for studying the glass transition.

In this introductory chapter, I will briefly introduce the basics of the glass transition and dynamics, as well as some polymer basics in the first section. In the later sections, I will provide a general description of the current understanding of how density and modulus are related to dynamics and the glass transition in both bulk and thin films scenarios.

1.2 Introduction to polymer glasses

1.2.1 Dynamics of glasses

Glasses are non-equilibrium materials that are amorphous and lack long-range order, in contrast to crystals which exhibits long-range order in the form of lattice. Common glass formers range from small molecules like SiO_2 (window glass) to giant molecules like polymers (plastics). When the system is in equilibrium, units are allowed to rearrange freely, while as less thermal energy is available at lower temperature, the units are required to move cooperatively for a rearrangement to occur. Such cooperative motion of the units in the system is called α-relaxation. Glasses are formed when the system is cooled faster than the time required for the system to rearrange into an equilibrium structure, effectively freezing into place, resulting in a frustrated packing configuration. Packing frustration of the units leaves the system trapped in a disordered, non-equilibrium configuration, which is the glassy state. The process of the system falling out of equilibrium upon cooling into a non-equilibrium glassy state is called the glass transition.

The mystery of the glass transition originates from the challenge to understand the dramatic slowing down of the dynamics by 10-14 orders of magnitude in the temperature range $\sim$50 K just above the glass transition temperature while the system is still in equilibrium, often referred to as the supercooled regime.[1] At very high temperatures, the molecules in the system have enough thermal energy to slide past each other and the temperature dependence of the relaxation time follows a simple activated process with an Arrhenius temperature dependence:

$$\tau \propto \exp\left(\frac{E_a}{k_{\mathrm{B}}T}\right), \tag{1.1}$$

where E_a is the activation energy barrier that is independent of temperature and k_{B}

is the Boltzmann's constant. When the temperature decreases, the relaxation time becomes longer because less thermal energy is available. Figure 1.1 demonstrates a typical Arrhenius plot where the logarithmic α-relaxation time $\log \tau_\alpha$ is plotted as a function of reciprocal temperature $1/T$. The equilibrium liquid regime that follows the Arrhenius temperature dependence is represented by the red line and the corresponding activation energy barrier can be determined from the slope of a linear fit to the red line. As the temperature drops (moving to the right of the $1/T$ axis), passing the Arrhenius temperature T_A which is the onset of cooperative motion, the system enters the supercooled liquid regime when the relaxation time reaches $\sim 10^{-10}$ s.[2] In the supercooled liquid regime, the temperature dependence of the relaxation time no longer follows the Arrhenius line. Instead, such non-Arrhenius behavior can be well fit by the Vogel, Fulcher, Tammann (VFT) equation:

$$\tau_\alpha = \tau_\infty \exp\left(\frac{B}{T - T_0}\right), \tag{1.2}$$

where τ_∞ is the relaxation time at very high temperature, B is a material-specific temperature scale and T_0 is the "Vogel–Fulcher temperature" at which the relaxation time appears to diverge to infinity.[3–5] Further down the $1/T$ axis at lower temperatures, decoupling of the α relaxation (main structural relaxation) and β relaxation (secondary relaxation) take place at a critical temperature T_C called the dynamic crossover when the relaxation time is approximately $10^{-8} - 10^{-6}$ s, where the β relaxation still follows the linear Arrhenius trend (brown dashed line).[6]

Similar to Eqn. 1.1, the VFT equation (Eqn.1.2) can also be viewed as an activated process with a temperature-dependent activation energy $E_a(T)$, where $E_a(T)$ grows with decreasing temperature. In 1965, Adam and Gibbs introduced the idea of a cooperatively rearranging region (CRR), corresponding to a certain number of units (z) that need to move collectively for a rearrangement to occur.[7] Hence, the increase

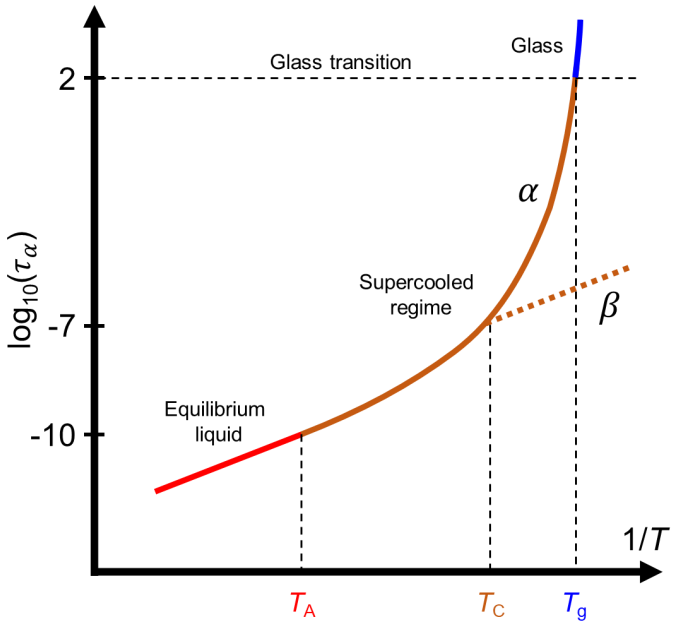

Figure 1.1: Schematic of an Arrhenius plot: logarithm of the α-relaxation time log τ_α as a function of reciprocal temperature $1/T$. At temperature above the Arrhenius temperature T_A, the system follows a simple Arrhenius temperature dependence (red line). Entering the supercooled liquid regime (brown curve) when $\tau_\alpha \sim 10^{-10}$ s, the dynamics now follow a non-Arrhenius trend where τ_α slows down drastically with decreasing temperature. A dynamic crossover occurs when $\tau_\alpha \sim 10^{-8} - 10^{-6}$ s at the critical temperature T_C, leading to a splitting of the α and β process. The glass transition happens at T_g upon further cooling when τ_α approaches 100 s.

in the effective activation energy has been related to the growing number of units that undergo collective local motion at these lower temperatures.[7–9] More specifically, the growth of the effective activation energy barrier can be treated as an increase in the size of the CRR: $E_a(T) = zE_a^*$, where E_a^* is a temperature independent activation energy for a single unit. Experimentally, the effective size of CRR has been found to be around a few nanometers near the glass transition temperature T_g.[10–13] Upon further cooling, the activation energy barrier for cooperative rearrangements grows too large to be overcome within the available time scale, resulting in dynamic arrest and packing frustration. The glass transition temperature T_g is commonly defined as the temperature when the α-relaxation time reaches 100 s, above which the system transitions into its glassy state (blue line).

1.2.2 Glass transition

The glass transition is associated with packing frustration that leads to the dynamic arrest of the units in the system. Packing frustration takes place as the system densifies, usually upon cooling for thermal-quenched glasses. At high temperature in the liquid state, the thermal energy is sufficient for the system to explore all possible configurations, such that the system is in equilibrium. As the temperature decreases, the available thermal energy is not enough for the system to explore all possible configurations on an experimentally accessible time scale, and the system falls out of equilibrium, being trapped in a non-equilibrium state, which is named the glassy state. Such a transition from the liquid state to the glassy state is called the glass transition and the temperature of the glass vitrification is defined as the glass transition temperature T_{g}.

The experimentally observed glass transition is referred to as a kinetic transition because T_{g} depends on the rate at which the system is densified, where for thermal-quenched glasses, T_{g} usually depends on cooling rate. As graphed in Figure 1.2, specific volume (inverse of density, $v(T) = 1/\rho(T)$) is plotted as a function of temperature for a typical polymer glass. The glass transition temperature T_{g} is typically defined experimentally as the intersection of linear fits to the liquid regime and the glassy regime. At a high enough temperature ($T > T_{\mathrm{A}}$), the system is in the equilibrium liquid state (red line) where the molecules have sufficient thermal energy to slide by each other freely. Then approaching the crystallization point at T_{m}, the system is going to either crystallize (purple line) into an ordered crystalline state or bypass crystallization into a supercooled liquid regime (brown line).[14]

If we assume that the system successfully avoided crystallization and is in the supercooled liquid regime, the system is still in equilibrium but the dynamics start to slow down dramatically. At a higher cooling rate, the system has less time to explore the different possible configurations in the molecular packing, resulting in the

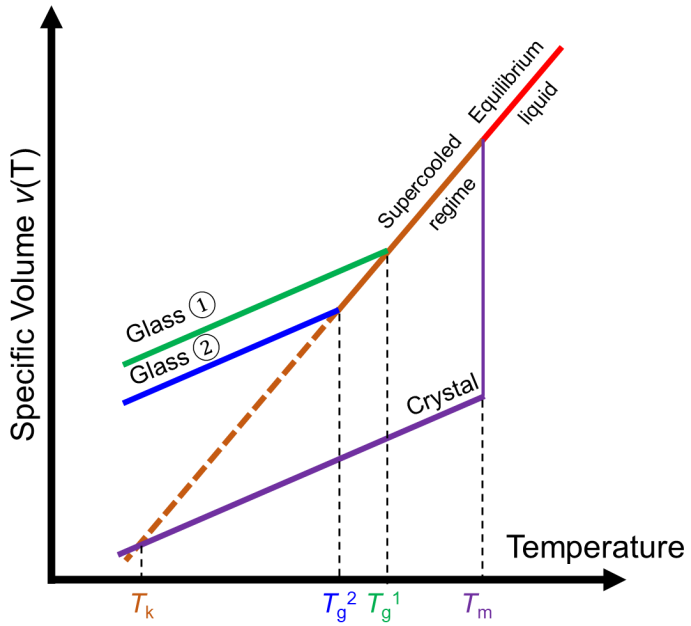

Figure 1.2: Schematic of specific volume as a function of temperature for a glass forming material. At a very high temperature above the crystallization point T_m, the system is in an equilibrium liquid state. If crystallization (purple line) is avoided, the system will enter a supercooled liquid regime where the system is still in equilibrium but the dynamics starts to slow down drastically. Depending on different cooling rates, the system will fall out of equilibrium at different T_gs, resulting in different glasses: higher cooling rate leads to glass 1 (green line) and slower cooling rate leads to glass 2 (blue line). If the system could be cooled infinitely slowly, it would follow the extrapolation of the supercooled liquid line and (theoretically) reach an ideal glassy state at the Kauzmann temperature T_k.

system falling out of equilibrium sooner at a higher T_g (T_g^1) forming a less stable glass (Glass 1, green line). In contrast, if the system is cooled at a lower cooling rate, it will remain in equilibrium following the supercooled liquid line for a longer time and fall out of equilibrium into an entropically more favored state compared to Glass 1 at a lower T_g (T_g^2), forming a more stable glass (Glass 2, blue line).[15] The actual difference between T_g^1 and T_g^2 is less exaggerated than that shown in the schematic, where decreasing the cooling rate by an order of magnitude would only decrease T_g by $\sim 3-5$ K.[16–18] This cooling rate dependent kinetic arrest of the molecular motion points to the essence of glass transition being a kinetic transition, where

whether a true thermodynamic transition hides beneath the kinetic transition has remained a debate for decades.[3,4,14,19–22] Further down the equilibrium supercooled liquid line, if the system could be cooled infinitely slowly, theoretically, it is thought that an ideal glassy state would be reached at the intersection of the extrapolation of the supercooled liquid line (dashed orange) and the crystalline line (purple) at the Kauzmann temperature T_{k}.[4,21,23] This ideal glassy state is supposed to have the same entropy as the corresponding crystalline state, which represents a hypothetical global minimum on the potential energy landscape (PEL).[4,24,25]

1.2.3 Polymer basics and polymeric glasses

Polymers are long-chain molecules consisting of a large number of repeat units called monomers. The contour size of a polymer molecule is usually described by its molecular weight (M) which is the product of the degree of polymerization N (number of repeat units) and the molecular weight of the monomer (single repeat unit) M_0, $M = N \times M_0$. In practice, molecules in a polymer system possess a distribution of different degrees of polymerization, characterized by the polydispersity which is the ratio of the weight-average molecular weight M_{w} to the number-average molecular weight M_{n}. Even though the contour length of a polymer molecule could extend to micron size, it usually coils up where the spatial size is often described by the radius of gyration R_{g} on the scale of tens of nanometers. Despite the fact that a polymer molecule has a large number of repeat units connected via covalent bonds, packing frustration associated with the glass transition only occurs at the cooperative segmental level for polymers, which usually involves monomers from many different chains. Recent theoretical work that treats polymers melts as disconnected spheres with a diameter of order the Kuhn length, predicts the temperature dependence of the α-relaxation behavior that agrees well with experimental data.[26] This particular feature makes polymer glasses exhibit similar characteristics to other small-molecule

glass formers. This also explains why T_g has little dependence on molecular weight for high molecular weight polymers and chain connectivity does not play an important role in the glass transition.[27–29] In addition, polymers usually form glasses because crystallization can be easily avoided due to the relatively slow relaxation dynamics of polymers and the stereo-irregularities in chemical structures that prevent the polymer molecules from forming ordered crystalline structures. Therefore, only a modest cooling rate is needed to bypass crystallization compared to the high cooling rates required by metallic glasses.

1.3 How are density and dynamics related?

1.3.1 Density considered as a key factor to understand the glass transition

The dynamics of polymer melts slow down dramatically in the relatively short temperature range just above T_g, which is followed by the dynamical arrest at T_g. However, over the same temperature range, there is only comparatively little change to the local structure or density of the material. For instance, if one takes two snapshots of the positions of all the units of a glass former at temperatures right above and right below T_g, there is little difference between the two snapshots. Nonetheless, the units are free to move in the supercooled regime above T_g but locked in place in the glassy state below T_g. This idea is further demonstrated in Figure 1.3, where specific volume (Fig. 1.3(a)) and density (Fig. 1.3(b)) are plotted as a function of temperature. The brown circles correspond to the states right above T_g in the supercooled liquid regime, while the blue circles correspond to the states right below T_g in the glassy state. Only minor differences exist in volume and density across the deflection point at T_g. In contrast, as shown in Fig. 1.3(c), where the logarithmic relaxation time is graphed as a function of $1/T$, the differences in dynamics across the glass transition

are more significant compared to the structural changes. Recent studies have found that even a tiny change in density can have a strong impact on dynamics.[30–34] Hence, how density or local structure is related to dynamics remains an open question in the glass transition field.

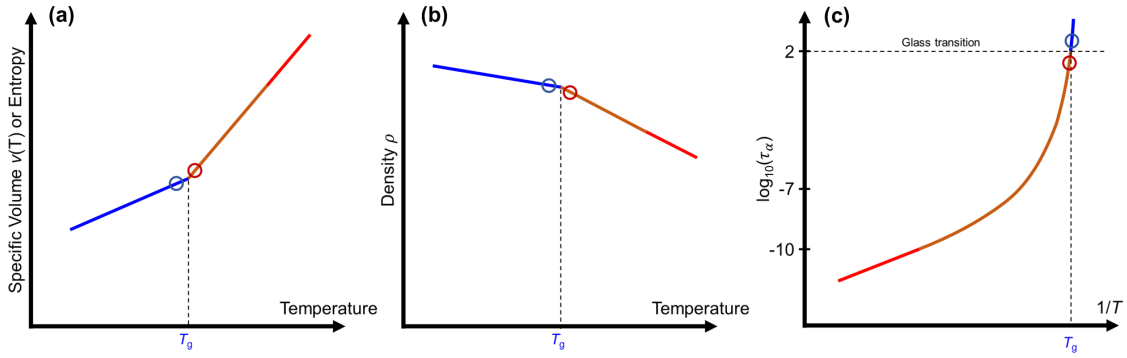

Figure 1.3: Schematics of (a) specific volume vs T, (b) density vs T and (c) logarithmic relaxation time log τ_α vs $1/T$. The brown circles correspond to the states right above T_g in the supercooled liquid regime, while the blue circles correspond to the states right below T_g in the glassy state. Little changes in the structure or density can contribute to a significant change in dynamics.

Historically, due to the fact that density is the inverse of specific volume, the density of the system has long been associated with the concept of "free volume". Even though the term free volume has been defined in multiple ways in the literature,[27,31,35–40] the most common definition of free volume is $V_{\text{free}} = V - V_{\text{occ}}$, which is the total volume V subtracted by some measure of the "occupied" volume V_{occ}.[32] The basic idea of the free volume theory is that molecules need a certain amount of "free volume" for the neighboring units to redistribute so that rearrangement of the central unit can take place. White and Lipson proposed a V_{free}-based "cooperative free volume" (CFV) model that is capable of describing general temperature T and

volume V-dependent structural relaxation behavior.[41,42] This CFV model separates the temperature and volume contributions as multiplicative coupled contributions that dictate the cooperative segmental dynamics in the form of[41,42]

$$\tau(T,V) \propto \exp[f(T) \times g(V)] \ . \tag{1.3}$$

The free volume is defined as $V_{\text{free}} = V - V_{\text{hc}}$, where the "hardcore" volume V_{hc} is the characteristic limiting hardcore volume at close packing, which is a material-specific constant.[41,42] White and Lipson determined V_{hc} by analyzing thermodynamic (PVT) data using their locally correlated lattice (LCL) equation of state.[32]

Within the free volume framework, changes to the dynamics have often been associated with fluctuations in density (compressibility) in theoretical works trying to understand the glass transition. The free volume theory would suggest a simple correlation between the density and dynamics where lower density would lead to faster dynamics and often faster dynamics are taken to imply lower density, because larger free volume (lower density) is available for the units in the system to rearrange. Such a simple correlation built on the free volume concept has been adopted by numerous theories studying the glass transition,[32] and has been shown to work reasonably well for bulk systems.[31]

Density has also been an important material property that is intensively studied in the field of computer simulation. The local packing density which can be easily calculated is usually considered equivalent to the local mass density, even though they are not strictly equivalent in all cases. In contrast to the simple correlation between density and dynamics proposed by the free volume theory, computer simulations have found that the local mobility and density are not simply correlated,[43–48] where specifically the density profile of polymer thin films are not directly correlated to the dynamical gradients.[44,45,49–51] It raises the interest of studying the density in confined

systems with interfaces and exploring the correlation between the experimentally measured density and dynamics.

1.3.2 Confinement effects in polymer thin films

It is believed that the glass transition is associated with the packing frustration of a growing cooperative lengthscale as the system temperature decreases. Therefore, reducing one of the dimensions of a system to a point which is comparable to its corresponding cooperative lengthscale (nanoscale) is a motivation for studying polymer thin films. For polymer thin films, the size of the system can easily be controlled in only one dimension by simply decreasing the film thickness, resulting in a relatively simplified system compared to other systems where the size is reduced in all dimensions (e.g. polymer nanocomposites). With the film thickness being confined to the nanometer range, deviations from bulk properties have been observed, such as the glass transition temperature T_g,[17,43,52–56] and modulus,[57–63] which is often referred to as nanoconfinement effects or confinement effects. The underlying cause of such confinement effects appears to be perturbations at the boundaries or interfaces of the system.[64] As the thickness of the film is reduced, the surface-to-volume ratio increases, which means that the perturbations occurring at the interfaces become a more significant component in the film-average properties of the system. From an engineering perspective, understanding the fundamental physics behind these confinement effects would be beneficial to the development and manufacturing of modern microelectronic circuits which involve polymers with nanoscale structures.[65–67]

Among those properties that deviate from the bulk value with decreasing film thickness, the glass transition temperature T_g has been the most studied property, characterized by a range of experimental techniques. The first work that reported shifts in T_g with decreasing film thickness was done by Keddie, Jones and Cory.[68,69] The film-average T_g of polystyrene (PS) thin films supported on silicon substrates was

observed to be ≈ 20 K below the bulk T_g ($T_g^{bulk} \approx 100°C$ for PS) for film thicknesses $h \approx 15$ nm when measured by ellipsometry. This $T_g(h)$ behavior was initially understood as the presence of a free surface layer with enhanced mobility due to fewer nearest neighbors for the segments at the free surface (polymer-air interface) than in the film interior. The thickness of this surface layer was assumed to be described by a power law behavior:

$$\xi(T) = A\left(1 - \frac{T}{T_g^{bulk}}\right)^{-1/\delta}, \tag{1.4}$$

where $\xi(T)$ would increase drastically as the temperature approaches T_g until divergence. For polymer thin films, when the size of the surface layer $\xi(T)$ reaches the film thickness ($\xi(T) = h$), it means that the system temperature reaches T_g (T = $T_g(h)$). Then Eqn. 1.4 can be written as:

$$T_g(h) = T_g^{bulk}\left[1 - \left(\frac{A}{h}\right)^{\delta}\right], \tag{1.5}$$

where the experimentally measured $T_g(h)$ data can be well fit by this functional form. Measurements of freestanding PS films with free surfaces on both sides showed a stronger reduction in film-average T_g, supporting the hypothesis that the T_g depression is due to the free surface layer with enhanced mobility.[52,70–72] This hypothesis was confirmed separately by two different methods, capping the top of the film to remove the free surface effect[73] and a fluorescence method to probe the local T_g.[74] In the first study, a PS film was sandwiched between two neutral substrates (gold and aluminum), no deviation from bulk T_g was observed for film thickness down to ≈ 7 nm when no free surface was introduced to the system and the $T_g(h)$ decrease could be recovered when the aluminum capping layer was removed.[73] In the second study, a 14-nm-thick fluorescence labelled (fluorophore:pyrene) probe layer was positioned at different locations of a bulk PS film: the free surface, film interior and the interface next to a silica substrate, where the free surface was reported to have a local T_g that

is 32 K below T_g^{bulk} while the results at the film interior and the substrate interface still indicated a local T_g the same as the bulk value.[74] With the evidence from these two studies, it has been understood that the shifts in T_g in polymer thin films originates from the perturbations to dynamics occurring at the free surface (polymer-air interface), which propagate deeper into the film, resulting in a gradient in dynamics. Similar T_g depression due to the enhanced mobility at the polymer-air interface has also been observed for poly(methyl methacrylate) PMMA films,[75] where the strength of the free surface effect of PMMA is roughly one third of that of PS.[76–79]

Despite the perturbations to dynamics caused by the polymer-air interface, similar phenomena have been reported in other systems resulting from the polymer-substrate interface[65,67,75] or a polymer-polymer interface.[80,81] For the polymer-substrate interface, attractive interactions between the polymer and the substrate (e.g. hydrogen bonding) can slow down dynamics near the substrate interface, inducing an increase in local T_g. For instance, PMMA is believed to have an attractive interaction with the native oxide layer atop a silica substrate. Local fluorescence measurements by the Torkelson group showed a +10 K increase in local T_g near the substrate interface and a −7 K reduction in local T_g near the free surface,[75] confirming that the competing dynamical perturbations from the free surface and the substrate interface lead to the slight increase in film-average T_g with decreasing film thickness.[67,69,75] Details of dynamical gradients in polymer thin films will be further discussed in detail in Chapter 4, Section 4.3.4.

1.3.3 Summary of literature on density changes in thin polymer films

Although density changes in thin polymer films have drawn a lot of interest for decades, experimentally characterizing changes in mass density of polymer thin films is quite challenging. For a bulk material, the mass density can be easily measured by

its mass divided by its volume. However, for polymer thin films, measuring its mass is a nearly impossible task. Even for experimental techiniques that have been used to characeterize density of thin polymer films, the signal associated with polymer thin films usually approaches the sensitivity limits of the experimental technique. A range of experimental techniques have been used to characterize or infer mass density, including well establised techniques such as neutron reflectivity (NR), x-ray reflectivity (XRR) ellipsometry and Brillouin light scattering (BLS),[82–88] as well as novel techniques such as nanoparticle adsorption and magnetic levitation.[87,89,90] In 1998, Wallace et al. measured thin PS films on Si-H substrates with twin neutron scattering, demonstrating no change to density within their $\pm 1\%$ error down to 6.5 nm thick films.[82] Another early effort in the same year by Forrest et al. characterized the thickness dependence of the phonon velocity of the S_0 mode for thin freestanding PS films ($h = 22.4 - 190$ nm) by BLS, finding no systematic changes to the mass density within $\pm 1\%$ error with decreasing film thickness.[83] In contrast, enormous increases in mass density ($\approx 25\%$) with decreasing film thickness for thin PS films ($h < 30 - 40$ nm) have been claimed by several recent studies based on the results of XRR, ellipsometry, and nanoparticle adsorption.[84,85,87] However, these claimed density increases are physically unrealistic for these thin polymer films in their amorphous state. For PS in its bulk crystalline state, it is only $\approx 5 - 8\%$ denser than its bulk amorphous state.[91,92] Hence, claiming a $\approx 25\%$ increase in mass density suggests that the amorphous state of PS thin films could form into a configuration that is several times denser in packing than the crystalline state, which is sterically inaccessible.

Despite the enormous increases in mass density interpreted from the experimental results measured by several techniques being physically unrealistic, it is still worth noting that such similar results observed by different techniques would indicate interesting physics related to the thin film geometry that are not well captured by the current analysis. During the data analysis procedure of many modern experimen-

tal techniques, including NR, XRR, and ellipsometry, a layer model is often used to extract physical properties (electron density, scattering density, refractive index and film thickness) from the raw experimental data. Due to the nature of the multi-layer structure of the thin polymer film samples (e.g. polymer film layer, native oxide layer and silicon substrate layer for a typical PS thin film sample), a layer model can well represent the distribution of the material properties in each layer when such differences are sufficiently distinguishable between the layers. Commonly, the material properties of the layer of interest (the polymer film in most cases) is assumed to be homogeneous and isotropic within the layer for the purpose of simplifying the model.[82,84–88,93] For example, a Cauchy layer model is widely used in analyzing ellipsometry data where the refractive index of the polymer film is assumed to be homogeneous throughout the film. This assumption of a homogeneous film remains valid for bulk films, and sometimes thin films when the property of interest (e.g. film thickness) is not noticeably affected by the spatial distribution of another property (e.g. refractive index). However, the homogeneous film assumption may not be correct for film thicknesses ≤ 100 nm, as many studies have suggested property changes in nanoconfined geometries.[17,43,52,53,55,56,94]

Besides, when inferring mass density from the experimentally measured physical quantities (e.g. refractive index or electron density), additional equations such as the Lorentz-Lorenz relation[95,96] are often used.[84–87] The Lorentz-Lorenz equation (Eqn. 1.6)

$$L = \frac{n^2 - 1}{n^2 + 2} = \frac{\alpha N_A}{3\epsilon_0 M_0}\rho \ , \tag{1.6}$$

relates the macroscopic refractive index n to the microscopic molecular polarizability α, where the Lorentz parameter L is proportional to the mass density ρ via the constants: Avogadro's number N_A, the permittivity of free space ϵ_0, the monomer molecular weight M_0, and the molecular polarizability α. Although the Lorentz-Lorenz equation has been widely used in many circumstances, the underlying as-

sumption in its derivation is often neglected. As the first term in a series expansion excluding higher order terms that account for local electric field,[97,98] the Lorentz-Lorenz equation assumes a homogeneous and isotropic distribution for the molecular dipoles of the material, where this assumption is hardly satisfied for a polymer thin film. Several studies have reported density variations with depth in thin polymer films,[99–101] contradicting the assumed homogeneous and isotropic dipole distribution. Previous work from our group addressed some of these issues by examining in detail the use of ellipsometry to characterize changes in density for PS thin films based on refractive index measurements. Huang and Roth confirmed that the measured refractive index was robust for film thicknesses $h \geq 20$ nm where the film thickness and refractive index can still be independently resolved.[86] This study also evaluated the inherent assumptions of isotropic uniform polarizability to validate the use of the Lorentz-Lorenz relation in thin PS films. They suggested that the apparent increase in density may result from a loss of uniform polarizability, which leads to my motivation of investigating different polymers and their spatial distribution of density.

So far, the field has not reached an agreement on how density actually changes in polymer thin films under confinement, with the discussed complexity associated with the experimental technique and data analysis. The interesting physics behind such shared enormous apparent increases in density could be a gradient in density induced by the perturbation from the interface. Another related open question would be whether the dynamical gradients are locally driven by the local structure and/or density modified by the interfacial perturbation. Therefore, I will be exploring the fundamental physics behind the enormous apparent increase in density and addressing these questions by comparing the density/refractive index behavior in different polymers under confinement.

1.4 How are modulus and the glass transition related?

1.4.1 Modulus behavior of bulk polymers

The long chain nature of polymers leads to an important feature which is viscoelasticity, where the system behaves like a solid under short time scales and behaves like a liquid under long time scales.[102,103] Figure 1.4 plots the logarithm of modulus as a function of logarithmic time or temperature, demonstrating different regimes of relaxation for a polymer system. At short time scales or low temperatures below T_g, the system remains in the glassy regime, where only local vibrational and rotational motions are activated while molecular units are undergoing packing frustration, resulting in a solid-like GPa (10^9 Pa) modulus. The glass transition is commonly defined at ~100 s (details mentioned in Section 1.2.1). On passing through the glass transition, for polymers chains with small molecular weights that are unentangled, the system will immediately transition to liquid flow (dotted curve). For polymers with high enough molecular weights to induce entanglement effects, the system will transition into the rubbery plateau regime where the modulus is on the order of MPa (10^6 Pa). Under this circumstance, viscous flow can only occur at sufficiently long times or high enough temperature, which is identified as the terminal flow regime. The length of the rubbery plateau has a strong dependence on the molecular weight where the onset of terminal flow at the reptation time τ_{rep} scales with $\sim M^{3.4}$ due to tube dynamics caused by entanglements (primarily reptation).[103–107] As shown in Fig. 1.4, terminal flow for medium molecular weight polymers (dashed curve) occurs at shorter times / lower temperature than that for the high molecular weight polymers (solid curve). Therefore, for entangled polymers, viscous flow and diffusion of the polymer chains are decoupled from the glass transition.

Experimentally, for bulk systems, the modulus of the material is often measured

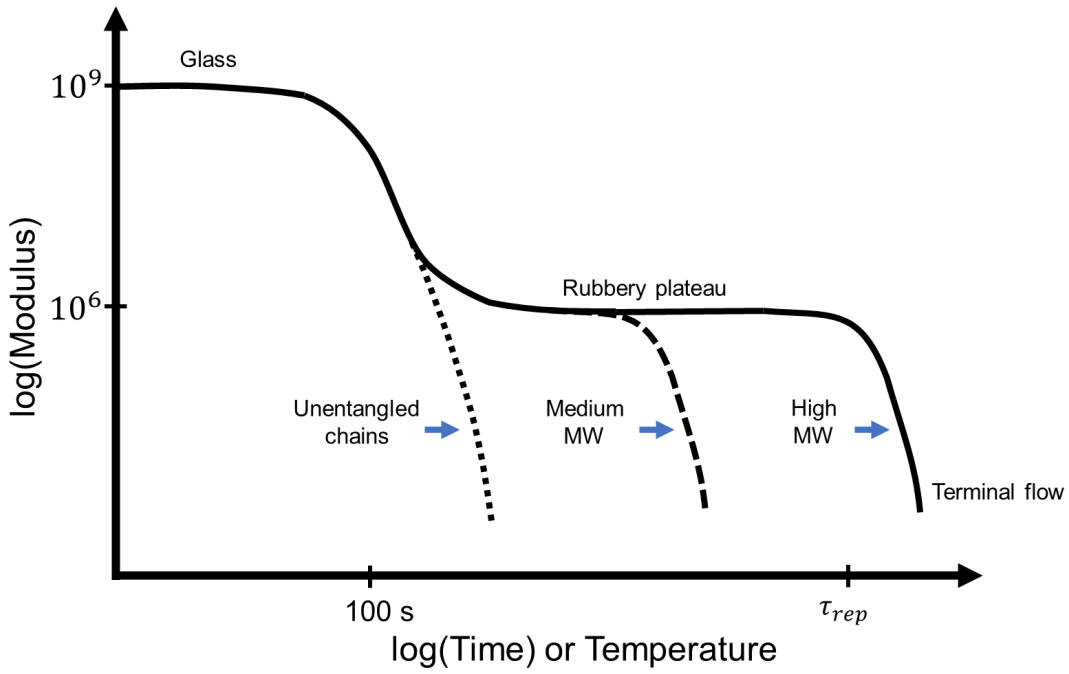

Figure 1.4: Schematic of a modulus master curve: the logarithm of modulus as a function of the logarithm of time or temperature for polymers with different molecular weights. The glass transition is commonly defined at $\sim$ 100 s. For unentangled polymers, the system transitions from the glassy state ($\sim 10^9$ Pa) to flow immediately. In contrast, entangled polymers transition from the glassy state to the rubbery plateau ($\sim 10^6$ Pa) before terminal flow finally occurs at the reptation time $\tau_{rep} \sim M^{3.4}$.

by dynamic mechanical analysis (DMA), which applies an oscillating strain to a sample and measures the dynamic stress response. The complex modulus G^* can be determined from the dynamic response, where the real and imaginary components are referred to as the storage (G') and loss (G'') modulus, respectively. The span of the time scale in Fig. 1.4 can reach $\sim$12 orders of magnitude for high molecular weight polymers, where no single experimental technique is capable of covering such broad time scales. Therefore, in practice, the modulus of the material is usually collected over several decades at different temperatures and then shifted along the time (or frequency) axis to overlap the data. This superposition of data collected at different temperatures is called time-temperature superposition. For a given reference temperature $T_{\rm ref}$ (usually taken to be $T_{\rm g}^{\rm bulk}$ of the polymer), the amount required to shift the

curve at each temperature along the time (or frequency) axis is determined by the factor a_T, which follows the Williams, Landel, and Ferry (WLF) equation:[35]

$$\log(a_T) = \log\left[\frac{\eta(T)}{\eta(T_{\text{ref}})}\right] = -\frac{C_1(T - T_{\text{ref}})}{C_2 + (T - T_{\text{ref}})} \ , \tag{1.7}$$

where C_1 and C_2 are tabulated fitting parameters for a given material and T_{ref} is the reference temperature. The WLF equation is mathematically equivalent to the VFT equation (Eqn.1.2) but more frequently used in the polymer field.

1.4.2 Previous efforts to investigate modulus changes in thin polymer films

It is widely acknowledged that polymer thin films under confinement undergo shifts in T_{g} with decreasing film thickness. Given that modulus and the glass transition are correlated in bulk, one would imagine that modulus would change in polymer thin films. The open question is whether it would be a simple shift corresponding to the position of the glass transition in the modulus master curve, or if it would change the overall shape as well as the magnitude of the glassy and rubbery modulus.

Even though methods such as DMA are sufficient to characterize the modulus of bulk systems, they are not applicable to polymer thin films where small loads and very precise load cells are required, not to mention the difficulty in keeping the integrity of the fragile films. Therefore, several new experimental methods have been developed to probe the changes in modulus of polymer thin films, such as surface wrinkling,[58,59,108,109] ultrathin film tensile tester (UFT),[60,61] nanoindentation[110] and Brillouin light scattering[111–113] for measuring glassy modulus, bubble inflation for measuring rubbery modulus,[62,63,114] as well as nanoparticle embedding for measuring surface compliance in both the glassy and rubbery regime.[115,116]

Surface wrinkling is a technique developed by Stafford et al.[58,59,108,109] that pro-

duces periodic wrinkles by deforming a thin stiff film adhered to a much softer thick substrate (often PDMS) after exceeding a critical strain. The spacing between the wrinkles λ can be directly related to the plane-strain moduli for the substrate (E_s) and thin film (E_f) as well as the thickness of the thin polymer film h by the following equation:

$$\lambda = 2\pi h \left(\frac{E_f}{3E_s} \right)^{\frac{1}{3}} . \tag{1.8}$$

With this technique, the elastic moduli of PS and PMMA films have been found to decrease with decreasing film thickness for film thicknesses below ~ 40 nm, with the trend for PS films being more pronounced.[59] Even though surface wrinkling has been considered as a decent choice to measure the modulus of polymer thin films, it is still subject to several inherent limitations. Due to the significant mismatch in modulus between the softer substrate and the stiffer film required to form the wrinkle, the presence of an adjacent rubbery layer (PDMS) could have an impact on the local stiffness of the polymer film on top.[117] Besides, only the value of the elastic modulus (Young's modulus) in the glassy state at room temperature can be determined with this method, instead of a full stress-strain curve. In addition, the deformation of the substrate has to remain in its linear elastic regime.

The ultrathin film tensile tester (UFT) and its successor the uniaxial tensile tester for ultrathin films (TUTTUT) were developed by Crosby et al. to measure the stress-strain curve by stretching a thin polymer film floated on liquid while monitoring the deflection of the cantilever that the polymer film is clamped to.[60,118] Such methods have reported a decrease in the glassy Young's modulus of PS films with decreasing film thickness for films below ~ 25 nm, qualitatively in agreement with the surface wrinkling results but showing a lower reduction in modulus at a thinner film thickness. In addition, the requirement of contact with the liquid restrains its application to only hydrophobic polymer films as well as the temperature range it can work in. A updated method called the Tensile tester for Ultrathin Freestanding Films (TUFF) has been

developed by the same group to measure freestanding PS films, showing constant elastic modulus down to film thickness of 30 nm.[61]

In general, modulus seems to decrease with decreasing film thickness for thin polymer films in the glassy state,[57] while there are a few results that disagree with this argument. Nanoindentation, which presses a hard tip with known mechanical properties into the film of interest, suggests an increase in modulus with decreasing film thickness.[110] However, the stress field introduced by the tip is nontrivial and becomes influenced by the substrate as the film becomes thinner. As a contact probe, the dynamics of the free surface could also be perturbed by the tip, which may lead to a different confinement condition when compared to other techniques. Brillouin light scattering (BLS), which samples the cubic elastic tensor from the changes in the energy of the phonons at GHz frequencies, demonstrates no changes to the elastic modulus down to 29 nm.[111–113] However, for film thicknesses below 40 nm, whether there is sufficient material to accurately capture the small shifts in modulus under confinement with this technique is questionable.[57] Due to its nature of sampling at high frequency (GHz), the invariant modulus in thin films could result from the suppression of confinement effects at high frequency (short time scale).[18]

The modulus of the rubbery plateau has been characterized by a nanobubble inflation technique developed by McKenna et al..[62,63,114] A thin polymer film is prepared on a porous substrate and inflated through those holes in the substrate, resulting in a biaxial stretch of the film. The time-dependent size of the bubble height is measured by atomic force microscopy (AFM), providing information about the creep compliance of the thin film. Results from the bubble inflation experiment suggest stiffening of the film in the rubbery region for a range of polymers.[62,63,114] To reconcile the modulus changes in both the glassy and rubbery regime for polymer thin films, the most relevant evidence to date is the result from nanoparticle embedding by McKenna et al.[115,116] Nanoparticles deposited on the surface of the film spontaneously embed into

the polymer film, where the evolution of the embedment process is impacted by the surface stifness. The surface compliance of the polymer film is calculated from the embedment depth monitored by AFM. With the results collected at different temperatures, surface softening in the glassy regime and surface stiffening in the rubbery regime have been found for PS and poly(α-methylstyrene) (PαMS).[116]

Even though these results have suggested surface softening in the glassy regime and surface stiffening in the rubbery regime, this piece of evidence is still not enough to understand the changes in the modulus curve for polymers under confinement. As suggested by Vogt, the modulus changes under confinement could be spatially inhomogeneous rather than a uniform change.[57] Therefore, a non-contact local probe of modulus would be very informative of the changes to the local modulus for polymer thin films.

1.5 Dissertation outline

This dissertation consists of six chapters illustrating the research I have accomplished towards the goal of understanding how changes in material properties (density and modulus) are related to the glass transition and dynamics for polymer thin films.

Chapter 2 introduces the two main experimental techniques that are used in the research included in this dissertation, ellipsometry and fluorescence spectrometry. Fundamental physics and mechanisms of these techniques will be covered in this chapter. In addition, details of the optical modeling for ellipsometry are also included, as they are relevant to the discussion of limitations in the conventional data analysis in the literature.

Density changes have long been considered as a possible explanation for the thickness-dependent shifts to T_g in nanoconfined systems. Chapter 3 explores the density changes in polymer thin films with ellipsometry. We have found similar apparent increases in the thickness-dependent refractive index trends $n(h)$ for three different polymers, PS, PMMA and poly(2-vinyl pyridine) (P2VP), despite the differences in polymer-silica substrate interactions. The nearly identical trends between PS and P2VP suggest the chemical structure and nature of the molecular dipole orientations may play a role in the observed behavior. We tested for possible non-uniform film polarizability by varying molecular weight, polydispersity, and forming films from bilayers as well as altering the substrate surface chemistry. However, none of these seems to be the cause of the large unphysical apparent increase in density. We suspect the use of homogeneous (uniform and isotropic) layer approximations, typical of data analysis in many thin film techniques, can lead to unphysical results when film inhomogeneities associated with non-uniform polarizability are present. A version of this chapter was published as:

Y. Han, X. Huang, A.C.W. Rohrbach, and C.B. Roth, "Comparing Refractive Index and Density Changes with Decreasing Film Thickness in Thin Supported Films Across Different Polymers," *The Journal of Chemical Physics* **2020**, *153*, 044902.

Continuing the work described in Chapter 3, we address film inhomogeneities associated with strong dynamical gradients frequently observed in such thin polymer films in Chapter 4. In this chapter, we have explored the use of an ellipsometric optical layer model with a depth-dependent refractive index gradient to model thin polymer films of PMMA, PS, and P2VP. Specifically we proposed a gradient linear in the magnitude of the refractive index, Cauchy parameter $A(z)$, with depth. From the ellipsometric fits to the linear gradient model, we demonstrate the presence of a strong positive gradient in the magnitude of the refractive index (%grade) for PMMA and PS thin films. In contrast, P2VP films, show a refractive index gradient that primarily fluctuates about zero for all film thicknesses. Counter to common expectations of a simple free volume correlation between density and dynamics, we find that the direction of the refractive index (density) gradient indicates a higher density near the free surface, which we rationalize based on the observed faster free surface dynamics needed to create vapor deposited stable glasses with optimized denser molecular packings. A version of this chapter was published as:

Y. Han and C.B. Roth, "Gradient in Refractive Index Reveals Denser Near Free Surface Region in Thin Polymer Films," *The Journal of Chemical Physics* **2021**, *155* , 144901.

Perturbations caused by interfacial effects lead to changes in local material properties in polymer thin films under nanoconfinement. Fluorescence has been used to probe such local material properties due to the probe's sensitivity in the ambient environment of the polymer matrices (e.g. temperature, density, modulus and local polarity), which is often reflected as characteristic spectral changes of the fluorophores. In Chapter 5, we developed a new method using perylene doped in a

range of polymers, polystyrene (PS), poly(methyl methacrylate) (PMMA), poly(2-vinyl pyridine) (P2VP) and polycarbonate (PC). We demonstrate the temperature dependence of perylene doped in various polymer matrices. We defined a fluorescence intensity "shift factor" $\log(a_T)$ based on the intensity ratio. We find the nonradiative decay process of perylene doped in polymers reflect the local polymer dynamics transitioning from the liquid to glassy regime. The nonradiative decay process is influenced by cooperative α-relaxation in the liquid regime, and the local β-relaxation in the glassy regime.

Bibliography

[1] C. B. Roth, R. R. Baglay. Fundamentals of polymers and glasses. *Polymer Glasses* **2016**, 3–22.

[2] R. Richert. Supercooled liquid dynamics: Advances and challenges. *Structural Glasses and Supercooled Liquids: Theory, Experiment, and Applications* **2012**, 1–30.

[3] L. Berthier, G. Biroli. Theoretical perspective on the glass transition and amorphous materials. *Reviews of Modern Physics* **2011**, *83*, 587.

[4] A. Cavagna. Supercooled liquids for pedestrians. *Physics Reports* **2009**, *476*, 51–124.

[5] E.-J. Donth, *The glass transition: relaxation dynamics in liquids and disordered materials*, *Vol. 48*, Springer Science & Business Media, **2001**.

[6] V. N. Novikov, A. P. Sokolov. Universality of the dynamic crossover in glass-forming liquids: A "magic" relaxation time. *Physical Review E* **2003**, *67*, 031507.

[7] G. Adam, J. H. Gibbs. On the temperature dependence of cooperative relaxation properties in glass-forming liquids. *The Journal of Chemical Physics* **1965**, *43*, 139–146.

[8] F. W. Starr, J. F. Douglas, S. Sastry. The relationship of dynamical heterogeneity to the Adam-Gibbs and random first-order transition theories of glass formation. *The Journal of Chemical Physics* **2013**, *138*, 12A541.

[9] B. A. Pazmiño Betancourt, J. F. Douglas, F. W. Starr. String model for the dynamics of glass-forming liquids. *The Journal of Chemical Physics* **2014**, *140*, 204509.

[10] S. A. Reinsberg, X. Qiu, M. Wilhelm, H. W. Spiess, M. D. Ediger. Length scale of dynamic heterogeneity in supercooled glycerol near Tg. *The Journal of Chemical Physics* **2001**, *114*, 7299–7302.

[11] U. Tracht, M. Wilhelm, A. Heuer, H. Feng, K. Schmidt-Rohr, H. W. Spiess. Length scale of dynamic heterogeneities at the glass transition determined by multidimensional nuclear magnetic resonance. *Physical Review Letters* **1998**, *81*, 2727.

[12] B. M. Erwin, R. H. Colby. Temperature dependence of relaxation times and the length scale of cooperative motion for glass-forming liquids. *Journal of Non-crystalline Solids* **2002**, *307*, 225–231.

[13] E. Hempel, G. Hempel, A. Hensel, C. Schick, E. Donth. Characteristic length of dynamic glass transition near T g for a wide assortment of glass-forming substances. *The Journal of Physical Chemistry B* **2000**, *104*, 2460–2466.

[14] G. Biroli, J. P. Garrahan. Perspective: The glass transition. *The Journal of Chemical Physics* **2013**, *138*, 12A301.

[15] P. G. Debenedetti, F. H. Stillinger. Supercooled liquids and the glass transition. *Nature* **2001**, *410*, 259–267.

[16] R. Greiner, F. Schwarzl. Thermal contraction and volume relaxation of amorphous polymers. *Rheologica acta* **1984**, *23*, 378–395.

[17] M. D. Ediger, J. A. Forrest. Dynamics near free surfaces and the glass transition in thin polymer films: a view to the future. *Macromolecules* **2014**, *47*, 471–478.

[18] Z. Fakhraai, J. A. Forrest. Probing slow dynamics in supported thin polymer films. *Physical Review Letters* **2005**, *95*, 025701.

[19] L. Berthier, G. Biroli, J.-P. Bouchaud, L. Cipelletti, W. van Saarloos, *Dynamical heterogeneities in glasses, colloids, and granular media*, *Vol. 150*, OUP Oxford, **2011**.

[20] J. C. Dyre. Colloquium: The glass transition and elastic models of glass-forming liquids. *Reviews of Modern Physics* **2006**, *78*, 953.

[21] M. D. Ediger, C. A. Angell, S. R. Nagel. Supercooled liquids and glasses. *The Journal of Physical Chemistry* **1996**, *100*, 13200–13212.

[22] C. A. Angell, K. L. Ngai, G. B. McKenna, P. F. McMillan, S. W. Martin. Relaxation in glassforming liquids and amorphous solids. *Journal of Applied Physics* **2000**, *88*, 3113–3157.

[23] W. Kauzmann. The nature of the glassy state and the behavior of liquids at low temperatures. *Chemical Reviews* **1948**, *43*, 219–256.

[24] M. D. Ediger, P. Harrowell. Perspective: Supercooled liquids and glasses. *The Journal of Chemical Physics* **2012**, *137*, 080901.

[25] D. Wales, et al., *Energy landscapes: Applications to clusters, biomolecules and glasses*, Cambridge University Press, **2003**.

[26] S. Mirigian, K. S. Schweizer. Dynamical theory of segmental relaxation and emergent elasticity in supercooled polymer melts. *Macromolecules* **2015**, *48*, 1901–1913.

[27] T. G. Fox, P. J. Flory. The glass temperature and related properties of polystyrene. Influence of molecular weight. *Journal of Polymer Science* **1954**, *14*, 315–319.

[28] H. J. Unidad, M. A. Goad, A. R. Bras, M. Zamponi, R. Faust, J. Allgaier, W. Pyckhout-Hintzen, A. Wischnewski, D. Richter, L. J. Fetters. Consequences

of increasing packing length on the dynamics of polymer melts. *Macromolecules* **2015**, *48*, 6638–6645.

[29] G. B. McKenna. Glass formation and glassy behavior. *Pergamon Press plc, Comprehensive Polymer Science: the Synthesis, Characterization, Reactions & Applications of Polymers.* **1989**, *2*, 311–362.

[30] C. M. Roland, S. Hensel-Bielowka, M. Paluch, R. Casalini. Supercooled dynamics of glass-forming liquids and polymers under hydrostatic pressure. *Reports on Progress in Physics* **2005**, *68*, 1405 – 1478.

[31] R. P. White, J. E. G. Lipson. Free Volume in the Melt and How It Correlates with Experimental Glass Transition Temperatures: Results for a Large Set of Polymers. *ACS Macro Letters* **2015**, *4*, 588–592.

[32] R. P. White, J. E. G. Lipson. Polymer Free Volume and Its Connection to the Glass Transition. *Macromolecules* **2016**, *49*, 3987–4007.

[33] S. F. Swallen, K. L. Kearns, M. K. Mapes, Y. S. Kim, R. J. McMahon, M. D. Ediger, T. Wu, L. Yu, S. Satija. Organic glasses with exceptional thermodynamic and kinetic stability. *Science* **2007**, *315*, 353–356.

[34] S. S. Dalal, M. D. Ediger. Molecular Orientation in Stable Glasses of Indomethacin. *The Journal of Physical Chemistry Letters* **2012**, *3*, 1229 – 1233.

[35] M. L. Williams, R. F. Landel, J. D. Ferry. Mechanical properties of substances of high molecular weight. 19. The temperature dependence of relaxation mechanisms in amorphous polymers and other glass-forming liquids. *Journal of the American Chemical Society* **1955**, *77*, 3701–3707.

[36] A. K. Doolittle. Studies in Newtonian flow. II. The dependence of the viscosity of liquids on free-space. *Journal of Applied Physics* **1951**, *22*, 1471–1475.

[37] M. H. Cohen, D. Turnbull. Molecular transport in liquids and glasses. *The Journal of Chemical Physics* **1959**, *31*, 1164–1169.

[38] T. G. Fox Jr, P. J. Flory. Second-order transition temperatures and related properties of polystyrene. I. Influence of molecular weight. *Journal of Applied Physics* **1950**, *21*, 581–591.

[39] T. G. Fox Jr, P. J. Flory. Further studies on the melt viscosity of polyisobutylene. *The Journal of Physical Chemistry* **1951**, *55*, 221–234.

[40] R. Simha, R. F. Boyer. On a general relation involving the glass temperature and coefficients of expansion of polymers. *The Journal of Chemical Physics* **1962**, *37*, 1003–1007.

[41] R. P. White, J. E. G. Lipson. Explaining the T, V-dependent dynamics of glass forming liquids: The cooperative free volume model tested against new simulation results. *The Journal of Chemical Physics* **2017**, *147*, 184503.

[42] R. P. White, J. E. G. Lipson. A Simple New Way To Account for Free Volume in Glassy Dynamics: Model-Free Estimation of the Close-Packed Volume from PVT Data. *The Journal of Physical Chemistry B* **2021**, *125*, 4221–4231.

[43] J. Baschnagel, F. Varnik. Computer simulations of supercooled polymer melts in the bulk and in confined geometry. *Journal of Physics: Condensed Matter* **2005**, *17*, R851.

[44] P. Z. Hanakata, J. F. Douglas, F. W. Starr. Local variation of fragility and glass transition temperature of ultra-thin supported polymer films. *The Journal of Chemical Physics* **2012**, *137*, 244901.

[45] P. Z. Hanakata, B. A. P. Betancourt, J. F. Douglas, F. W. Starr. A unifying framework to quantify the effects of substrate interactions, stiffness, and rough-

ness on the dynamics of thin supported polymer films. *The Journal of Chemical Physics* **2015**, *142*, 234907.

[46] F. Varnik, J. Baschnagel, K. Binder. Reduction of the glass transition temperature in polymer films: A molecular-dynamics study. *Physical Review E* **2002**, *65*, 021507.

[47] A. Shavit, R. A. Riggleman. Influence of backbone rigidity on nanoscale confinement effects in model glass-forming polymers. *Macromolecules* **2013**, *46*, 5044–5052.

[48] A. Shavit, R. A. Riggleman. Physical aging, the local dynamics of glass-forming polymers under nanoscale confinement. *The Journal of Physical Chemistry B* **2014**, *118*, 9096–9103.

[49] Y. Zhou, S. T. Milner. Short-Time Dynamics Reveals Tg Suppression in Simulated Polystyrene Thin Films. *Macromolecules* **2017**, *50*, 5599–5610.

[50] W. Zhang, F. W. Starr, J. F. Douglas. Reconciling computational and experimental trends in the temperature dependence of the interfacial mobility of polymer films. *The Journal of Chemical Physics* **2020**, *152*, 124703.

[51] D. M. Sussman, S. S. Schoenholz, E. D. Cubuk, A. J. Liu. Disconnecting structure and dynamics in glassy thin films. *Proceedings of the National Academy of Sciences* **2017**, *114*, 10601 – 10605.

[52] J. A. Forrest, K. Dalnoki-Veress. The glass transition in thin polymer films. *Advances in Colloid and Interface Science* **2001**, *94*, 167–195.

[53] C. B. Roth, J. R. Dutcher. Glass transition and chain mobility in thin polymer films. *Journal of Electroanalytical Chemistry* **2005**, *584*, 13–22.

[54] M. Alcoutlabi, G. B. McKenna. Effects of confinement on material behaviour at the nanometre size scale. *Journal of Physics: Condensed Matter* **2005**, *17*, R461.

[55] D. S. Simmons. An emerging unified view of dynamic interphases in polymers. *Macromolecular Chemistry and Physics* **2016**, *217*, 137–148.

[56] K. S. Schweizer, D. S. Simmons. Progress towards a phenomenological picture and theoretical understanding of glassy dynamics and vitrification near interfaces and under nanoconfinement. *The Journal of Chemical Physics* **2019**, *151*, 240901.

[57] B. D. Vogt. Mechanical and viscoelastic properties of confined amorphous polymers. *Journal of Polymer Science Part B: Polymer Physics* **2018**, *56*, 9–30.

[58] C. M. Stafford, C. Harrison, K. L. Beers, A. Karim, E. J. Amis, M. R. VanLandingham, H.-C. Kim, W. Volksen, R. D. Miller, E. E. Simonyi. A buckling-based metrology for measuring the elastic moduli of polymeric thin films. *Nature materials* **2004**, *3*, 545–550.

[59] C. M. Stafford, B. D. Vogt, C. Harrison, D. Julthongpiput, R. Huang. Elastic moduli of ultrathin amorphous polymer films. *Macromolecules* **2006**, *39*, 5095–5099.

[60] Y. Liu, Y.-C. Chen, S. Hutchens, J. Lawrence, T. Emrick, A. J. Crosby. Directly measuring the complete stress–strain response of ultrathin polymer films. *Macromolecules* **2015**, *48*, 6534–6540.

[61] R. K. Bay, A. J. Crosby. Uniaxial extension of ultrathin freestanding polymer films. *ACS Macro Letters* **2019**, *8*, 1080–1085.

[62] P. A. O'connell, G. B. McKenna. Rheological measurements of the thermoviscoelastic response of ultrathin polymer films. *Science* **2005**, *307*, 1760–1763.

[63] P. A. O'Connell, G. B. McKenna. Dramatic stiffening of ultrathin polymer films in the rubbery regime. *The European Physical Journal E* **2006**, *20*, 143–150.

[64] C. B. Roth, K. L. McNerny, W. F. Jager, J. M. Torkelson. Eliminating the enhanced mobility at the free surface of polystyrene: fluorescence studies of the glass transition temperature in thin bilayer films of immiscible polymers. *Macromolecules* **2007**, *40*, 2568–2574.

[65] D. S. Fryer, P. F. Nealey, J. J. de Pablo. Thermal probe measurements of the glass transition temperature for ultrathin polymer films as a function of thickness. *Macromolecules* **2000**, *33*, 6439–6447.

[66] D. S. Fryer, P. F. Nealey, J. J. de Pablo. Scaling of Tg and reaction rate with film thickness in photoresist: A thermal probe study. *Journal of Vacuum Science & Technology B: Microelectronics and Nanometer Structures Processing, Measurement, and Phenomena* **2000**, *18*, 3376–3380.

[67] M. K. Mundra, S. K. Donthu, V. P. Dravid, J. M. Torkelson. Effect of spatial confinement on the glass-transition temperature of patterned polymer nanostructures. *Nano Letters* **2007**, *7*, 713 – 718.

[68] J. L. Keddie, R. A. L. Jones, R. A. Cory. Size-Dependent Depression of the Glass Transition Temperature in Polymer Films. *Europhysics Letters* **1994**, *27*, 59–64.

[69] J. L. Keddie, R. A. L. Jones, R. A. Cory. Interface and surface effects on the glass-transition temperature in thin polymer films. *Faraday Discussions* **1994**, *98*, 219.

[70] J. A. Forrest, K. Dalnoki-Veress, J. R. Stevens, J. Dutcher. Effect of free surfaces on the glass transition temperature of thin polymer films. *Physical Review Letters* **1996**, *77*, 2002.

[71] J. Mattsson, J. A. Forrest, L. Börjesson. Quantifying glass transition behavior in ultrathin free-standing polymer films. *Physical Review E* **2000**, *62*, 5187.

[72] K. Dalnoki-Veress, J. A. Forrest, C. Murray, C. Gigault, J. R. Dutcher. Molecular weight dependence of reductions in the glass transition temperature of thin, freely standing polymer films. *Physical Review E* **2001**, *63*, 031801.

[73] J. S. Sharp, J. A. Forrest. Free Surfaces Cause Reductions in the Glass Transition Temperature of Thin Polystyrene Films. *Physical Review Letters* **2003**, *91*, 235701.

[74] C. J. Ellison, J. M. Torkelson. The distribution of glass-transition temperatures in nanoscopically confined glass formers. *Nature Materials* **2003**, *2*, 695 – 700.

[75] R. D. Priestley, M. K. Mundra, N. J. Barnett, L. J. Broadbelt, J. M. Torkelson. Effects of Nanoscale Confinement and Interfaces on the Glass Transition Temperatures of a Series of Poly(n-methacrylate) Films. *Australian Journal of Chemistry* **2007**, *60*, 765–771.

[76] C. B. Roth, J. R. Dutcher. Glass transition temperature of freely-standing films of atactic poly(methyl methacrylate). *The European Physical Journal E* **2003**, *12*, 103–107.

[77] C. B. Roth, A. Pound, S. W. Kamp, C. A. Murray, J. R. Dutcher. Molecular-weight dependence of the glass transition temperature of freely-standing poly(methyl methacrylate) films. *The European Physical Journal E* **2006**, *20*, 441–448.

[78] K. Paeng, M. D. Ediger. Molecular Motion in Free-Standing Thin Films of Poly(methyl methacrylate), Poly(4-tert-butyl styrene), Poly(α-methyl styrene), and Poly(2-vinyl pyridine). *Macromolecules* **2011**, *44*, 7034–7042.

[79] K. Paeng, R. Richert, M. D. Ediger. Molecular mobility in supported thin films of polystyrene, poly(methyl methacrylate), and poly(2-vinyl pyridine) probed by dye reorientation. *Soft Matter* **2012**, *8*, 819 – 826.

[80] R. R. Baglay, C. B. Roth. Communication: Experimentally determined profile of local glass transition temperature across a glassy-rubbery polymer interface with a T g difference of 80 K. *The Journal of Chemical Physics* **2015**, *143*, 111101.

[81] R. R. Baglay, C. B. Roth. Local glass transition temperature T g (z) of polystyrene next to different polymers: Hard vs. soft confinement. *The Journal of chemical physics* **2017**, *146*, 203307.

[82] W. E. Wallace, N. C. Beck Tan, W. L. Wu, S. Satija. Mass density of polystyrene thin films measured by twin neutron reflectivity. *The Journal of Chemical Physics* **1998**, *108*, 3798–3804.

[83] J. A. Forrest, K. Dalnoki-Veress, J. R. Dutcher. Brillouin light scattering studies of the mechanical properties of thin freely standing polystyrene films. *Physical Review E* **1998**, *58*, 6109.

[84] S. Ata, K. Kuboyama, K. Ito, Y. Kobayashi, T. Ougizawa. Anisotropy and densification of polymer ultrathin films as seen by multi-angle ellipsometry and X-ray reflectometry. *Polymer* **2012**, *53*, 1028–1033.

[85] G. Vignaud, M. S. Chebil, J. K. Bal, N. Delorme, T. Beuvier, Y. Grohens, A. Gibaud. Densification and Depression in Glass Transition Temperature in Polystyrene Thin Films. *Langmuir* **2014**, *30*, 11599–11608.

[86] X. Huang, C. B. Roth. Changes in the temperature-dependent specific volume of supported polystyrene films with film thickness. *The Journal of Chemical Physics* **2016**, *144*, 234903.

[87] A. Beena Unni, G. Vignaud, J. P. Chapel, J. Giermanska, J. K. Bal, N. Delorme, T. Beuvier, S. Thomas, Y. Grohens, A. Gibaud. Probing the Density Variation of Confined Polymer Thin Films via Simple Model-Independent Nanoparticle Adsorption. *Macromolecules* **2017**, *50*, 1027 – 1036.

[88] Y. Li, J. Q. Pham, K. P. Johnston, P. F. Green. Contact Angle of Water on Polystyrene Thin Films: Effects of CO2 Environment and Film Thickness. *Langmuir* **2007**, *23*, 9785–9793.

[89] J. Giermanska, S. B. Jabrallah, N. Delorme, G. Vignaud, J.-P. Chapel. Direct experimental evidences of the density variation of ultrathin polymer films with thickness. *Polymer* **2021**, *228*, 123934.

[90] S. E. Root, R. Gao, C. K. Abrahamsson, M. S. Kodaimati, S. Ge, G. M. Whitesides. Estimating the Density of Thin Polymeric Films Using Magnetic Levitation. *ACS Nano* **2021**, DOI: 10.1021/acsnano.1c04798.

[91] J. Brandrup, E. H. Immergut, E. A. Grulke, A. Abe, D. H. Bloch (Eds.), *Polymer Handbook 4th ed.*, of *Wiley: New York*, Wiley: New York, **1999**.

[92] J. N. Hay. Crystallization kinetics of high polymers: Isotactic polystyrene. *Journal of Polymer Science, Part A* **1965**, *3*, 433–447.

[93] G. Reiter. Mobility of Polymers in Films Thinner than Their Unperturbed Size. *Europhysics Letters* **1993**, *23*, 579–584.

[94] C. B. Roth. Polymers under nanoconfinement: Where are we now in under-

standing local property changes? *Chemical Society Reviews* **2021**, *50*, 8050–8066.

[95] M. Born, E. Wolf, *Principles of Optics*, Cambridge University Press, New York, **2006**.

[96] N. W. Ashcroft, N. D. Mermin, *Solid State Physics*, Saunders College Publishing, Philadelphia, **1976**.

[97] S. Y. Larsen, R. D. Mountain, R. Zwanzig. On the Validity of the Lorentz–Lorenz Equation Near the Critical Point. *The Journal of Chemical Physics* **1965**, *42*, 2187–2190.

[98] D. Beysens, P. Calmettes. Temperature dependence of the refractive indices of liquids: Deviation from the Lorentz–Lorenz formula. *Journal of Chemical Physics* **1977**, *66*, 766–771.

[99] C. Bollinne, V. W. Stone, V. Carlier, A. M. Jonas. Density Perturbations in Polymers Near a Solid Substrate: An X-ray Reflectivity Study. *Macromolecules* **1999**, *32*, 4719–4724.

[100] A. Beena Unni, K. Chat, K. Balin, K. Adrjanowicz. Connecting the density distribution and segmental dynamics of confined polymer films. *Nano-Structures & Nano-Objects* **2020**, *23*, 100519.

[101] A. van der Lee, L. Hamon, Y. Holl, Y. Grohens. Density Profiles in Thin PMMA Supported Films Investigated by X-ray Reflectometry. *Langmuir* **2001**, *17*, 7664–7669.

[102] E. Riande, R. Diaz-Calleja, M. Prolongo, R. Masegosa, C. Salom, *Polymer viscoelasticity: stress and strain in practice*, CRC Press, **1999**.

[103] J. D. Ferry, *Viscoelastic properties of polymers*, John Wiley & Sons, **1980**.

[104] M. Rubinstein, R. H. Colby, et al., *Polymer Physics*, *Vol. 23*, Oxford university press New York, **2003**.

[105] M. Doi, S. F. Edwards. Dynamics of concentrated polymer systems. Part 1.—Brownian motion in the equilibrium state. *Journal of the Chemical Society, Faraday Transactions 2: Molecular and Chemical Physics* **1978**, *74*, 1789–1801.

[106] P.-G. de Gennes. Reptation of a polymer chain in the presence of fixed obstacles. *The Journal of Chemical Physics* **1971**, *55*, 572–579.

[107] P. C. Hiemenz, T. P. Lodge, *Polymer Chemistry*, CRC press, **2007**.

[108] J. M. Torres, C. M. Stafford, B. D. Vogt. Elastic modulus of amorphous polymer thin films: relationship to the glass transition temperature. *ACS Nano* **2009**, *3*, 2677–2685.

[109] J. M. Torres, C. M. Stafford, B. D. Vogt. Impact of molecular mass on the elastic modulus of thin polystyrene films. *Polymer* **2010**, *51*, 4211–4217.

[110] C. A. Tweedie, G. Constantinides, K. E. Lehman, D. J. Brill, G. S. Blackman, K. J. Van Vliet. Enhanced stiffness of amorphous polymer surfaces under confinement of localized contact loads. *Advanced Materials* **2007**, *19*, 2540–2546.

[111] J. A. Forrest, A. C. Rowat, K. Dalnoki-Veress, J. R. Stevens, J. R. Dutcher. Brillouin light scattering studies of the mechanical properties of polystyrene/polyisoprene multilayered thin films. *Journal of Polymer Science Part B: Polymer Physics* **1996**, *34*, 3009–3016.

[112] L. Sun, J. R. Dutcher, L. Giovannini, F. Nizzoli, J. R. Stevens, J. L. Ord. Elastic and elasto-optic properties of thin films of poly (styrene) spin coated onto Si (001). *Journal of Applied Physics* **1994**, *75*, 7482–7488.

[113] W. Cheng, R. Sainidou, P. Burgardt, N. Stefanou, A. Kiyanova, M. Efremov, G. Fytas, P. F. Nealey. Elastic properties and glass transition of supported polymer thin films. *Macromolecules* **2007**, *40*, 7283–7290.

[114] P. A. O'Connell, J. Wang, T. A. Ishola, G. B. McKenna. Exceptional property changes in ultrathin films of polycarbonate: glass temperature, rubbery stiffening, and flow. *Macromolecules* **2012**, *45*, 2453–2459.

[115] T. B. Karim, G. B. McKenna. Unusual surface mechanical properties of poly (α-methylstyrene): Surface softening and stiffening at different temperatures. *Macromolecules* **2012**, *45*, 9697–9706.

[116] T. B. Karim, G. B. McKenna. Comparison of surface mechanical properties among linear and star polystyrenes: Surface softening and stiffening at different temperatures. *Polymer* **2013**, *54*, 5928–5935.

[117] Y. J. Gagnon, C. B. Roth. Local Glass Transition Temperature Tg (z) Within Polystyrene Is Strongly Impacted by the Modulus of the Neighboring PDMS Domain. *ACS Macro Letters* **2020**, *9*, 1625–1631.

[118] R. K. Bay, S. Shimomura, Y. Liu, M. Ilton, A. J. Crosby. Confinement effect on strain localizations in glassy polymer films. *Macromolecules* **2018**, *51*, 3647–3653.

Chapter 2

Experimental Methods

2.1 Synopsis

In this chapter, I will give a general introduction of two major experimental techniques that are used in the dissertation research, ellipsometry and fluorescence spectroscopy. Ellipsometry has been used to characterize the film thickness and refractive index of polymer thin films, where the refractive index is then used to infer changes in mass density. Besides, fluorescence spectroscopy has been used to monitor the changes in the emission spectrum of perylene, a temperature and pressure-sensitive fluorophore. Such changes induced by the polymer matrices surrounding the fluorophore can be informative of the local dynamics, as well as the stress or stiffness of the material.

2.2 Ellipsometry

2.2.1 Basics of ellipsometry and instrumentation

Ellipsometry is an optical technique that has been used to characterize surfaces and thin films in many fields. The core mechanism of ellipsometry is that it measures the changes in the polarization of light reflected off the sample.[1,2] The name of ellipsom-

etry is related to the fact that the polarization state of the light is often elliptically polarized.

The ellipsometer that is used is this study is a J.A, Woollam M-2000 spectroscopic ellipsometer. A schematic of this ellipsometer is shown in Figure 2.1, where the essential components are the light source, a polarizer, a rotating compensator the sample of interest, an analyzer and a detector. The light source used in this ellipsometer is a quartz tungsten halogen (QTH) bulb with wavelengths from 350 nm to 2000 nm, which covers the whole visible light range we are interested in (choice of wavelength range will be explained in Section 2.2.3). The fixed polarizer ($+45°$) is a linear polarizer than converts the unpolarized light generated by the light source into linear polarized light. The rotating compensator (sometimes also called a retarder) is a quarter waveplate that introduces a phase delay of $\delta = \pi/2$ between the perpendicular polarizations. It converts the linear polarized light into elliptically polarized light, unless the linear polarized light is at an angle of $45°$ to the fast-axis of the compensator which then results in circular polarized light. The elliptically polarized light shines on the sample of interest at an incident angle of θ. Upon reflection off the sample, the polarization state of the light changes depending on the sample's optical property. Then the reflected light is converted back into linear polarized light by the analyzer which is a fixed linear polarizer placed orthogonal to the polarizer ($-45°$). After the analyzer, the beam is spread onto the detector which is a charge-coupled device (CCD) array where the intensity of the beam is measured at hundreds of wavelengths simultaneously (193-1000 nm).

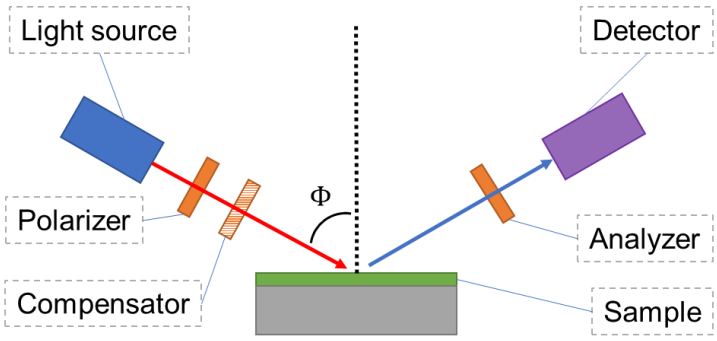

Figure 2.1: Schematic of a spectroscopic ellipsometer with rotating compensator. Unpolarized light is generated by the light source then polarized by the linear polarizer. The rotating compensator ($1/\lambda$ waveplate) converts the linear polarized light into elliptically polarized light. The polarization state of the light changes upon reflections with the sample at an incident angle of Φ. After the analyzer (linear polarizer orthogonal to the polarizer), the light is dispersed on to the detector (CCD array) for spectroscopic measurements.

2.2.2 Light reflection at interfaces

The change in polarization state upon reflection can be quantitatively described by the Fresnel equations.[1,2] We take the case of reflection off a planar surface that separates two semi-infinite media with different refractive indices as an example, as it is very similar to our thin film sample geometry. We assume that above the interface is air with a refractive index of 1, and the reflection of light takes place in this upper space. The lower space below the interface is the material of interest, where the refracted light does not reflect back because the lower space is semi-infinite. With respect to the plane of incidence (the plane that contains the normal line and the incident light beam), the polarization of the light can be classified into two linear polarized components, p- (parallel to the plane of incidence) and s- (perpendicular to the plane of incidence) polarized light. According to Fresnel equations, the amplitude reflection coefficients (Fresnel coefficients) describe the ratio of the magnitude of the electric field of the reflected light E_r to that of the incident light E_i. The Fresnel coefficients

of the p- and s-polarized light[2] are expressed by

$$r_{\mathrm{p}} \equiv \frac{E_{\mathrm{rp}}}{E_{\mathrm{ip}}} = \frac{n_2 \cos\theta_1 - n_1 \cos\theta_2}{n_2 \cos\theta_1 + n_1 \cos\theta_2} \tag{2.1}$$

$$t_{\mathrm{p}} \equiv \frac{E_{\mathrm{tp}}}{E_{\mathrm{ip}}} = \frac{2 n_1 \cos\theta_1}{n_2 \cos\theta_1 + n_1 \cos\theta_2} \tag{2.2}$$

$$r_{\mathrm{s}} \equiv \frac{E_{\mathrm{rs}}}{E_{\mathrm{is}}} = \frac{n_1 \cos\theta_1 - n_2 \cos\theta_2}{n_1 \cos\theta_1 + n_2 \cos\theta_2} \ . \tag{2.3}$$

$$t_{\mathrm{s}} \equiv \frac{E_{\mathrm{ts}}}{E_{\mathrm{is}}} = \frac{2 n_1 \cos\theta_1}{n_1 \cos\theta_1 + n_2 \cos\theta_2} \ . \tag{2.4}$$

In equation 2.1 to 2.4, n_1 and n_2 are refractive index of the air and the material, where θ_1 and θ_2 are angle of incidence and angle of refraction, respectively, which are relate by Snell's law.

As mentioned in Section 2.2.1, ellipsometry measures the changes in the polarization state of the light reflected off the sample, where in practice, the changes in polarization are expressed as the variations of light reflection with the p- and s-polarizations. The amplitude ratio and phase difference of the p- and s-polarizations can be described by a complex number ρ, which is the ratio of the Fresnel coefficients for p- and s-polarized light[1,2],

$$\rho \equiv \frac{r_{\mathrm{p}}}{r_{\mathrm{s}}} \equiv \tan\Psi \exp(i\Delta) \ . \tag{2.5}$$

Equation 2.5 is the fundamental equation of ellipsometry, where Ψ and Δ are the raw data measured by the ellipsometer that are fed into the optical layer model (Section 2.2.3) to determine the optical properties of the sample. In practice, when measured by spectroscopic ellipsometry (like the one used in this study), Ψ and Δ are often measured as a function of wavelength $(\Psi(\lambda), \Delta(\lambda))$.

2.2.3 Optical modeling of the sample

To interpret the raw $\Psi(\lambda)$ and $\Delta(\lambda)$ data measured by the ellipsometer, an optical layer model is required to describe the optical quantities of the sample. Specifically, for the polymer thin films in this study, the optical model usually has a multilayer structure, in correspondence to the nature of the multiple layers in the thin film sample (e.g. polymer film, native oxide layer & silicon substrate). Most polymers are transparent (extinction coefficient $k = 0$) in the wavelength range of visible light (400-1000 nm). Thus, the dispersion in refractive index of polymers can be well described by the Cauchy model,[1,2]

$$n = A + \frac{B}{\lambda^2} + \frac{C}{\lambda^4} + ... \quad k = 0 \ , \tag{2.6}$$

where n is the refractive index and A, B and C are called Cauchy parameters.

For a typical polymer film sample, the optical layer model consists of a Cauchy layer for the polymer film with a film thickness h, a layer for the native oxide layer that is naturally present on the surface of the silicon substrate, and a silicon substrate that is thick enough to neglect any back reflection. A schematic of the Cauchy layer model describing such a polymer sample is shown in Figure 2.2, where the ray diagram demonstrates the reflections and refractions occurring at multiple interfaces. The calculation of the Fresnel coefficients for the whole sample requires the consideration of Fresnel coefficients (Eqn. 2.1 to 2.4) at each of the interfaces, as well as the optical path inside each layer. According to Eqn. 2.5, simulated (Ψ,Δ) can be calculated from the Fresnel coefficients of the sample. To minimize the difference between the simulated and experimentally measured (Ψ,Δ), iterations of nonlinear fitting (Levenberg–Marquardt) are performed to find the best-fit values for the fitting parameters in the optical layer model (h, A, B and C).

For a common homogeneous film where the construction of optical layer model

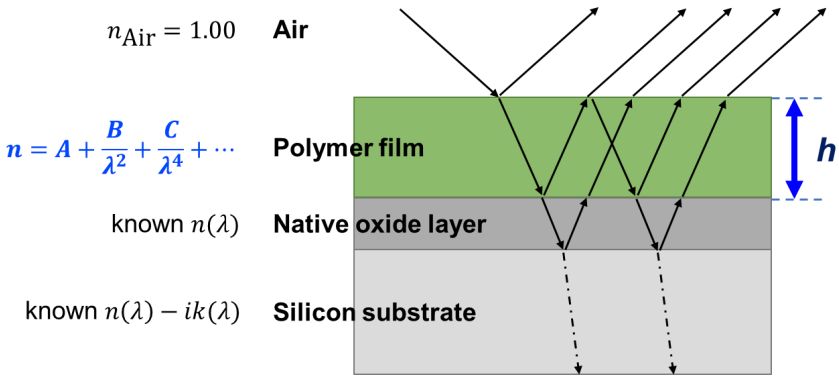

Figure 2.2: Schematic of a Cauchy layer model for a polymer film of film thickness h atop a silicon substrate. Ray diagram demonstrates the multiple reflections and refractions at various interfaces. The optical layer model consists a polymer film for which the dispersion is described by the Cauchy equation (Eqn. 2.6), a 1.25 nm thick native oxide layer and a semi-infinite silicon substrate.

only involves several layers, the explicit solution from the Fresnel coefficients can be easily calculated. However, for a film with a continuous gradient in refractive index where the refractive index of the material changes with depth into the film, calculations of the Fresnel coefficients can be nontrivial. The logistics of implementing a continuous gradient in refractive index within the optical layer model requires dividing up the polymer layer into a fixed number of discrete slices with successively different refractive indices, called grade layer method. Within each slice of the graded layer, the refractive index of the slice can be considered as isotropic given the thickness of the slice is sufficiently small.[2–5] In this case, the calculation of the Fresnel coefficients for a layer with a gradient in refractive index turns into a problem of how to calculate the Fresnel coefficients for a system of stratified layers. In this section, we will introduce the Hayfield and White 2×2 transfer matrix method[4,6] that is mathematically straightforward and works well for demonstration, while the more generalized Berreman 4×4 transfer matrix formalism[2,3,7] will be used to evaluate the gradient in refractive index in thin polymer films (Chapter 4).

If the stratified layers are viewed as a black box, as shown in Figure 2.3, the mag-

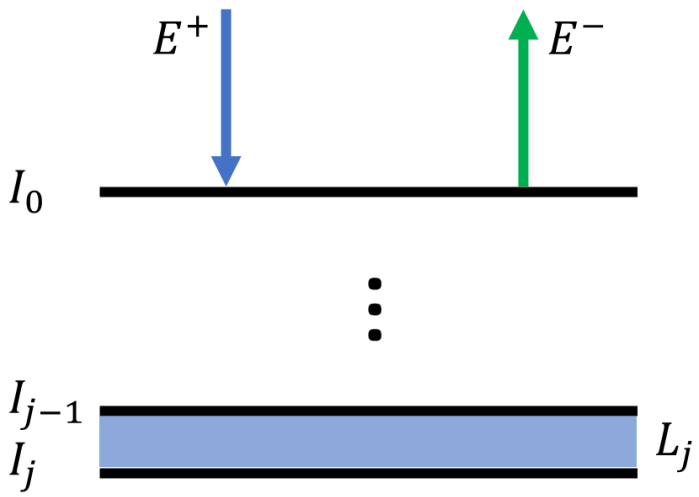

Figure 2.3: Schematic of transfer matrices in stratified layers. E^+ and E^- are the magnitude of the electric field for the incident and reflected light. I_j represents the transfer matrix of the j-th interface while L_j represents the transfer matrix of the j-th layer. I_0 is transfer matrix for the polymer-air interface on the incidence side.

nitude of the electric field of the incident (positive direction, "+") and reflected light (negative direction, "−") can be generalized as E^+ and E^-, respectively. According to Fresnel equations, the magnitude of the electric field changes at each interface and across each layer due to reflection and refraction, where each interface and each layer interior can be treated as optical elements that can be represented by transfer matrices.[4,6] The transfer matrices of the j-th interface I_j and the j-th layer L_j can be expresses by

$$I_j = \begin{pmatrix} 1/t_j & r_j/t_j \\ r_j/t_j & 1/t_j \end{pmatrix} , \tag{2.7}$$

$$L_j = \begin{pmatrix} e^{i\delta_j} & 0 \\ 0 & e^{-i\delta_j} \end{pmatrix} . \tag{2.8}$$

Here, r_j and t_j are the Fresnel reflection and transmission coefficients for polarized

light at the j-th interface, while δ_j is the phase lag across the j-th layer given by $\delta_j = \frac{2\pi n_j d}{\lambda} cos\phi$, with refractive index n_j, layer thickness d, wavelength of incident light λ and angle of incidence ϕ of the layer.

Changes in the incident and reflected electric field (E_j^+ and E_j^-) at the interfaces and across the layer are subject to the transfer matrices of the j-th interface I_j and the j-th layer L_j. For stratified layers with n layers, the collective transfer matrix of the stratified layers M is given by:

$$M = I_0 \prod_{j=1}^{n} L_j I_j, \tag{2.9}$$

where I_0 is the transfer matrix of the polymer-air interface. The magnitude of the electric field for the whole system (n layers) can then be expressed in matrix from as

$$\begin{pmatrix} E^+ \\ E^- \end{pmatrix} = \begin{pmatrix} M_{11} & M_{12} \\ M_{21} & M_{22} \end{pmatrix} \begin{pmatrix} E_n^+ \\ E_n^- \end{pmatrix} \ . \tag{2.10}$$

Since there is no reflection on the other end of the stratified layers, $E_n^- = 0$ and the magnitude of the electric field follows the simple reflection and transmission relation, $E^- = rE^+$ and $E_n^+ = tE^+$, the elements of matrix M can be written as

$$M_{11} = 1/t \ , \ M_{21} = r/t \ . \tag{2.11}$$

Therefore the reflection coefficients of the film can then be calculated as

$$r = \frac{M_{21}}{M_{11}} \tag{2.12}$$

for both p- and s- polarized light, leading to ellipsometric parameters Ψ and Δ.

2.3 Fluorescence

2.3.1 Basics of fluorescence

Fluorescence is a process involving the absorption and emission of a photon, inducing transitions between different electronic states.[8] The molecule that fluoresces is usually referred to as a fluorophore, where the fluorophore can be doped in the system (free molecule) or covalently attached to a component of the system (bonded molecule). Figure 2.4 shows the schematic of a Perrin-Jablonski diagram which demonstrates the transitions between electronic states of a fluorophore. Electrons of the molecule stay at the ground state (S_0) when not excited. Upon absorption of a photon, the electrons are promoted to electronic states with higher energy (S_1), which is referred to as the excited state. Depending on the energy of the photon being absorbed, the electrons will be distributed to different vibronic bands within S_1. This absorption process usually takes place on the time scale of 10^{-15} s. Then the vibrational relaxation of the fluorophore will dissiplate energy and bring the electrons in the vibronic bands with higher energy back to the lowest vibronic band of the excited state S_1, at a time scale of 10^{-12} - 10^{-10} s. From the lowest vibronic band of S_1, the electrons can return to the ground state via two kinds of transitions, nonradiative and radiative. Fluoresence is the radiative transition of an electron from the excited state S_1 to various vibronic bands in the ground state S_0, at a time scale of 10^{-10} - 10^{-7} s, which is the lifetime of the excited state S_1. In this process, a photon of corresponding energy is emitted (radiative) that is the fundamental signal of a fluorescence probe. In contrast, nonradiative transitions do not involve the emission of a photon. Instead, the excess energy between S_1 and S_0 is dissipated through intramolecular vibrations/rotations and intermolecular collisions, occurring at a time scale of 10^{-11} - 10^{-9} s.

For a given number of electrons in the excited state, the resulting fluorescence intensity is determined by the competition between radiative and nonradiative tran-

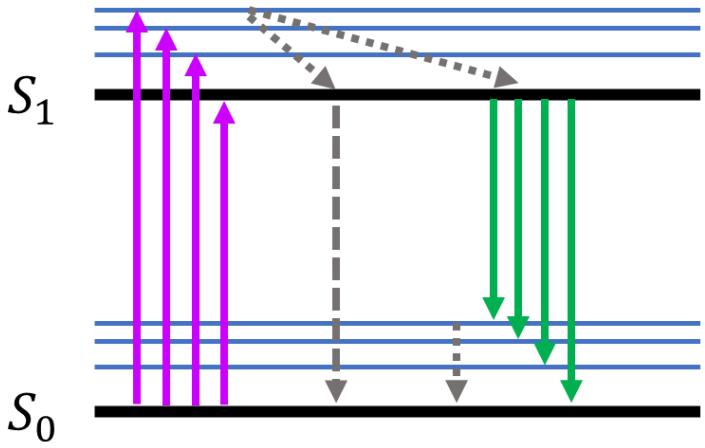

Figure 2.4: Schematic of Perrin-Jablonski diagram. S_0 is the ground state and S_1 is the excited state. Upon absorption of photons, electrons at S_0 are promoted to different vibronic bands in S_1 (purple solid arrow). Vibrational relaxation (gray dotted arrow) will bring electrons at higher energy vibronic bands to the one with the lowest vibronic bands. Fluorescence is the process of the electrons returning to different vibronic bands in S_0 from the lowest vibronic band in S_1 (green solid arrow). The electrons can also return to S_0 via nonradiative decay (gray dashed arrow) without the emission of photons.

sitions. The rate of nonradiative transitions is significantly influenced by the temperature of the environment since both the intramolecular vibrations/rotations and intermolecular collisions are more prevalent at higher temperature, which in turn diminishes the number of electrons that decay via the radiative transition (fluoroscence).

The shape of the fluorescence spectrum is one of the key features that has been used to analyze fluorescence signals. As mentioned before, the different energies of the emitted photons correspond to the different energy gaps between the S_1 state and the vibronic bands in the S_0 state. In practice, the emitted light forms a continuous spectrum as a function of wavelength with a few peaks, rather than several discrete wavelengths. The emission spectrum is measured when the excitation light is fixed at a certain wavelength while the emission intensity is monitored at different wavelengths. Similarly, the excitation spectrum can be obtained by fixing the emission wavelength and monitoring the emission intensity change as a function of excitation wavelength.

Even though the emission and excitation spectra are continuous, the location and the magnitude of the spectrum are still determined by the energy gaps and the probabilities of the corresponding electronic transitions. Given that the spacings between the vibronic bands in the excited state S_1 and the ground state S_0 are often similar, this will lead to similar energy gaps and probabilities of electronic transitions. Therefore, the magnitude and relative spacing of the peaks for the emission spectrum and the excitation spectrum are often symmetric to each other, which is known as the "Mirror image rule".[8]

2.3.2 Instrumentation of fluorescence

The experimental apparatus we used to characterize fluorescence spectra is a PTI QuantaMaster fluorescence spectrometer. A schematic of the fluorescence spectrometer is graphed in Figure 2.5, demonstrating the fundamental workflow of the instrument. The light source in the system is a xenon arc lamp which generates continuous light in the range of 240-1200 nm. A particular wavelength is selected by the excitation monochromator from this broadband of light, while in practice, the distribution of the light around the selected wavelength (bandpass) is adjusted by the width of the slit on the monochromator. A neutral density (ND) filter is placed at the outlet of the excitation monochromator to attenuate the intensity of the excitation beam because high excitation light intensity would result in severe photobleaching. The beam then goes through a beam splitter, where a portion of the excitation light is introduced into the reference cell (RCQC), which is a photodiode that monitors the real-time changes in the excitation light intensity to account for fluctuations in the intensity of the light generated by the light source.

The sample (polymer film) is usually prepared on fused silica via spincoating or water transfer technique. A transparent fused quartz cover is placed atop the film to limit oxygen quenching and sublimation of the fluorophore. The sample is enclosed

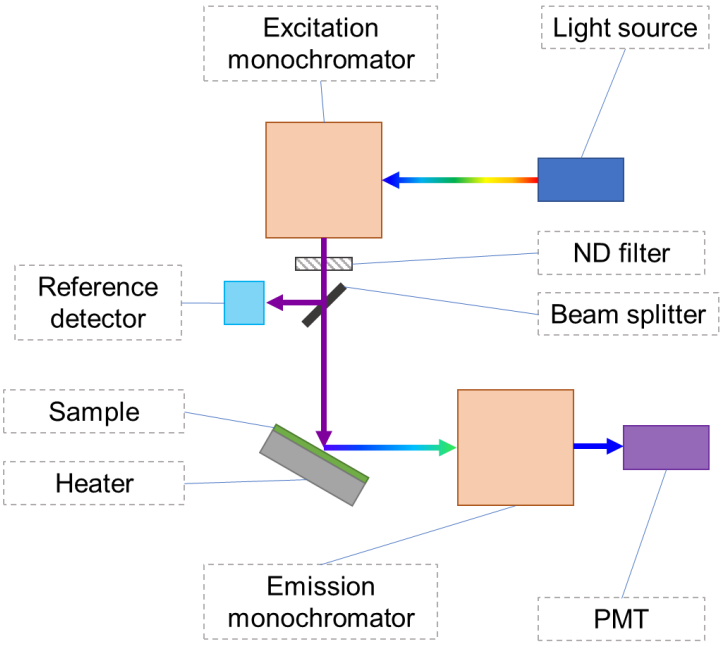

Figure 2.5: Schematic of the fluorescence spectrometer used. Broadband light is generated by the light source and then narrowed to the excitation wavelength by the excitation monochromator. The ND filter attenuates the intensity of the excitation light to reduce photobleaching. A portion of the excited light enters the reference detector via the beam splitter to account for the fluctuation in lamp intensity. The fluoresence signal of the sample upon excitation is selected by the emission monochromator and passed to the PMT detector.

in an Instec HCS402 heater to provide temperature control of the sample, where the sample is aligned off the 45° angle from the incident beam on purpose to prevent excitation light from being reflected into the detector. The fluorescence signal enters the emission monochromator that selects a particular wavelength of light of which the intensity is measured by the photomultiplier tube (PMT).

Bibliography

[1] H. G. Tompkins, *A User's Guide to Ellipsometry*, Academic Press, Inc., San Diego, CA, **1993**.

[2] H. Fujiwara, *Spectroscopic Ellipsometry: Principles and Applications*, John Wiley & Sons, Ltd., West Sussex, England, **2007**.

[3] M. Schubert, *Theory and Application of Generalized Ellipsometry* in *Handbook of Ellipsometry*, H. G. Tompkins, E. A. Irene (Eds.), William Andrew Publishing, Springer, Norwich, NY, **2005**, pp. 637 – 717.

[4] R. M. A. Azzam, N. M. Bashara, *Ellipsometry and Polarized Light*, Elsevier Science Publishers, Amsterdam, **1987**.

[5] F. Abelès, *Optical Properties of Inhomogeneous Films* in *Ellipsometry in the Measurement of Surfaces and Thin Films*, E. Passaglia, R. R. Stromberg, J. Kruger (Eds.), National Bureau of Standards Miscellaneous Publication 256, U.S. Government Printing Office, Washington, DC, **1964**, pp. 41 – 58.

[6] P. C. S. Hayfield, G. W. T. White, *An Assessment of the Suitability of the Drude-Tronstad Polarised Light Method for the Study of Film Growth on Polycrystalline Metals* in *Ellipsometry in the Measurement of Surfaces and Thin Films*, E. Passaglia, R. R. Stromberg, J. Kruger (Eds.), National Bureau of Standards Miscellaneous Publication 256, U.S. Government Printing Office, Washington, DC, **1964**, pp. 157 – 199.

[7] D. W. Berreman. Optics in Stratified and Anisotropic Media: 4×4-Matrix Formulation. *Journal of the Optical Society of America* **1972**, *62*, 502.

[8] B. Valeur, M. N. Berberan-Santos, *Molecular fluorescence: principles and applications*, John Wiley & Sons, **2012**.

Chapter 3

Comparing Refractive Index and Density Changes with Decreasing Film Thickness in Thin Supported Films Across Different Polymers

A version of this chapter was published as Yixuan Han, Xinru Huang, Alan C. W. Rohrbach, and Connie B. Roth, *The Journal of Chemical Physics*, 153, 044902 (2020).

3.1 Introduction

To better understand the underlying phenomena associated with changes to the glass transition in thin films and other confined geometries, efforts to measure and correlate these effects to other property changes are highly valued. In this vein, characterizing changes to the material density in thin polymer films with decreasing film thickness has drawn interest over the years, especially given that even tiny changes (<1 %) in density can have a strong impact on dynamics.[1–5] Experimental techniques such as

neutron reflectivity (NR),[6,7] x-ray reflectivity (XRR),[8–11] and ellipsometry[10–14] have typically been used to measure material density in thin films, while other techniques such as Brillouin light scattering (BLS)[15] have been used to characterize other film properties related to mass density. Early efforts from the late 1990s by Wallace et al.[7] (NR) and Forrest et al.[15] (BLS) demonstrated no change to the mass density of thin polystyrene (PS) films down to film thicknesses of 6 nm within an experimental error of ±1 %. In contrast, several recent studies have claimed enormous increases (∼25 %) in the mass density of PS films with decreasing film thickness below ∼30 nm–40 nm based on results from XRR, ellipsometry, and other methods.[10,11,14] However, such large increases in mass density are physically unrealistic given that the crystalline state of PS is only ∼5 %–8 % denser than amorphous PS.[16,17]

Experimental measurements of mass density in thin films are challenging because the amount of material present providing the measurement signal is very small, frequently confronting the sensitivity limits of the technique. In addition, the analysis and interpretation of the results usually require some appropriate model to fit the data that is often based on inherent assumptions, which may break down in the thin film limit.[12] For example, x-ray and neutron reflectivity, as well as ellipsometry, typically rely on the selection of an appropriate layer model to fit and analyze the raw data, where common equations with their own intrinsic assumptions are routinely used to treat the various layers.[7–11,14,18,19] In these models, the polymer film is usually treated as a simple homogeneous layer.[7,10,11,13,14,18] Finally, to convert the measured quantity such as refractive index or electron density to mass density, additional equations such as the common Lorentz-Lorenz relation are frequently used.[10,11,14] The observation, by so many different experimental techniques of a physically unrealistic large apparent increase in the material density of polymer films with decreasing thickness suggests that some other property of the film is changing, which makes the standard analysis followed by these methods unreliable.

A recent study by our group addressed some of these issues by examining in detail the use of ellipsometry to characterize density changes in thin PS films based on the measurements of the refractive index.[12] Temperature-dependent measurements of the refractive index $n(T)$ were done on thin PS ($M_w = 650$ kg/mol, $M_w/M_n = 1.06$) films supported on silicon to quantify shifts in the liquid $n(T = T_g^{bulk} + 15\ K)$ and glassy $n(T = T_g^{bulk} - 45\ K)$ state quantities with decreasing film thickness h. The common Lorentz-Lorenz relation was then used to infer changes in the specific volume v_{sp} (inverse of density) of the material as it relates the macroscopic (continuum) quantity refractive index n to the microscopic polarizability of the material.[20,21] An examination of the ellipsometry layer model fitting concluded that the measured refractive index values $n(h)$ were robust for film thicknesses $h \geq 20$ nm, while thinner films with $h \approx 10$ nm suffered from fitting limitations due to ellipsometry's inherent difficulty to independently resolve h and n from the measured optical thickness.[12] (Because of this, in the present study, we only discuss $n(h)$ values for $h \geq 20$ nm.) The validity of the Lorentz-Lorenz relation for use in thin films was also considered by evaluating the inherent assumptions of isotropic uniform polarizability in its derivation.[12]

For film thicknesses $h \geq 20$ nm where the measurements were believed to be robust, small non-monotonic shifts in refractive index $n(h)$ and specific volume $v_{sp}(h)$ with decreasing film thickness were reported.[12] The small increase in $v_{sp} = 0.4 \pm 0.2$ % (decrease in density) from $h \approx 120$ nm to 65 nm was attributed to the predicted film expansion by White and Lipson's thermodynamic model,[22] associated with a reduction in attractive energy between polymer segments from the missing interactions at the free surface. For film thickness $h < 65$ nm, where reductions in the glass transition temperature $T_g(h)$ of PS begin to occur, a decrease in v_{sp} (increase in density) was found.[12] This observation is consistent with other reports in the literature, indicating that dynamical perturbations due to interface effects in thin films are uncorrelated with density changes.[23–25] For film thicknesses below ~30 nm–40

nm, a large apparent increase in density was seen as the measured refractive index $n(h)$ appeared to increase dramatically,[12] consistent with the recent reports of large density increases.[10,11,13,14] Huang and Roth speculated that these unrealistically large apparent increases in $n(h)$ and density may result from a loss of uniform polarizability within the thin films, invalidating the standard analysis methods used to extract these quantities.[12] Interestingly, the same shifts in $n(h)$ were observed for both the liquid and glassy regimes, indicating that the behavior was present even in the equilibrium liquid state.

In the present work, we test these previous interpretations by comparing the thickness-dependent refractive index trends $n(h)$ for three different polymers and assess the impact of molecular weight, polydispersity, chain conformation, and surface chemistry treatment. A subsequent study by White and Lipson[26] has suggested that the presence of attractive substrate interactions with the polymer can cause film contraction counteracting the film expansion effects of the free surface, predicting opposing trends in specific volume (density) with decreasing film thickness. We aim to test this prediction by comparing the $n(h)$ trends of poly(2-vinyl pyridine) (P2VP) and poly(methyl methacrylate) (PMMA), which have attractive polymer–silica substrate interactions[27–33] with those of PS, which has a neutral polymer–silica substrate interaction.[34–36] Following the method of our previous work,[12] we use ellipsometry to measure the temperature dependence of the refractive index $n(T)$ for films of different thicknesses supported on silicon wafers with native oxide layers (silica interface interactions), and examine the thickness dependent changes in the liquid $n(T = T_g^{bulk} + 15\ K)$ and glassy $n(T = T_g^{bulk} - 45\ K)$ regimes. We also evaluate possible sources of non-uniform polarizability within thin films caused by confinement of the polymer chains and surface orientation of molecular dipole units.

3.2 Experimental methods

Polystyrene (PS) with molecular weights $M_w = 650$ kg/mol, $M_w/M_n = 1.06$ from Pressure Chemical, $M_w = 245$ kg/mol, $M_w/M_n = 2.0$ from Sigma Aldrich, and $M_w = 48$ kg/mol, $M_w/M_n = 1.01$ from Scientific Polymer Products, were used as received. PS $M_w = 650$ kg/mol data from our previous study Ref. 12 are also graphed. Poly(methyl methacrylate) (PMMA) with $M_w = 815$ kg/mol, $M_w/M_n = 1.09$ from Scientific Polymer Products, and poly(2-vinyl pyridine) (P2VP) with $M_w = 650$ kg/mol, $M_w/M_n = 1.08$ from Scientific Polymer Products, and $M_w = 643$ kg/mol, $M_w/M_n = 1.18$ from Polymer Source, were also obtained. The P2VP from Scientific Polymer Products was dried under vacuum for 24 h at 110 °C to remove any residual monomer.[30] Polymer films were made by spin-coating solutions of PS or PMMA dissolved in toluene, or P2VP dissolved in butanol, onto 2 cm × 2 cm silicon wafers (Wafernet) with 1.25 nm thick native oxide layers.[12] Films of different thicknesses were obtained by varying the solution concentration (0.5 wt%-5.0 wt%) and spin-speed (1000-3000 rpm). All films were annealed at T_g^{bulk} + 20 K under vacuum for 12 h to remove any residual solvent and facilitate chain relaxation. Stacked bilayer films of $M_w = 650$ kg/mol PS were fabricated by floating a second 35 nm thick film from mica onto a 35 nm thick film on silicon, where both layers were first separately annealed under vacuum at 120 °C for 12 h prior to floating. The assembled bilayers were then annealed either for 10 min at 120 °C (corresponding to $\sim 1/10$ the reptation time τ_d) or 40 min at 150 °C (corresponding to $\sim 50\ \tau_d$).

Temperature-dependent film thicknesses $h(T)$ and index of refraction $n(T)$ data were measured using spectroscopic ellipsometry (Woollam M-2000) at an angle of incidence of 65° for samples cooled at 1 °C/min after being equilibrated at T_g^{bulk} + 45 K for 20 min on the ellipsometer hotstage (Instec HSC 302) to remove thermal history. Raw $\Psi(\lambda)$ and $\Delta(\lambda)$ data for $\lambda = 400$ nm-1000 nm were fit to an optical

layer model consisting of a transparent Cauchy layer,

$$n(\lambda) = A + \frac{B}{\lambda^2} + \frac{C}{\lambda^4}, \tag{3.1}$$

for the polymer and a 1.25 nm native oxide layer atop a semi-infinite silicon substrate. Following our previous work,[12] the Cauchy C parameter was held fixed at the bulk value, resulting in three fitting parameters for each film: h, A, and B. The refractive index parameters for the silicon substrate and the thin native oxide layer were taken from the literature as part of the Woollam analysis software.[37] Based on a multi-wavelength analysis of multiple silicon wafers performed by Woollam, the refractive index of the native silicon oxide layer is modeled using the Sellmeier equation

$$n_{\mathrm{SiOx}}(\lambda) = \left[\epsilon(\infty) + \frac{A\lambda^2}{\lambda^2 - B^2} - E\lambda^2\right]^{1/2}, \tag{3.2}$$

with parameter values $\epsilon(\infty) = 2.374$ for the index offset, $A = 0.6152$ for the amplitude, $B = 0.115$ μm for the center energy, and $E = 0.01059$ $\mu\mathrm{m}^{-2}$ for the position of the pole in the infrared. This $n_{\mathrm{SiOx}}(\lambda)$ parameterization produces extremely good fits to the native oxide layer of the silicon substrates we use. We have verified that the $n(h)$ trends for the polymer films we report are robust to alternative parameterizations of the native oxide layer with any reasonable h_{SiOx} and n_{SiOx} values that model the silicon substrates well. Our previous study also verified that the polymer film thickness h and refractive index $n(\lambda)$ parameters obtained from fitting the $\Psi(\lambda)$ and $\Delta(\lambda)$ data to this three layer optical model were robust to reasonable selections of the wavelength range and Cauchy C parameter used.[12] The mean squared error (MSE) function minimized by the Woollam software,[38,39] which functions as a χ^2 parameter, produced well-defined minima for film thicknesses h greater than ≈ 10 nm. Only for the thinnest films of $h = 10$ and 13 nm did the MSE minimum become poorly defined, especially for the B Cauchy parameter, making the refractive index values for $h \lesssim 15$

nm, which were anomalously large, suspect. Therefore, such thin films were excluded from the discussion of thickness-dependent refractive index $n(h)$ shifts, as they are in the present work. Bulk values of the glass transition temperature T_g^{bulk} were determined from ellipsometry measurements of thick films (average of measurements for films typically > 400 nm) on cooling at 1 °C/min with T_g identified as the intersection of linear fits to the liquid and glassy regimes of the temperature-dependent film thickness $h(T)$ data: $T_g^{bulk} = 96$ °C for 650 kg/mol PS, $T_g^{bulk} = 98$ °C for 245 kg/mol PS, $T_g^{bulk} = 95$ °C for 48 kg/mol PS, $T_g^{bulk} = 115$ °C for 815 kg/mol PMMA, and $T_g^{bulk} = 94$ °C for both the 650 kg/mol P2VP and 643 kg/mol P2VP.

Phenyl-capped silicon substrates were prepared by modifying the surface chemistry of the silicon substrates following the procedure outlined in Ref. 40. Chloro(dimethyl)phenylsilane (Sigma Aldrich, 98%) was spin-coated onto silicon precleaned with 10 vol.% hydrochloric acid (HCl) and rinsed with filtered deionized water.[41] The substrates were then annealed at 80 °C under vacuum for 5 h to covalently bond the phenylsilane to the hydroxyl groups on the surface. Any remaining unreacted chloro(dimethyl)phenylsilane was rinsed away with toluene and filtered deionized water. Water contact angle measurements showed that the phenyl-capped surfaces were more hydrophobic with a contact angle of $\approx 45°$, indicating a surface coverage of ≈ 25 % phenyl rings,[42] compared to the $\approx 0°$ contact angle for the native SiO_x/Si substrates. PS films were then spin-coated atop the phenyl-capped substrates and annealed at 120 °C under vacuum for 12 h to match the preparation procedure of other samples made on silicon with native oxide layers.

3.3 Results and discussion

3.3.1 Comparing refractive index trends in thin films of P2VP, PMMA, and PS

Our group's previous work investigating shifts in the refractive index n for PS films with decreasing film thickness h observed non-monotonic changes below $h \leq 130$ nm, including a large distinctive increase in index for very thin films.[12] These shifts in refractive index n were interpreted through the Lorentz-Lorenz equation,[20,21]

$$L = \frac{n^2 - 1}{n^2 + 2} = \frac{\alpha N_A}{3\epsilon_0 M_0}\rho, \tag{3.3}$$

where the Lorentz parameter L is directly proportional to the mass density ρ of the material via the constants: Avogadro's number N_A, the permittivity of free space ϵ_0, the monomer molecular weight M_0, and the molecular polarizability α. The work was initially motivated by a theoretical study from White and Lipson[22] that predicted increases in specific volume $\sim$0.5 % for thin free-standing PS films associated with missing contacts at the free surface, which was suggested to be correlated with the reductions in average glass transition temperature $T_g(h)$ seen experimentally. Thus, in our study we used the Lorentz-Lorenz relation to define an effective specific volume $v_{sp} \equiv 1/L$, where the shifts in refractive index n with decreasing film thickness were interpreted as an increase in v_{sp} (decrease in density) of 0.4$\pm$0.2 % from $h \approx 120$ to 65 nm, followed by a strong v_{sp} decrease (increase in density) below 65 nm. Given that the v_{sp} increase was comparable in magnitude, we associated it with the film expansion prediction by White and Lipson.[22] However, experimentally, this film expansion occurred at film thicknesses larger than where any changes to $T_g(h)$ are observed. In fact, where the $T_g(h)$ decrease begins at $h \approx 65$ nm, is where we observed the start of the large and precipitous decrease in v_{sp} (increase in density), suggesting that density

and dynamics are not simply correlated.

This large increase in refractive index n with decreasing film thickness, giving a large apparent increase in density, is consistent with other literature reports.[10,11,13,14] However, because of the unphysical nature of the observation, we assessed other possible causes, concluding[12] that limitations in obtaining unambiguous fits to ellipsometric layer models was a concern for $h \lesssim 15$ nm because of the inherent difficulty of the technique at independently resolving h and n for very thin films.[43,44] We also assessed the validity of applying the Lorentz-Lorenz equation to very thin films given the underlying assumptions in its derivation, determining that the requirement for isotropic uniform polarization of the material would likely limit its applicability as film thicknesses approached ≈ 20 nm.[12] Thus, we attributed the large apparent increase in film density to possible deviations from uniform polarizability in very thin films.[12] We note that our previous study also addressed concerns that the observed behavior was simply resulting from poor optical contrast between the polymer film and native oxide layer of the underlying silicon by demonstrating that the same shifts in refractive index $n(h)$ and $v_{sp}(h)$ were obtained when the PS films were placed on aluminum oxide (AlO_x) coated silicon wafers.[12]

In the present work, we revisit and test these conclusions by comparing similar measurements of refractive index n shifts with decreasing film thickness h across three different polymers: P2VP and PMMA, with PS from our previous study,[12] as well as additional measurements of PS with different molecular weights. Follow-up work by White and Lipson has since adapted their theoretical model to account for attractive interactions between the polymer and underlying substrate, proposing that such attractive interactions could counter the film expansion induced by the free surface.[26] Specifically their model introduced a parameter to describe the strength of interfacial interaction with the substrate, where significant attractive interactions could overcome the film expansion induced by the free surface resulting in v_{sp} shifts

in the opposite direction than those predicted for PS with a neutral silica interface interaction. Both P2VP and PMMA have been reported as having attractive interactions with silica substrates[27–33] making them an ideal choice for comparison. To limit the amount of data processing and inherent assumptions we apply to the measured values, in the present work we focus our comparisons on the trends in refractive index n themselves, without inferring density changes through the Lorentz-Lorenz relation.

Figure 3.1(a) graphs the temperature-dependent refractive index $n(T)$ of P2VP (650 kg/mol) films for a number of different film thicknesses. Data were collected by ellipsometry on cooling at 1 °C/min where the raw $\Psi(\lambda)$ and $\Delta(\lambda)$ data for $\lambda = 400 - 1000$ nm were fit to a standard Cauchy model for the polymer layer atop silicon substrates with an SiO_x native oxide layer. Although the full wavelength-dependent refractive index $n(\lambda)$ of the polymer is fit (see eq. 3.1), for the purposes of graphing we plot the $n(\lambda)$ data evaluated at $\lambda = 632.8$ nm, corresponding to the HeNe laser wavelength. $n(T)$ data for bulk films ($h = 359$ and 713 nm) overlap, but thinner films show vertical shifts, where a slight decrease in n is observed for intermediate film thicknesses ($h \approx 85$ nm) followed by more a pronounced increase for thinner films ($h \lesssim 60$ nm). The $n(T)$ curves primarily exhibit simple vertical shifts for different film thicknesses with little change in the shape of the curve, meaning both the liquid and glassy regimes are affected in a similar manner. These vertical shifts in the $n(T)$ curves are extremely reproducible with multiple samples consistently showing the same small shifts. This behavior exhibited by P2VP appears identical to what we previously observed for PS films in Ref. 12.

To more explicitly examine the thickness dependence of these shifts in refractive index, we focus on values at representative temperatures corresponding to the liquid $n(T = 110\ °C)$ and glassy $n(T = 50\ °C)$ regimes, evaluated based on an average of the data at $T \pm 2\ °C$ around these values. Figure 3.1(b) plots the $n(T)$ values as a function of film thickness h for two different P2VP molecular weights ($M_w =$

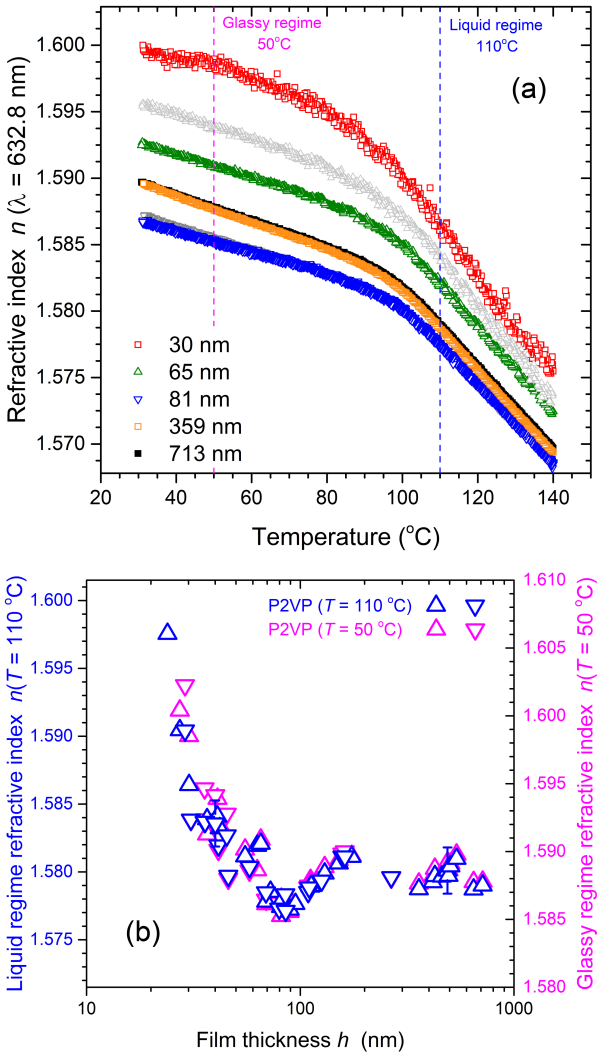

Figure 3.1: (a) Temperature dependence of refractive index $n(T)$ for P2VP (650 kg/mol) films measured on cooling at 1 °C/min for different film thicknesses: 713 nm (solid black squares), 359 nm (open orange squares), 81 nm (blue downward triangles), 65 nm (green upward triangles), 30 nm (red squares). Also shown in gray are data for 89 nm (downward triangles) and 41 nm (upward triangles) films to demonstrate reproducibility and consistency in $n(T)$ shifts. (b) Film thickness dependence of the refractive index showing the same shifts in the liquid regime at $n(T = 110\ °C)$ (blue) and glassy regime at $n(T = 50\ °C)$ (magenta) for P2VP films: 650 kg/mol from Scientific Polymer Products (upward pointing triangles) and 643 kg/mol from Polymer Source (downward pointing triangles). Representative error bars are included corresponding to two standard deviations ($\approx 95\%$ confidence interval) of the sample-to-sample variability for film thicknesses $h \geq 130$ nm.

650 kg/mol from Scientific Polymer Products and 643 kg/mol from Polymer Source).

The refractive index values for the liquid and glassy regimes have been overlaid by

aligning the average value for thick films ($h > 300$ nm). The error associated with the repeated measurement of a single film is only ± 0.0005 and has been represented by the size of the symbols. The scatter in the data demonstrates the sample-to-sample variability, where we have marked the span of the bulk data by plotting representative error bars. These error bars of ± 0.0017 for the P2VP data correspond to twice the standard deviation ($\approx 95\%$ confidence interval) for the data with $h \geq 130$ nm. The one in the bulk regime has been placed on a datapoint coinciding with the average value. With decreasing film thickness, the refractive index $n(h)$ data begin having small deviations from bulk for thickness $h \lesssim 100$ nm, exhibiting a slight minimum at $h \approx 85$ nm followed by a sharp increase in refractive index well above the bulk value for the thinnest films $h \lesssim 50$ nm.

In Figure 3.1(b), the vertical span of the y-axes for both the liquid and glassy regimes are identical to easily confirm that the refractive index shifts with film thickness are the same in both the liquid and glassy state. Thus, this effect is not the result of some non-equilibrium glassy behavior, but occurs even in the equilibrium liquid state. For the remainder of this study we graph only the liquid state values for clarity in making comparisons between different polymers, but we emphasize that the same index shifts are observed in the glassy regime, as was already demonstrated for PS in Ref. 12.

Identical measurements were collected for PMMA (815 kg/mol) films, where the refractive index of the liquid and glassy regimes were sampled at equivalent temperatures above ($T = T_{\mathrm{g}}^{\mathrm{bulk}} + 15$ K) and below ($T = T_{\mathrm{g}}^{\mathrm{bulk}} - 45$ K) the bulk glass transition temperature. Figure 3.2 plots the liquid regime refractive index $n(T = T_{\mathrm{g}}^{\mathrm{bulk}} + 15$ K) as a function of film thickness h for PMMA ($M_{\mathrm{w}} = 815$ kg/mol), P2VP ($M_{\mathrm{w}} =$ 650 kg/mol and 643 kg/mol), and PS ($M_{\mathrm{w}} = 650$ kg/mol) films. Again, the size of the symbols represent the error of a single measurement, while the sample-to-sample variability in the bulk data ($h \geq 130$ nm) are indicated by representative error bars

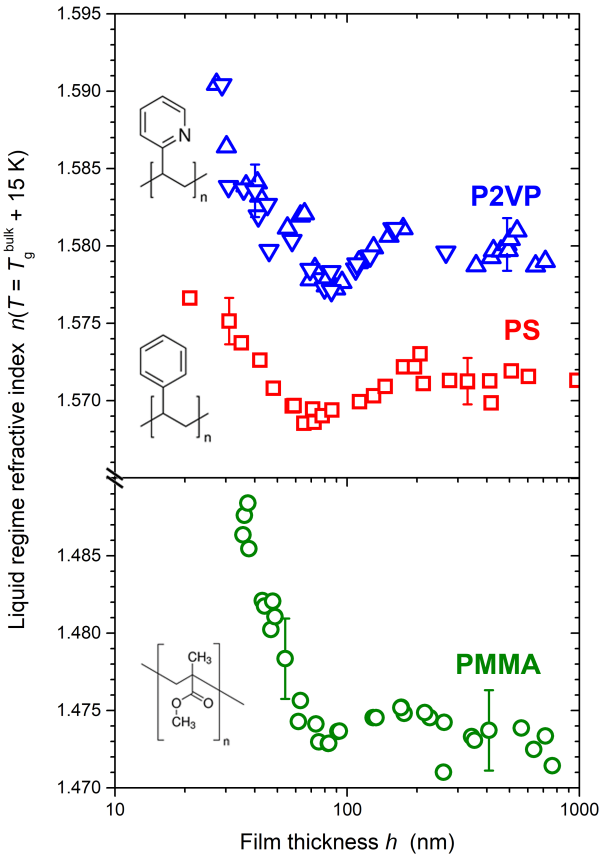

Figure 3.2: Refractive index in the liquid regime at $T = 110$ °C for P2VP ($M_w = 650$ kg/mol data, blue upward pointing triangles; $M_w = 643$ kg/mol data, blue downward pointing triangles) and PS ($M_w = 650$ kg/mol data from Ref. 12, red squares), and at $T = 130$ °C for PMMA ($M_w = 815$ kg/mol, green circles) as a function of film thickness h, all showing similar behavior in both length scale and magnitude. Representative error bars (two standard deviations) identify the sample-to-sample variability for film thicknesses $h \geq 130$ nm. Inset: Chemical structures for the three polymers.

corresponding to two standard deviations (± 0.0015 for PS and ± 0.0026 for PMMA). A second representative error bar is included in the thin film regime for each data set indicating where the $n(h)$ values increase outside of this two standard deviations. All three polymers exhibit similar trends in $n(h)$ with minor deviations from bulk occurring for $h \lesssim 100$ nm, followed by a large distinctive increase in refractive index for the thinnest films. Given the range of variability in the bulk films ($h \geq 130$ nm), we focus only on the increase in $n(h)$ values that occur for thin films. There are small

differences in the film thickness at which this large increase in $n(h)$ begins for the three different polymers: below $h \approx 50$ nm for P2VP, $h \approx 40$ nm for PS, and $h \approx 65$ nm for PMMA.

The fact that all three polymers exhibit nearly the same trends in $n(h)$ despite P2VP and PMMA having attractive substrate interactions with the underlying SiO_x/Si substrate interface,[27–33] while PS does not,[34–36] invalidates the hypothesis made in our earlier work[12] that the slight increase in v_{sp} (decrease in refractive index) between $h \approx 120$ to 65 nm for PS films was due to the film expansion prediction by the White and Lipson model[22,26] as P2VP and PMMA would be expected to exhibit opposite shifts to PS. Remarkably both P2VP and PS are extremely similar in their behavior with PMMA exhibiting slight differences. Inset in Fig. 3.2 we show the chemical structures for the three polymers and note that both P2VP and PS have similar ring-type structures, while the PMMA monomer size is smaller and more flexible. In the next section we consider whether these factors play a role in the observed $n(h)$ behavior.

We note that Beena Unni et al.[14] recently compared changes in refractive index with decreasing film thickness for PMMA and PS, observing a decrease in $n(h)$ for PMMA with decreasing film thickness. Their ellipsometry measurements were done by holding the film thickness fixed at a value measured by XRR, and then fitting $n(\lambda)$ from $\lambda = 288 - 1700$ nm using the Sellmeier dispersion relation. We have been unable to reproduce their $n(h)$ trend for PMMA by following a similar analysis method using our own data. It is worth recognizing that all these thin film methods (XRR and ellipsometry) inherently assume a uniform homogeneous layer for the polymer film, which we believe is the likely underlying cause for the large, unphysical apparent changes in film properties observed by a range of different methods. This is also true for the nanoparticle adsorption measurement put forward by Beena Unni et al.[14] that infers refractive index changes from van der Waals attractions assuming a constant

and uniform Hamaker constant for the polymer film. Green et al.[13] similarly inferred refractive index trends from contact angle measurements using a spreading coefficient based on a uniform Hamaker constant for the underlying polymer film. All these methods suffer from the same inherent assumption of a uniform and homogeneous layer for the polymer film.

3.3.2 Large apparent increase in refractive index: Testing sources of film inhomogeneities

We consider now possible sources for the refractive index shifts with decreasing film thickness $n(h)$ given that a similar behavior is observed for all three polymers. In Figure 3.3 we examine more closely the similarities and differences in $n(h)$ between the polymers by shifting the P2VP and PMMA data sets vertically [$n(h) - 0.0086$ for P2VP and $n(h) + 0.0980$ for PMMA] to overlap the bulk values with that for PS. Graphed in this manner, we can clearly observe that the magnitude of the large increase in $n(h)$ for thin films below $h \approx 40 - 65$ nm is comparable for all three polymers, with the effect being most pronounced in PMMA.

Our previous work[12] speculated that this large increase in refractive index with decreasing film thickness, which can be interpreted as an apparent increase in film density that becomes unphysical in magnitude for very thin films, could result from a loss of uniform isotropic polarizability within the polymer film. Such inhomogeneities in film properties would be incompatible with inherent assumptions in how data analysis is typically done. Ellipsometry layer model fitting to convert experimentally measured $\Psi(\lambda)$ and $\Delta(\lambda)$ data to film thickness h and refractive index $n(\lambda)$ utilizes a homogeneous Cauchy layer equation (eq. 3.1) to model the wavelength dependence of the refractive index of the polymer layer. Inherent in the use of this equation is the assumption that the polymer film is uniform, isotropic and transparent. Use of this Cauchy equation is extremely common and gives excellent fits to the data,

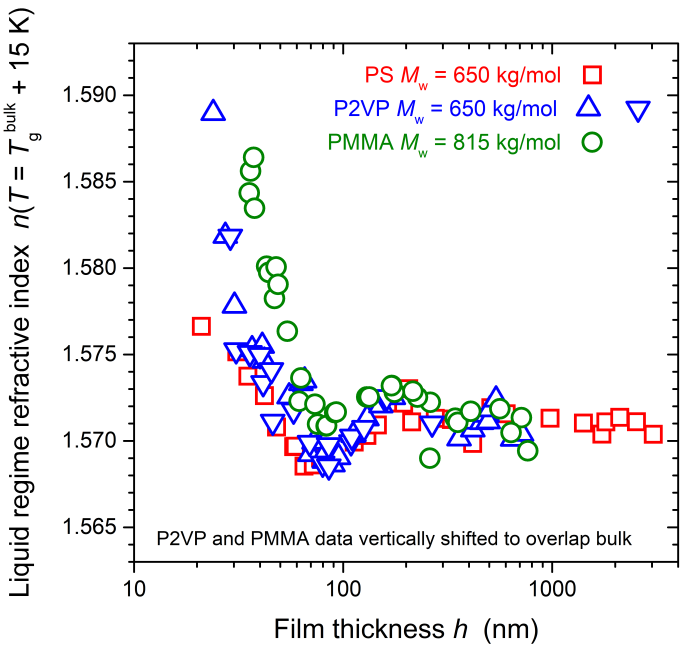

Figure 3.3: Comparison of film thickness trends in the liquid regime refractive index $n(T = T_g^{\text{bulk}} + 15 \text{ K})$ of PS, P2VP, and PMMA, where the data in Fig. 3.2 have been vertically shifted ($n_{\text{P2VP}} - 0.0086$ and $n_{\text{PMMA}} + 0.0980$) to overlap with that of PS. P2VP and PS $n(h)$ data appear to collapse on top of each other, while the $n(h)$ PMMA data exhibits a sharper upward trend starting at a larger film thickness.

routinely resulting in mean squared error (MSE) values between 1-2,[12] including for the data sets in the present study. However, such layer model fits to samples are not unique; nor does a good fit imply that the correct model is being used. Perhaps one of the first indications that a given layer model may not be quite correct is when fit parameters become unrealistic. This type of data analysis where measurement values are interpreted by fitting to a layer model representation of the sample geometry is commonly used to analyze data from ellipsometry, as well as X-ray and neutron reflectivity measurements.[7–11,14,18,19] Perhaps this is why results from different experimental techniques can all yield similar unphysical results.[10,11,14]

Without knowing more specifics about how film properties are altered in thin films, we are left to speculate what changes may be occurring with decreasing film thickness that could account for the behavior and possibly allow us to formulate a more accurate layer model. For example, one possibility is that film properties are

becoming anisotropic as the polymer chains are confined to a smaller film thickness in the perpendicular direction. We have tried fitting the $\Psi(\lambda)$ and $\Delta(\lambda)$ data to an anisotropic layer model that utilizes different Cauchy parameters parallel and perpendicular to the plane of the film. However, this introduces additional fitting parameters and the resulting fits are no better than the already excellent fits obtained with a simple uniform Cauchy model with no anisotropy. In general, small amounts of film anisotropy are challenging to reliably characterize for film thicknesses $h < 100$ nm because as the optical path length of the light through the film decreases, most of the change in polarization that the ellipsometer measures will come from the reflection at the interfaces. Thus, by simply comparing fit quality for different layer models, we cannot conclusively identify or eliminate the presence of film anisotropy or other orientational difference in film properties.

Instead, we proceed by taking a more experimental approach to test and identify possible sources of film inhomogeneities responsible for the observed $n(h)$ trends. If we return to Fig. 3.3 and examine more closely the similarities and differences between the three different polymers, we see that the smaller shifts or undulations in $n(h)$ in the intermediate thickness range (40-65 $< h <$ 200 nm) are nearly identical for PS and P2VP, whereas in this region the $n(h)$ data are flatter for PMMA. Given the chemical structures of the three polymers, we speculate that the rigid ring-type side group of PS and P2VP that forms the dominant molecular dipole in the system could be undergoing slight orientational ordering leading to nonuniformities in film polarization that vary with film thickness. As the molecular dipoles on the side group of PMMA are more flexible, perhaps this effect is more muted at these intermediate thicknesses. Such orientation of molecular dipoles could arise from either distortions of the chain conformations within the thin films or be caused by preferential alignment of molecular dipoles at the substrate interface that are propagated further into the film interior. Below we test these two hypotheses as possible sources of film

inhomogeneities.

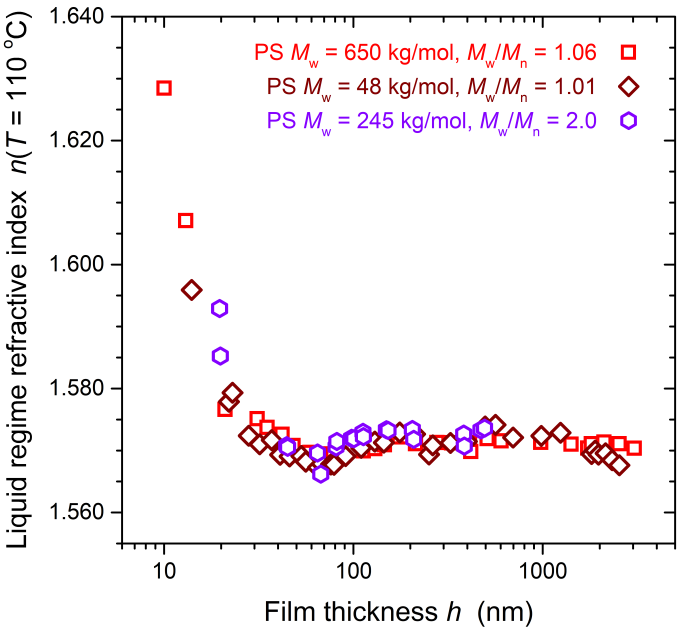

Figure 3.4: Identical film thickness trends for the liquid regime refractive index $n(T = 110\ °C)$ of PS films with three different molecular weights and polydispersities: $M_w = 650$ kg/mol, $M_w/M_n = 1.06$ (red squares, data from Ref. 12), $M_w = 48$ kg/mol, $M_w/M_n = 1.01$ (brown diamonds), and $M_w = 245$ kg/mol, $M_w/M_n = 2.0$ a secondary standard (purple hexagons).

The data presented in Figs. 3.2 and 3.3 are all for high molecular weight (M_w = 650-800 kg/mol) monodisperse polymers. If the observed $n(h)$ behavior were being caused by distorted chain conformations inside the film inducing non-uniform orientation of the molecular dipoles then we would expect a molecular weight dependence to the $n(h)$ trends. In particular, lower molecular weight chains would be less distorted and therefore likely result in films with more uniform polarization. Figure 3.4 plots the film-thickness dependence of the refractive index shifts $n(h)$ for PS films with three different molecular weights, comparing the $M_w = 650$ kg/mol ($M_w/M_n = 1.06$) data from Ref. 12 with data for a much lower molecular weight $M_w = 48$ kg/mol ($M_w/M_n = 1.01$) and a polydisperse secondary standard $M_w = 245$ kg/mol ($M_w/M_n = 2.0$). All three molecular weights exhibit exactly the same $n(h)$ trends independent of chain length or polydispersity. We note that Green et al. also previously measured

the same increase in refractive index with decreasing film thickness for different PS molecular weights.[13]

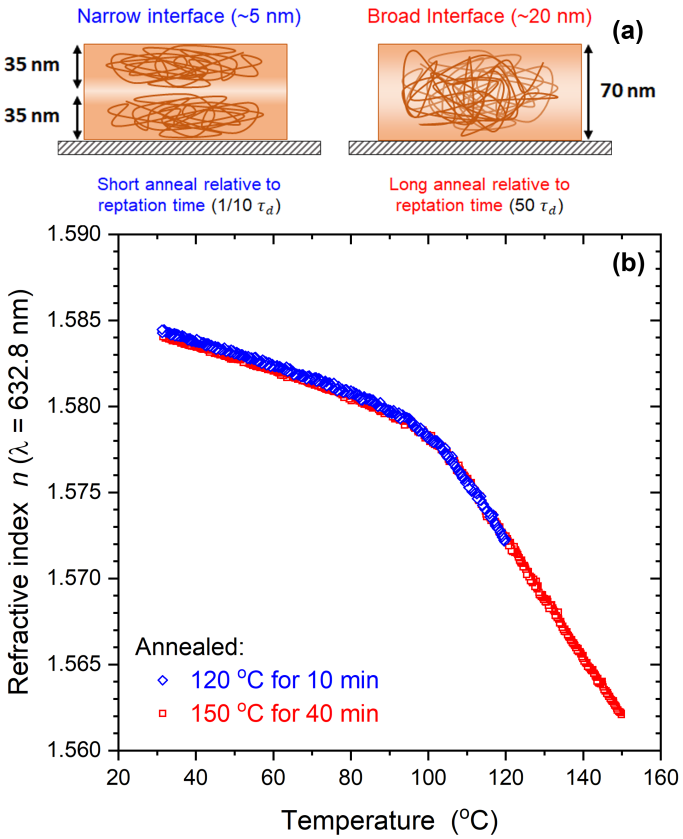

Figure 3.5: (a) Schematic of PS ($M_w = 650$ kg/mol) bilayer sample formed by stacking two 35 nm thick layers atop each other. A short 10 min anneal at 120 °C (corresponding to $\sim 1/10\ \tau_d$) gives a narrow $\sim$ 5 nm interface (blue data), while a long 40 min anneal at 150 °C (corresponding to $\sim$ 50 τ_d) gives a broader $\sim$ 20 nm interface (red data). (b) Temperature dependence of the refractive index $n(T)$ demonstrating overlap of the data.

A more stringent test demonstrating that distorted chain conformations do not have any impact on the measured refractive index of the film is given by the data shown in Figure 3.5. We assembled a 70 nm thick bilayer film by stacking two 35 nm thick PS layers ($M_w = 650$ kg/mol) atop each other. A thickness of 70 nm was selected for its proximity to the minimum in the $n(h)$ trend (see Fig. 3.2). A short anneal of the film for only 10 min at 120 °C, corresponds to $\approx 1/10\tau_d$ the reptation time, resulting in a narrow interface of $\approx$ 5 nm.[45,46] This creates a consolidated film

with no air gaps, but leaves the chain conformations primarily localized to only one half of the film, and thus quite distorted. The measured temperature dependence of the refractive index $n(T)$ is plotted in Fig. 3.5. The same sample can then be annealed again for a much longer time at a higher temperature, 40 min at 150 °C corresponding to $\approx 50\tau_d$, allowing the chains to expand and diffuse across the entire width of the film. Based on measurements of chain interdiffusion,[45,46] we would estimate an interfacial width between the layers of $\approx$ 20 nm. From the graph in Fig. 3.5, we can see that the same $n(T)$ curve is traced out by the sample even after the chains have been allowed to expand. The benefit of this test is that it can be done on the same sample avoiding sample-to-sample variations and any small differences associated with sample alignment on the ellipsometer.

Another potential source of non-uniform polarization for the samples could be caused by preferential orientation of the molecular dipoles near the substrate interface. Depending on molecular packing, this could result in an inhomogeneous distribution of polarization within the film. Surface chemistry of the substrate is an important factor that influences the local orientation of molecular dipoles in the polymer near this interface. Therefore, modifying the surface chemistry of the substrate should alter the orientation of molecular dipoles at the interface, and change the refractive index $n(h)$ behavior if this is an underlying cause for film inhomogeneities. We treated the silicon substrate with chloro(dimethyl)phenylsilane to cap the silicon surface with phenyl rings.[40] This creates a distinctly different surface chemistry compared to the hydroxyl covered surface of native SiO_x/Si substrates used in the rest of our study. Such differences in surface chemistry should cause changes in dipole alignment of the PS phenyl rings. A recent study demonstrated with sum frequency generation (SFG) vibrational spectroscopy that phenyl-capped substrates result in a perpendicular orientation of the PS phenyl rings relative to the substrate interface for chains adjacent to the surface because of favorable $\pi - \pi$ interactions, in contrast to

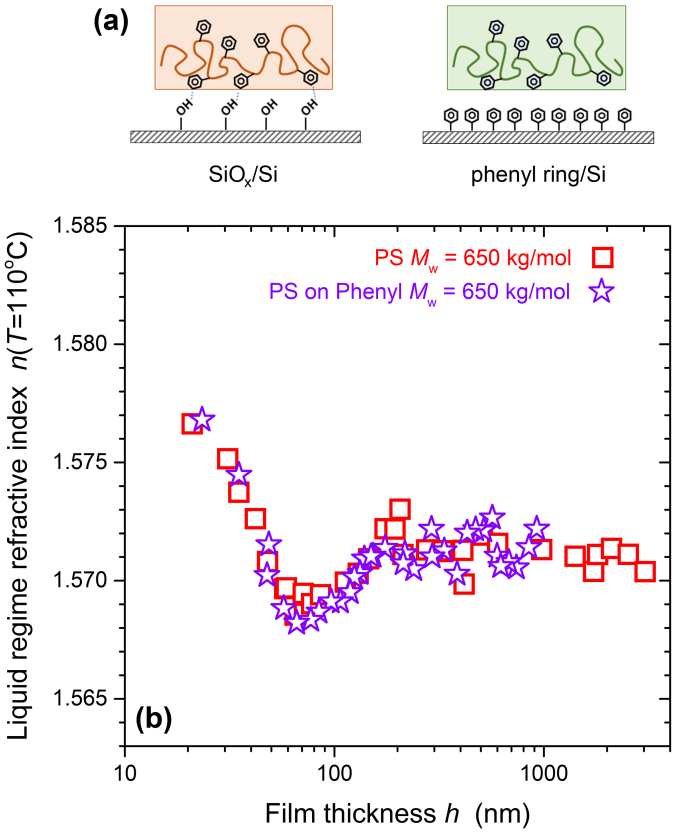

Figure 3.6: (a) Schematic of silicon surface chemistry for the two different substrates studied: PS films atop native SiO_x/Si with surface hydroxyl groups and phenyl capped silicon. (b) Film thickness trends of the liquid regime refractive index $n(T = 110\ ^\circ\mathrm{C})$ for PS films atop phenyl-capped Si (stars) are identical to those observed on native SiO_x/Si substrates (squares).

hydroxyl covered surfaces where the PS phenyl rings are oriented primarily parallel to the surface.[42] Figure 3.6 compares the $n(h)$ behavior of PS (M_w = 650 kg/mol) films supported on phenyl-capped Si relative to the data on SiO_x/Si surfaces. Again, the same $n(h)$ trend emerges, suggesting that preferential orientation of molecular dipoles near the substrate interface is also not the underlying cause of this behavior. Measurements on alkane coated Si substrates were also attempted, but dewetting of films prevented an accurate assessment of $n(h)$ trends.

Although these tests have ruled out chain distortion and substrate interface interactions as possible sources of molecular orientations, we still believe that incorrect modeling of non-uniform film polarization is the likely underlying cause of these ef-

fects. Another possible major source of film inhomogeneities in thin polymer films could be associated with the gradient in dynamics routinely reported in these films. For PMMA in particular, fluorescence measurements of the local T_g have demonstrated a decrease of -7 K near the free surface and an increase of $+10$ K near the silica substrate interface relative to T_g^{bulk}.[29] We note that Bollinne et al.[8] modeled their X-ray reflectivity measurements of PMMA films using a depth-dependent electron density gradient. Similarly, Sanyal et al. reported better fits to x-ray reflectivity curves with a depth dependent electron density profile for ≈80-nm thick PS films.[19] We will address this possible source of film inhomogeneity associated with a strong dynamical gradient perpendicular to the film in a separate publication as the ellipsometer layer modeling is rather involved.

3.4 Conclusions

In this study, we have used spectroscopic ellipsometry to measure and compare the film thickness-dependent refractive index $n(h)$ trends in the liquid and glassy regimes for supported films of P2VP, PMMA, and PS. Similar $n(h)$ trends are observed for all three polymers despite differences in polymer–silica substrate interactions, which invalidates our previous interpretation[12] of associating $n(h)$, and corresponding specific volume $v_{sp}(h)$, shifts with the interface driven film expansion and contraction mechanisms predicted by the White and Lipson thermodynamic model.[22,26] All three polymers exhibit a large distinctive increase in refractive index $n(h)$ for very thin films below $h \lesssim 40$ nm for PS, $h \lesssim 50$ nm for P2VP, $h \lesssim 65$ nm for PMMA. The surprising near equivalence in $n(h)$ trends for P2VP and PS, relative to that for PMMA, suggests the chemical structure and nature of the molecular dipole orientations may play a role in the observed behavior. We tested for possible non-uniform film polarizability due to (i) distortion and confinement of chain conformations by

varying molecular weight, polydispersity, and forming films from bilayers, and (ii) molecular dipole ordering near interfaces by varying the substrate surface chemistry. However, we found the $n(h)$ trends to be invariant under any of these changes suggesting that they are not the cause of the large unphysical apparent increase in density for very thin films recently reported by several studies using different experimental techniques.[10,11,14] Previous efforts had already ruled out limits in ellipsometer fitting accuracy and poor optical contrast with the substrate.[12] We suspect the use of homogeneous (uniform and isotropic) layer approximations, typical of data analysis in many thin film techniques, can lead to unphysical results when film inhomogeneities associated with non-uniform polarizability are present. Such inhomogeneities would certainly invalidate the use of equations like the Lorentz-Lorenz relation to infer density from refractive index values.[12] Future efforts will address film inhomogeneities associated with strong dynamical gradients frequently observed in such thin polymer films.

Bibliography

[1] C. M. Roland, S. Hensel-Bielowka, M. Paluch, R. Casalini. Supercooled dynamics of glass-forming liquids and polymers under hydrostatic pressure. *Reports on Progress in Physics* **2005**, *68*, 1405 – 1478.

[2] R. P. White, J. E. G. Lipson. Free Volume in the Melt and How It Correlates with Experimental Glass Transition Temperatures: Results for a Large Set of Polymers. *ACS Macro Letters* **2015**, *4*, 588–592.

[3] R. P. White, J. E. G. Lipson. Polymer Free Volume and Its Connection to the Glass Transition. *Macromolecules* **2016**, *49*, 3987–4007.

[4] S. F. Swallen, K. L. Kearns, M. K. Mapes, Y. S. Kim, R. J. McMahon, M. D. Ediger, T. Wu, L. Yu, S. Satija. Organic glasses with exceptional thermodynamic and kinetic stability. *Science* **2007**, *315*, 353–356.

[5] S. S. Dalal, M. D. Ediger. Molecular Orientation in Stable Glasses of Indomethacin. *The Journal of Physical Chemistry Letters* **2012**, *3*, 1229 – 1233.

[6] W.-L. Wu, W. J. Orts, J. H. Van Zanten, B. M. Fanconi. Density profile of spin cast polymethylmethacrylate thin films. *Journal of Polymer Science Part B: Polymer Physics* **1994**, *32*, 2475–2480.

[7] W. E. Wallace, N. C. Beck Tan, W. L. Wu, S. Satija. Mass density of polystyrene thin films measured by twin neutron reflectivity. *The Journal of Chemical Physics* **1998**, *108*, 3798–3804.

[8] C. Bollinne, V. Stone, V. Carlier, A. M. Jonas. Density perturbations in polymers near a solid substrate: An X-ray reflectivity study. *Macromolecules* **1999**, *32*, 4719–4724.

[9] A. van der Lee, L. Hamon, Y. Holl, Y. Grohens. Density profiles in thin PMMA supported films investigated by X-ray reflectometry. *Langmuir* **2001**, *17*, 7664–7669.

[10] S. Ata, K. Kuboyama, K. Ito, Y. Kobayashi, T. Ougizawa. Anisotropy and densification of polymer ultrathin films as seen by multi-angle ellipsometry and X-ray reflectometry. *Polymer* **2012**, *53*, 1028–1033.

[11] G. Vignaud, M. S. Chebil, J. K. Bal, N. Delorme, T. Beuvier, Y. Grohens, A. Gibaud. Densification and depression in glass transition temperature in polystyrene thin films. *Langmuir* **2014**, *30*, 11599–11608.

[12] X. Huang, C. B. Roth. Changes in the temperature-dependent specific volume of supported polystyrene films with film thickness. *The Journal of Chemical Physics* **2016**, *144*, 234903.

[13] Y. Li, J. Q. Pham, K. P. Johnston, P. F. Green. Contact angle of water on polystyrene thin films: Effects of CO2 environment and film thickness. *Langmuir* **2007**, *23*, 9785–9793.

[14] A. B. Unni, G. Vignaud, J. P. Chapel, J. Giermanska, J. K. Bal, N. Delorme, T. Beuvier, S. Thomas, Y. Grohens, A. Gibaud. Probing the density variation of confined polymer thin films via simple model-independent nanoparticle adsorption. *Macromolecules* **2017**, *50*, 1027–1036.

[15] J. A. Forrest, K. Dalnoki-Veress, J. R. Dutcher. Brillouin light scattering studies of the mechanical properties of thin freely standing polystyrene films. *Physical Review E* **1998**, *58*, 6109.

[16] J. Brandrup, E. H. Immergut, E. A. Grulke, A. Abe, D. H. Bloch (Eds.), *Polymer Handbook 4th ed.*, of *Wiley: New York*, Wiley: New York, **1999**.

[17] J. N. Hay. Crystallization kinetics of high polymers: Isotactic polystyrene. *Journal of Polymer Science, Part A* **1965**, *3*, 433–447.

[18] G. Reiter. Mobility of Polymers in Films Thinner than Their Unperturbed Size. *Europhysics Letters* **1993**, *23*, 579–584.

[19] M. K. Sanyal, J. K. Basu, A. Datta, S. Banerjee. Determination of small fluctuations in electron density profiles of thin films: Layer formation in a polystyrene film. *Europhysics Letters* **1996**, *36*, 265 – 270.

[20] M. Born, E. Wolf, *Principles of Optics*, Cambridge University Press, New York, **2006**.

[21] N. W. Ashcroft, N. D. Mermin, *Solid State Physics*, Saunders College Publishing, Philadelphia, **1976**.

[22] R. P. White, J. E. G. Lipson. Thermodynamic treatment of polymer thin-film glasses. *Physical Review E* **2011**, *84*, 041801.

[23] P. Z. Hanakata, B. A. P. Betancourt, J. F. Douglas, F. W. Starr. A unifying framework to quantify the effects of substrate interactions, stiffness, and roughness on the dynamics of thin supported polymer films. *The Journal of Chemical Physics* **2015**, *142*, 234907.

[24] P. Z. Hanakata, J. F. Douglas, F. W. Starr. Local variation of fragility and glass transition temperature of ultra-thin supported polymer films. *The Journal of Chemical Physics* **2012**, *137*, 244901.

[25] D. M. Sussman, S. S. Schoenholz, E. D. Cubuk, A. J. Liu. Disconnecting structure and dynamics in glassy thin films. *Proceedings of the National Academy of Sciences* **2017**, *114*, 10601 – 10605.

[26] R. P. White, C. C. Price, J. E. G. Lipson. Effect of Interfaces on the Glass Transition of Supported and Freestanding Polymer Thin Films. *Macromolecules* **2015**, *48*, 4132 – 4141.

[27] J. L. Keddie, R. A. L. Jones, R. A. Cory. Interface and surface effects on the glass-transition temperature in thin polymer films. *Faraday Discussions* **1994**, *98*, 219.

[28] M. K. Mundra, S. K. Donthu, V. P. Dravid, J. M. Torkelson. Effect of spatial confinement on the glass-transition temperature of patterned polymer nanostructures. *Nano Letters* **2007**, *7*, 713 – 718.

[29] R. D. Priestley, M. K. Mundra, N. J. Barnett, L. J. Broadbelt, J. M. Torkelson. Effects of nanoscale confinement and interfaces on the glass transition temperatures of a series of poly(n-methacrylate) films. *Australian Journal of Chemistry* **2007**, *60*, 765 – 771.

[30] C. B. Roth, K. L. McNerny, W. F. Jager, J. M. Torkelson. Eliminating the enhanced mobility at the free surface of polystyrene: Fluorescence studies of the glass transition temperature in thin bilayer films of immiscible polymers. *Macromolecules* **2007**, *40*, 2568–2574.

[31] A. P. Holt, P. J. Griffin, V. Bocharova, A. L. Agapov, A. E. Imel, M. D. Dadmun, J. R. Sangoro, A. P. Sokolov. Dynamics at the polymer/nanoparticle interface in poly(2-vinylpyridine)/silica nanocomposites. *Macromolecules* **2014**, *47*, 1837–1843.

[32] A. M. Jimenez, D. Zhao, K. Misquitta, J. Jestin, S. K. Kumar. Exchange Lifetimes of the Bound Polymer Layer on Silica Nanoparticles. *ACS Macro Letters* **2019**, *8*, 166–171.

[33] N. Jouault, M. K. Crawford, C. Chi, R. J. Smalley, B. Wood, J. Jestin, Y. B. Melnichenko, L. He, W. E. Guise, S. K. Kumar. Polymer chain behavior in polymer nanocomposites with attractive interactions. *ACS Macro Letters* **2016**, *5*, 523–527.

[34] C. J. Ellison, J. M. Torkelson. The distribution of glass-transition temperatures in nanoscopically confined glass formers. *Nature Materials* **2003**, *2*, 695 – 700.

[35] X. Huang, C. B. Roth. Optimizing the Grafting Density of Tethered Chains to Alter the Local Glass Transition Temperature of Polystyrene near Silica Substrates: The Advantage of Mushrooms over Brushes. *ACS Macro Letters* **2018**, *7*, 269 – 274.

[36] X. Huang, M. F. Thees, W. B. Size, C. B. Roth. Experimental Study of Substrate Roughness on the Local Glass Transition of Polystyrene. *The Journal of Chemical Physics* **2020**, *152*, 244901.

[37] C. M. Herzinger, B. Johs, W. A. McGahan, J. A. Woollam, W. Paulson. Ellipsometric determination of optical constants for silicon and thermally grown silicon dioxide via a multi-sample, multi-wavelength, multi-angle investigation. *Journal of Applied Physics* **1998**, *83*, 3323–3336.

[38] J. N. Hilfiker, N. Singh, T. Tiwald, D. Convey, S. M. Smith, J. H. Baker, H. G. Tompkins. Survey of methods to characterize thin absorbing films with Spectroscopic Ellipsometry. *Thin Solid Films* **2008**, *516*, 7979 – 7989.

[39] C. M. Herzinger, P. G. Snyder, F. G. Celii, Y. C. Kao, D. Chow, B. Johs, J. A. Woollam. Studies of thin strained InAs, AlAs, and AlSb layers by spectroscopic ellipsometry. *Journal of Applied Physics* **1996**, *79*, 2663–2674.

[40] J. Choi, N. Clarke, K. I. Winey, R. J. Composto. Polymer Diffusion from Attractive and Athermal Substrates. *Macromolecules* **2017**, *50*, 3038 – 3042.

[41] M. F. Thees, J. A. McGuire, C. B. Roth. Review and Reproducibility of Forming Adsorbed Layers From Solvent Washing of Melt Annealed Films. *Soft Matter* **2020**, *16*, 5366 – 5387.

[42] Y. Hong, Y. Li, F. Wang, B. Zuo, X. Wang, L. Zhang, D. Kawaguchi, K. Tanaka. Enhanced Thermal Stability of Polystyrene by Interfacial Noncovalent Interactions. *Macromolecules* **2018**, *51*, 5620–5627.

[43] H. Fujiwara, *Spectroscopic Ellipsometry: Principles and Applications*, John Wiley & Sons, Ltd., West Sussex, England, **2007**.

[44] H. G. Tompkins, *A User's Guide to Ellipsometry*, Academic Press, Inc., San Diego, CA, **1993**.

[45] R. A. L. Jones, R. W. Richards, *Polymers at Surfaces and Interfaces*, Cambridge University Press, Cambridge, UK, **1999**.

[46] A. Karim, A. Mansour, G. P. Felcher, T. P. Russell. Short-time relaxation at polymeric interfaces. *Physical Review B* **1990**, *42*, 6846–6849.

Chapter 4

Gradient in Refractive Index Reveals Denser Near Free Surface Region in Thin Polymer Films

A version of this chapter was published as Yixuan Han and Connie B. Roth, *The Journal of Chemical Physics*, 155, 144901 (2021).

4.1 Introduction

Many modern experimental techniques such as x-ray and neutron reflectivity, as well as ellipsometry, utilize a layer model in the data analysis procedure to interpret physical properties (electron density, refractive index, film thickness) from the raw experimental data. The layer model is informed by the intrinsic multilayer geometry of the samples, where it is common to assume a homogeneous layer for the material layer of interest (e.g., a polymer film). However, as studies routinely report property changes in thin nanoconfined geometries,[1–7] this homogeneous layer assumption may not be correct for film thicknesses $\lesssim$100 nm. The presence of interfaces and the finite size of the sample, intrinsic to the sample geometry, may perturb the homogeneity of

the polymer film.

Several recent studies using a variety of experimental techniques have reported large (≈25%) increases in the density and refractive index of thin polymer films with decreasing film thickness that are physically unrealistic.[8–12] The claimed density increases for these amorphous thin films would be many times higher than the bulk crystalline state (only ≈5%–8% denser than the bulk amorphous state),[13,14] a sterically unattainable packing state. We contend that the common underlying assumption of a homogeneous layer may likely be the source of the claimed unphysical results.

In our previous work, we used spectroscopic ellipsometry to investigate the film thickness dependence of the refractive index $n(h)$ in thin films of poly(2-vinyl pyridine) (P2VP), poly(methyl methacrylate) (PMMA), and polystyrene (PS).[15,16] We observed similar larger increases in $n(h)$ with decreasing film thickness $h \lesssim 40-65$ nm in both the liquid and glassy regimes for all three polymers assuming a simple homogeneous Cauchy layer model for the polymer film that could be interpreted as an unphysically large increase in density. Our group's first study on PS films had already addressed possible concerns associated with the limits in accuracy of ellipsometry fitting in thin films, and sufficient optical contrast with the substrate.[15] Observing similar results for all three polymers despite differences in attractive interactions with the underlying substrate interface, we speculated that these unphysically large increases in refractive index with decreasing film thickness could be an artifact of the ellipsometry modeling if inhomogeneities were present in the orientation of molecular dipoles.[16] Such film inhomogeneities would invalidate the common assumption of a homogeneous layer model for the polymer film that is routinely presumed in such data analysis. Our 2020 study experimentally tested for various possible sources of non-uniform polarizability in thin films that could account for the source of film inhomogeneity.[16] The observed anomalous trends in $n(h)$ were found to be independent

of polymer molecular weight and polydispersity. In addition, the creation of bilayer films to artificially distort and confine the polymer chains to only one-half of the film did not alter the measured deviation in refractive index of thin films relative to bulk. Substrates with different surface chemistries were also designed to alter the orientation of surface molecular dipoles. However, none of these factors altered the observed $n(h)$ trends that were anomalous. From this process of elimination and the observation that such anomalous $n(h)$ behaviors occur for film thicknesses $h \lesssim 40 - 65$ nm where deviations in film dynamics from bulk are routinely reported, we concluded that underlying film inhomogeneities associated with the strong depth-dependent dynamical gradients frequently observed in thin polymer films could be the fundamental origin of this anomalous behavior. In the present study, we address this proposition.

For nearly 25 years, decreases and increases in the glass transition temperature $T_g(h)$ with decreasing film thickness h have been reported in thin polymer films.[1,2,7,17,18] Frequently deviations from bulk behavior in the average film dynamics of thin films are observed for film thicknesses $h \lesssim 50 - 60$ nm.[17,18] Subsequent studies demonstrated that these film-average $T_g(h)$ shifts with decreasing film thickness result from local T_g changes at the interfaces that propagate into the film establishing a gradient in dynamics with depth from the interface.[6,7,19–21] A central question in understanding this phenomenon is whether a local change in density occurring near the interface is responsible for this local change in dynamics.[6,22] It is not uncommon for studies to assume some density change based on the observed shifts in local dynamics. Tiny changes in density of $\sim$0.5% would be sufficient to explain the observed dynamics.[23–25] In recent years, several computer simulation studies have found no such correlation between local density and local dynamics.[3,6,26–30] However, local density profiles in computer simulations frequently show artificial oscillations associated with the steric packing of spherical particles next to a sharp interface.[3,26,31] Thus, natural questions that arise are whether depth-dependent film inhomogeneities

exist that can be modeled as a depth-dependent gradient in refractive index, and whether such a gradient can be correlated with the known depth-dependent gradients in local dynamics.

To address this question, we investigate the fitting of spectroscopic ellipsometry data to an optical layer model that includes a polymer film layer with a depth-dependent gradient in refractive index, and compare these results with the commonly used homogeneous Cauchy layer model $n(\lambda) = A + \frac{B}{\lambda^2}$. For simplicity, we assume that the wavelength-dependent dispersion of the material $n(\lambda) \sim \frac{B}{\lambda^2}$ is the same, and treat the gradient as linear in magnitude, parameterizing $A(z)$ as linear in a depth-dependent position z within the polymer film. This linear gradient model is applied to three polymers (PMMA, PS, and P2VP) for which depth-dependent dynamical gradients have been well established.[6,7,19,21,32] We find that the resulting refractive index values using the linear gradient model are more physically realistic for thin films than those obtained using the simple homogeneous Cauchy layer model. Surprisingly, the direction of the observed gradient in refractive index with depth for PMMA and PS is opposite to what one might have guessed based on a simple free volume correlation between density and dynamics. Instead we observe an increase in the local refractive index and density near the free surface suggesting the enhanced mobility facilitates improved molecular packing as is observed in the formation of stable glasses. We discuss these results in the context of the existing literature on dynamical gradients in thin polymer films.

4.2 Experimental methods

In practice the experimental data collected for this study was from our previous work where the refractive index in thin polymer films fit using the homogeneous Cauchy layer model was investigated. Additional data on PS films were also collected

for this study. We mention here the pertinent details for interpreting the results presented; additional experimental details are provided in our previous work.[16] Films of polystyrene (PS) ($M_w = 650$ kg/mol, $M_w/M_n = 1.06$), poly(methyl methacrylate) (PMMA) ($M_w = 815$ kg/mol, $M_w/M_n = 1.09$), and poly(2-vinyl pyridine) (P2VP) ($M_w = 650$ kg/mol, $M_w/M_n = 1.08$, or $M_w = 643$ kg/mol, $M_w/M_n = 1.18$) were made by spin-coating solutions from toluene or butanol (for P2VP) onto silicon wafers. All films were then annealed at $T_g^{bulk} + 20$ K under vacuum for 12 h, where the bulk values of the glass transition temperature T_g^{bulk} are 96 °C for PS, 115 °C for PMMA, 94 °C for P2VP.

Temperature-dependent spectroscopic ellipsometry data were collected using a Woollam M-2000 ellipsometer at an angle of incidence of 65° on cooling at 1 °C/min immediately after samples had been reequilibrated at $T_g^{bulk} + 45$ K for 20 min on the ellipsometer hot stage (Instec HSC 302) to remove thermal history. $\Psi(\lambda)$ and $\Delta(\lambda)$ data were fit to an optical layer model for wavelengths $\lambda = 400-1000$ nm using Woollam's CompleteEASE software to obtain the polymer's film thickness and refractive index parameters. The optical layer model consisted of either a homogeneous Cauchy layer [$n(\lambda) = A + B/\lambda^2$] or linear gradient model for the polymer film atop a silicon wafer with 1.25 nm thick native oxide layer.[16]

The linear gradient model was constructed by converting a homogeneous Cauchy layer into a graded layer within the CompleteEASE software. We describe the scientific basis for this in section 4.3.1, but list here the specific details used in the Woollam software as this ellipsometer is accessible to many research labs. Using a *parametric* grade type, the Cauchy A parameter representing the magnitude of the refractive index was set to follow a linear grade equation with 31 slices, while the Cauchy B parameter was held fixed at the bulk value to retain the same dispersion relation. The resulting fit parameters are %grade representing the slope of the gradient (described in more detail in section 4.3.1), $A_{Midpoint}$ the refractive index at the midpoint of the

film and equivalent to the film average value, and the film thickness h.

4.3 Results and discussion

4.3.1 Linear gradient model in refractive index applied to PMMA thin films

As demonstrated by our previous work,[16] the use of homogeneous (uniform and isotropic) layer approximations can lead to unphysical results when film inhomogeneities associated with non-uniform polarizability are present. To resolve such large apparent increases in refractive index reported in the literature,[8–12,15,16] we consider allowing for a linear gradient in index of refraction for the polymer layer as opposed to treating the polymer film as homogeneous. This choice of allowing for a depth-dependent gradient in refractive index is based on the numerous literature studies that have demonstrated depth-dependent gradients in dynamics for thin polymer films.[6,7,19,21,32,33] We start with a linear gradient as the simplest form of a gradient, where the observation of such a gradient in refractive index would be able to provide us with information about the spatial distribution of the refractive index within the film.

Figure 4.1 outlines our proposed linear gradient model to fit a depth-dependent gradient in refractive index for the polymer film, as well as revisiting the details of the standard homogeneous Cauchy layer for comparison between the two models. Figure 4.1a (upper panel) shows a schematic of the standard homogeneous Cauchy layer model corresponding to the sample geometry of our films. This homogeneous model consists of a transparent Cauchy layer for the polymer and a 1.25 nm native oxide layer atop a semi-infinite silicon substrate.[15,16] Following common convention, the wavelength dependence of the refractive index is modeled through the Cauchy

dispersion equation,

$$n(\lambda) = A + \frac{B}{\lambda^2} + \frac{C}{\lambda^4} + \cdots , \tag{4.1}$$

which treats the index of refraction as a series expansion in wavelength.[15,34] In this study, we omit the C/λ^4 and higher rank terms to focus on the magnitude of the refractive index (parameter A) and dispersion (parameter B), resulting in three fitting parameters for the polymer layer: h, A, and B. Refractive index parameters for the thin native oxide layer and the silicon substrate are taken from the literature as part of the Woollam analysis software, as we justified in our previous work.[16] To better describe the spatial distribution of optical quantities, we define z as the depth-dependent position within the film, originating from the substrate interface ($z = 0$) to the free surface ($z = h$). Figure 4.1a (lower panel) graphs the refractive index parameter A as a function of position z, where no depth dependence is present in refractive index parameter A for a homogeneous film.

Figure 4.1b (upper panel) shows a schematic plot of the linear gradient model with the same sample geometry as the homogeneous model except for the presence of a linear gradient in refractive index within the polymer layer. The linear gradient model was constructed based on the idea of allowing for a continuous gradient in the refractive index in its simplest form. This inherent assumption of refractive index following a linear spatial distribution as a function of distance from the substrate may not be completely accurate, but is a starting point for our analysis. We construct the model of a linear gradient in refractive index for a polymer layer with film thickness h without changing the dispersion $n(\lambda)$ relation. The depth-dependent refractive index is thus still modeled with the Cauchy relation (eq. 4.1), but with parameter A being allowed to vary with depth (graded) to reflect the change in magnitude of refractive index. The parameter B is held fixed at the bulk value ($B = 0.00447\ \mu\text{m}^2$ for PMMA), such that the number of fitting parameters remains the same for the linear gradient model as the homogeneous model, avoiding the complexity of introducing extra fitting

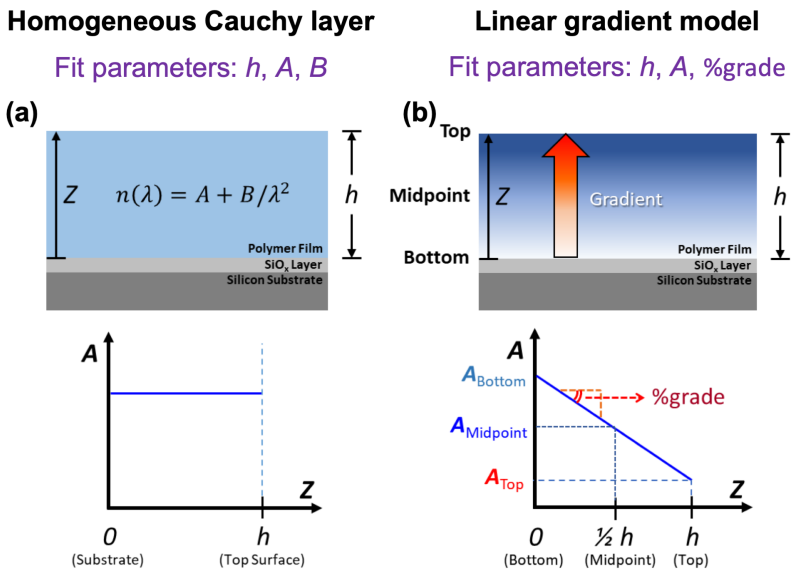

Figure 4.1: (a) (Upper panel) Schematic of homogeneous Cauchy layer model consisting of a polymer layer following the Cauchy dispersion relation (eq. 4.1), a 1.25 nm native oxide layer atop a semi-infinite silicon substrate. (Lower panel) Corresponding profile in refractive index parameter A as a function of depth-dependent position z. (b) (Upper panel) Schematic of linear gradient model with the same geometry as the homogeneous model except for a linear gradient in refractive index parameter A within the polymer layer. (Lower panel) Depth dependence of refractive index parameter $A(z)$ with a slope of %grade, schematic illustrates the negative %grade anticipated.

parameters.

A schematic of the linear profile in refractive index parameter $A(z)$ for the linear gradient model is graphed as a function of depth in Figure 4.1b (lower panel). Three fitting parameters are involved in the linear gradient model: the refractive index parameter A at the midpoint of the film ($z = \frac{1}{2}h$) A_{Midpoint}, the slope of the gradient in refractive index %grade, and the film thickness h. Due to the nature of the linear gradient, A_{Midpoint} is equivalent to the film average of the refractive index parameter A. The slope of the gradient in $A(z)$, %grade is defined as

$$\frac{\%\text{grade}}{100} = \frac{A_{\text{Top}} - A_{\text{Bottom}}}{A_{\text{Midpoint}}}\,, \tag{4.2}$$

where A_{Top} and A_{Bottom} represent the refractive index parameters A at the free surface

($z = h$) and at the substrate interface ($z = 0$), respectively. By this definition, %grade can either be positive or negative, where positive %grade means a higher index A value at the top of the film and a lower index A value at the bottom ($A_{\text{Top}} > A_{\text{Bottom}}$), while a negative %grade would mean the opposite.

The logistics of implementing a continuous gradient in refractive index within the optical layer model requires numerically dividing up the polymer layer into a series of slices each with a successively different refractive index value.[35–38] In the most generalized approach, calculations of the electromagnetic field components within the sample are done using the Berreman 4×4 transfer matrix formalism,[35,36,39] although for fully homogeneous and isotropic slices the more physically intuitive Hayfield and White 2×2 transfer matrix method can also be used.[37,40] In our work, we have used the more generalized 4×4 matrix formalism built into the Woollam CompleteEASE software, but we have also performed calculations in MATLAB using the Hayfield and White transfer matrix approach to verify that both methods produce equivalent results for the fully homogeneous and isotropic slices we are modeling. As described by Abelès,[38] the key issue with modeling a continuous gradient in refractive index with multiple slices is that a sufficient number of slices must be used to ensure that the relative difference in refractive index from slice to slice is small enough to not artificially introduce multiple reflections, and thereby accurately capture the continuous nature of the gradient. Determination of the number of slices needed are done through computational trials, where the number of slices are increased until the modeled parameters are reproducible to within the desired tolerance.[37,38] In the present work, we have found that at least >10 slices are needed to adequately approximate the continuous gradient and obtain model parameters within the variability of the data across different samples. The number of slices used do not impact the film average refractive index (equivalent to A_{Midpoint}) or the film thickness h, only the magnitude of the gradient, where for >30 slices, %grade is independent of the number of slices

to within the precision of the calculation. For the data presented in this study, the polymer film has been divided up into 31 slices, although we have also verified that the same film thickness trends in %grade are observed for 15 and 61 slices. An odd number is deliberately chosen to guarantee a slice at the midpoint of the film from which we can easily obtain the film average optical properties (A_{Midpoint}), as opposed to needing to average two of the middle slices. Thus, the continuous linear gradient model is implemented by assigning a slightly different $A(z)$ value to each successive slice following a linear gradient in the optical parameter A:

$$\begin{aligned} A(z) &= \frac{A_{\mathrm{Top}} - A_{\mathrm{Bottom}}}{h}\left(z - \frac{h}{2}\right) + A_{\mathrm{Midpoint}} \\ &= \frac{\%\mathsf{grade}}{100} \cdot \frac{A_{\mathrm{Midpoint}}}{h}\left(z - \frac{h}{2}\right) + A_{\mathrm{Midpoint}} \ . \end{aligned} \tag{4.3}$$

We start by applying the linear gradient model to PMMA films where the dynamical gradient with depth has been well established.[7,21,32,33] Ellipsometric data of $\Psi(\lambda)$ and $\Delta(\lambda)$ for PMMA films (M_{w} = 815 kg/mol) at different temperatures were collected on cooling at 1 °C/min from our previous work.[16] We fit these $\Psi(\lambda)$ and $\Delta(\lambda)$ data for $\lambda = 400{-}1000$ nm to our linear gradient model at a fixed temperature $T = T_{\mathrm{g}}^{\mathrm{bulk}} + 15$ K, when the film is in the equilibrium liquid state. The initial conditions for the fit parameters are chosen to be the bulk values from a homogeneous Cauchy layer fit, $A_{\mathrm{Midpoint}} = 1.4626$ as the film average value with %grade = 0. For thick films $h \gtrsim 45$ nm, we find the best fit values of A_{Midpoint} and %grade stay near these bulk values. However, for thinner films $h \lesssim 45$ nm, the %grade value begins deviating from zero, becoming progressively more positive for PMMA films with decreasing thickness. The value of A_{Midpoint} also increases slightly. We ensured that these best fit values corresponded to a well-defined global minimum in the parameter space by examining the χ^2 vs. fit parameter curves. Fits to PMMA thin films always gave a global minimum value with positive %grade value.

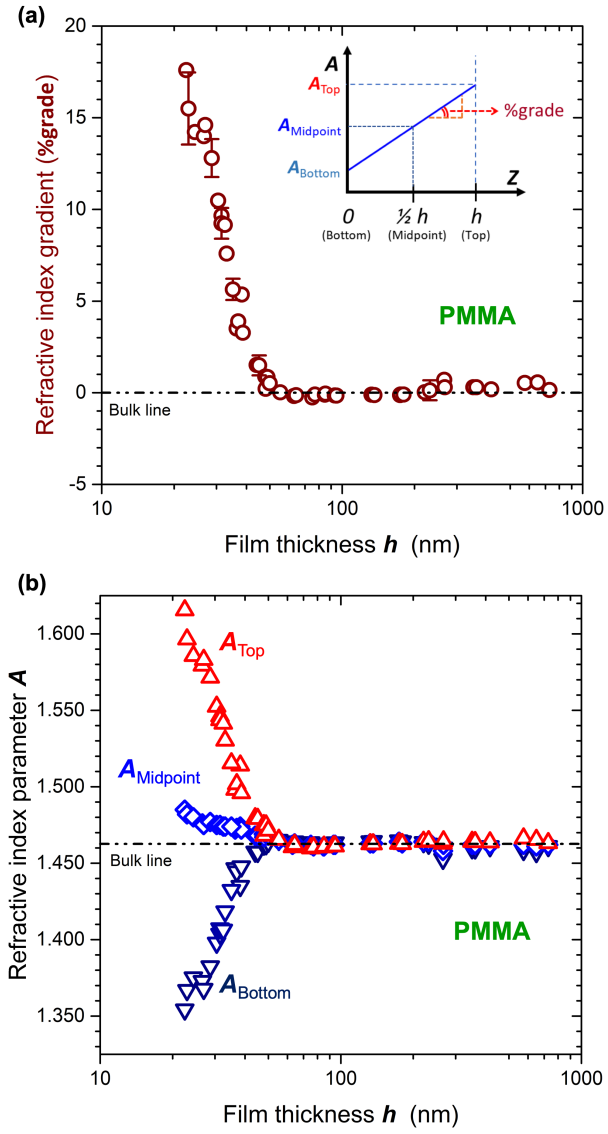

Figure 4.2: Linear gradient model applied to PMMA (M_w = 815 kg/mol) films in the liquid regime at $T = T_g^{bulk} + 15$ K: (a) Best fit refractive index gradient %grade parameter (circles) as a function of film thickness h. Inset: Corresponding depth profile $A(z)$ for positive %grade values. (b) Film thickness dependence of local refractive index parameters at the free surface A_{Top} ($z = h$, red upward pointing triangles), at the film midpoint $A_{Midpoint}$ ($z = \frac{1}{2}h$, blue diamonds), and at the substrate interface A_{Bottom} ($z = 0$, navy downward pointing triangles). Representative error bars have been added for the %grade parameter (see text for details), while the error of the local refractive index parameters A_{Top}, $A_{Midpoint}$, A_{Bottom} are all smaller than the symbol size.

Figure 4.2a graphs the gradient in refractive index parameter %grade in the equilibrium liquid state ($T = T_g^{bulk} + 15$ K) as a function of film thickness for PMMA.

For film thicknesses larger than ≈45 nm, %grade remains zero with little fluctuations, indicating the film is still homogeneous without a noticeable gradient in refractive index. For thicknesses $h \lesssim 45$ nm, a discernible increase is observed for the gradient in refractive index with decreasing film thickness, reaching a positive value of 17.6% in %grade for a 22.5 nm thick film. According to the definition of %grade (eq. 4.2), a positive value of %grade implies the magnitude of A_{Top} is higher, while A_{Bottom} is lower, relative to A_{Midpoint}. The inset of Fig. 4.2a shows a schematic of the refractive index profile as a function of depth $A(z)$, matching the positive value of %grade fit by the linear gradient model.

The error associated with the %grade fit parameter results from sample-to-sample variability across multiple different, but nominally identical samples, which is the dominant error for films of thickness $h \geq 35$ nm, and uncertainty from the fitting, which increases with decreasing film thickness becoming the dominant error for thin films $h \leq 35$ nm. Representative error bars have been included in Fig. 4.2a to indicate the size of these errors. The sample-to-sample variability of the %grade parameter is ±0.54, corresponding to twice the standard deviation (≈95% confidence interval), and has been determined from the scatter in the data for film thicknesses $h \geq 130$ nm. The uncertainty in each of the fit parameters is determined from the square root of the corresponding diagonal element from the covariance matrix C_{ii}, representing one standard deviation.[41] This fitting error that characterizes how well-defined the χ^2 minimum is with respect to variation of that fit parameter becomes larger than the sample-to-sample variability for very thin films, $h \leq 35$ nm. For example, this gives an error in the %grade value of ±2 for a 23 nm thick film.

To more explicitly examine the thickness dependence of the shifts in refractive index at different positions within the film, we focus on the refractive index at the free surface A_{Top} ($z = h$), at the midpoint A_{Midpoint} ($z = \frac{1}{2}h$), and at the substrate interface A_{Bottom} ($z = 0$). Figure 4.2b plots the liquid regime refractive index parameters A_{Top},

A_{Midpoint}, and A_{Bottom} as a function of film thickness sampled at the same temperature ($T = T_{\text{g}}^{\text{bulk}} + 15$ K) for PMMA. A_{Top} and A_{Bottom} are calculated from the value of A_{Midpoint} and %grade via eq. 4.3. With decreasing film thickness, A_{Top} exhibits a sharp increase for film thicknesses $h \lesssim 45$ nm, while A_{Bottom} exhibits a corresponding decrease, with A_{Midpoint} showing only a modest increase. Both the bulk sample-to-sample variability (± 0.0031) and the fitting error (± 0.0015 for the thinnest films) are smaller than the size of the symbols for these local refractive index values in Fig. 4.2b.

These differences in the local values of the refractive index parameter A indicate that the magnitude of the refractive index varies with depth within the film. Frequently, the Lorentz-Lorenz equation, $\frac{n^2-1}{n^2+2} = \frac{\alpha N_A}{3\epsilon_0 M_0}\rho$, has been used to convert values of the refractive index n to density ρ, where α is the molecular polarizability, M_0 the monomer molecular weight, N_A Avogadro's number, and ϵ_0 the permittivity of free space.[8–10,15] Use of this Lorentz-Lorenz relation in the present case would not be valid as its derivation requires isotropic and homogeneously distributed dipoles.[42,43] However, the general proportionality of this relation that the refractive index n is correlated with the density of molecular dipoles ρ, i.e., $n \propto \rho$, must still be true locally.[44,45] Thus, we believe that the observed gradient in refractive index parameter $A(z)$ is indicative of a gradient in molecular density $\rho(z)$ within the film. Even though we cannot numerically convert local $A(z)$ values to a local density profile $\rho(z)$, these results are able to inform us about the relative magnitude and direction of such a density gradient. Below in section 4.3.4, we will explore the implications of such a gradient in local structure with regards to the known dynamical gradients in these thin polymer films.

4.3.2 Fitting improvements of the linear gradient model over the homogeneous model

Overall, we find the linear gradient model is able to provide more physically realistic film properties and less correlated fitting parameters when compared to the homogeneous Cauchy layer model. With the same number of fitting parameters as the homogeneous model, the linear gradient model does not add additional complexity, making the fitting equally robust. It is worth noting that both the linear gradient model and the homogeneous model report the same thickness h for a given sample. The fits to the experimentally measured $\Psi(\lambda)$ and $\Delta(\lambda)$ data are equivalently good, with resulting mean squared error (MSE) values that are within experimental error the same. As such, fit quality alone is unable to distinguish one model as being more correct or accurate than the other. Woollam et al. has argued that MSE values alone are insufficient to favor one optical layer model over another and that one needs to consider how physical the resulting optical parameters are coming from the model.[46] Thus, given that we have two optical layer models with equivalently good fits to the experimental data, we consider here which model is the more physically realistic interpretation for the anomalous behavior obtained when measuring the refractive index of thin polymer films.

The linear gradient model, in essence, changes the interpretation of the large increases in refractive index $n(h)$ with decreasing film thickness that are observed in thin films. Use of the homogeneous Cauchy layer model treats the $n(h)$ increase as an increase in the magnitude of the average index value A and a change in the wavelength-dependent dispersion of the material B. This is not necessarily the most realistic assumption given that for very thin films, the change in polarization of the light occurring upon reflection from the film becomes primarily dominated by the interfaces such that the contribution from the wavelength-dependent material dispersion becomes negligible. Thus, given this decreased sensitivity to the B parameter for

very thin films, it is unlikely that the observed changes to the polarization of light on reflection of very thin films is due to a change in the wavelength-dependent dispersion of the material. In contrast, the linear gradient model treats the $n(h)$ increase in thin films as occurring from the development of a gradient in refractive index with depth within these thin films. This assumption has strong literature support as it has been well documented that such thin films exhibit a gradient in dynamics with depth.[6,7,19,21,32,33]

We first start by noting that if we simply apply the homogeneous Cauchy layer model to thin films holding the refractive index parameters fixed at the bulk value ($A = 1.4626$, $B = 0.00447$), fitting only the film thickness h, we find that the MSE parameter and residual of the fits become significantly worse in thin films than when allowing the A and/or B parameters to vary. Thus, there is strong indication from the fitting, as well as reports by other experimental studies,[8–10,12,15,16,47] that the refractive index of thin films is altered from bulk in some fashion. When the A and B parameters are allowed to vary, we observe a strong correlation in these two parameters where a change in the B parameter value may be compensating for the large unphysical increase in the A parameter value, resulting in an inaccurate capture of the change in refractive index of thin films.

In our previous study,[16] we investigated possible sources of film inhomogeneities that could be responsible for the large unphysical increases in refractive index $n(h)$ observed in thin films. By process of elimination, we determined that chain distortion by film confinement and molecular dipole ordering near interfaces were not the source of the film inhomogeneities. As a conclusion, we speculated that strong dynamical gradients frequently observed in thin polymer films may be the cause of film inhomogeneities. By using the linear gradient model, in this work we are able to explore the presence of a refractive index distribution inside polymer thin films and compare them to the dynamical gradients that constitute confinement effects.

We find that the linear gradient model provides best-fit values for the refractive index parameters A_{Midpoint} and %grade that are more consistent with bulk films down to thinner film thicknesses $h \approx 35 - 45$ nm, relative to that observed for fits using the homogeneous Cauchy layer model where the refractive index began strongly deviating from bulk values for films thinner than $h \approx 40 - 65$ nm.[16] The linear gradient model also seems more physical because it is more reasonable to assume that a depth-dependent refractive index could be present in such thin films exhibiting depth-dependent dynamics, compared with some average change in the wavelength-dependent dispersion (B parameter). In section 4.3.4, we will discuss how the observed depth-dependent refractive index changes determined from the linear gradient model fits compare with the previously observed depth-dependent dynamics in these thin films.

4.3.3 Linear gradient model in refractive index applied to PS and P2VP thin films

We apply now the linear gradient model in refractive index to thin supported films of PS and P2VP. Our previous work showed that when a simple homogeneous Cauchy layer model was applied to thin films, all three polymers, PS, P2VP, and PMMA, exhibited roughly the same unphysically large increase in $n(h)$ with decreasing film thickness below $h \lesssim 40{-}65$ nm, despite differences in substrate interactions between the different polymers.[16] From our previous study, temperature-dependent measurements of the refractive index $n(T)$ were collected for PS ($M_{\text{w}} = 650$ kg/mol) and P2VP ($M_{\text{w}} = 650$ and 643 kg/mol) thin films at different thicknesses. Here, we fit these $\Psi(\lambda)$ and $\Delta(\lambda)$ data, as well as additional data collected for the same 650 kg/mol PS, at $T = T_{\text{g}}^{\text{bulk}} + 15$ K to the linear gradient model, starting with initial fit parameters set at their respective bulk values: $A_{\text{Midpoint}} = 1.5501$ and $B = 0.00748$ μm^2 for PS, $A_{\text{Midpoint}} = 1.5543$ and $B = 0.0101$ μm^2 for P2VP, with %grade $= 0$ for both

polymers.

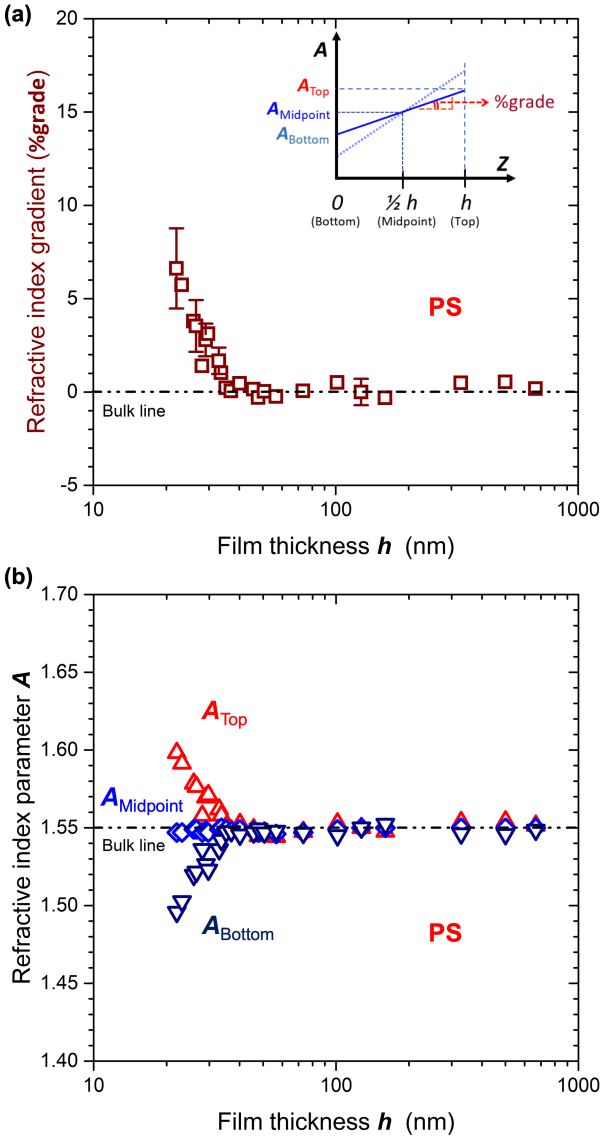

Figure 4.3: Linear gradient model applied to PS (M_w = 650 kg/mol) films in the liquid regime at $T = T_g^{bulk} + 15$ K: (a) Best fit refractive index gradient %grade parameter (squares) as a function of film thickness h. Inset: Corresponding depth profile $A(z)$ for positive %grade values (solid line), with dotted line showing that for PMMA from Fig. 4.2. (b) Film thickness dependence of refractive index values at the free surface A_{Top} ($z = h$, red upward pointing triangles), at the film midpoint $A_{Midpoint}$ ($z = \frac{1}{2}h$, blue diamonds), and at the substrate interface A_{Bottom} ($z = 0$, navy downward pointing triangles). Representative error bars have been added to the %grade parameters following the same criteria as described for PMMA, while the error of the local refractive index parameters A_{Top}, $A_{Midpoint}$, A_{Bottom} are all smaller than the symbol size.

Figure 4.3 graphs the thickness dependence of the refractive index gradient %grade(h), as well as the local refractive index parameters A_{Top}, A_{Midpoint}, and A_{Bottom} at different depths within the film for PS in the liquid regime ($T = T_{\mathrm{g}}^{\mathrm{bulk}} + 15$ K), following the same manner as shown in Fig. 4.2. Figure 4.3a shows that below ≈35 nm in film thickness, %grade begins to deviate from the bulk zero line and increases similar to PMMA. However, the magnitude of the increase in %grade(h) is significantly less than that observed for PMMA. For example, a 22.0 nm thick PS film exhibits a %grade value of 6.6%, roughly a factor of three smaller than the 17.6% observed for a 22.5 nm PMMA film. The inset of Figure 4.3a illustrates this reduced $A(z)$ gradient for PS (solid line), relative to that for PMMA (dotted line). PS also differs in that the onset of the gradient in refractive begins at a thinner value of the film thickness, ≈35 nm for PS compared with ≈45 nm for PMMA. The span of the vertical axes in Figure 4.3 for PS have been set to match that of Figure 4.2 for PMMA such that a direct comparison can be made of the magnitudes. The specific local refractive index values as a function of film thickness are shown in Figure 4.3b, where again A_{Top} increases and A_{Bottom} decreases with decreasing film thickness. Notably, the average refractive index value represented by A_{Midpoint} remains equivalent to bulk even for the thinnest films.

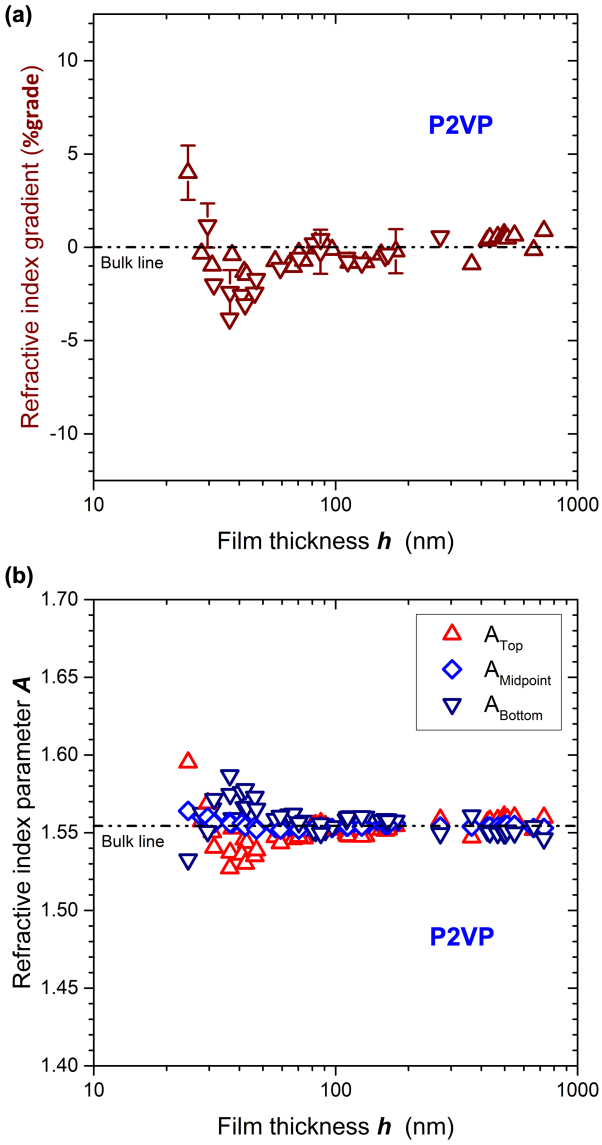

Figure 4.4: Linear gradient model applied to P2VP ($M_w = 650$ kg/mol and $M_w = 643$ kg/mol) films in the liquid regime at $T = T_g^{bulk} + 15$ K: (a) Best fit refractive index gradient %grade parameter ($M_w = 650$ kg/mol, upward pointing triangles; $M_w = 643$ kg/mol, downward pointing triangles) as a function of film thickness h. (b) Film thickness dependence of refractive index values at the free surface A_{Top} ($z = h$, red upward pointing triangles), at the film midpoint $A_{Midpoint}$ ($z = \frac{1}{2}h$, blue diamonds), and at the substrate interface A_{Bottom} ($z = 0$, navy downward pointing triangles). Representative error bars have been added to the %grade parameters following the same criteria as described for PMMA, while the error of the local refractive index parameters A_{Top}, $A_{Midpoint}$, A_{Bottom} are all smaller than the symbol size.

In Figure 4.4, we apply the linear gradient model to supported P2VP films. From our previous study, we found that when the homogeneous Cauchy layer model is

applied to thin films, P2VP films exhibit a nearly identical trend in refractive index $n(h)$ increase with decreasing film thickness to PS films, which we attributed to the similar ring-type chemical structure and corresponding molecular dipole of the two polymers.[16] Figure 4.4a graphs the thickness dependence of the refractive index gradient parameter %grade(h) for P2VP films in the liquid regime ($T = T_{\mathrm{g}}^{\mathrm{bulk}} + 15$ K), following the same manner shown in Figures 4.2 and 4.3. Again we have deliberately set the vertical spans of the y-axes to all be the same in this series of graphs (Figs. 4.2, 4.3 and 4.4) to enable direct comparison of the magnitude of these refractive index parameters across the different polymers. For P2VP films, the %grade parameter primarily fluctuates about zero for essentially all film thicknesses. For $h \gtrsim 50$ nm, the %grade values are within $\pm 1\%$, while for thinner films this grows to approximately $\pm 4\%$. Figure 4.4b plots the local refractive index parameters A_{Top}, A_{Midpoint} and A_{Bottom} as a function of film thickness for P2VP. Corresponding to the low values of %grade for this polymer, the local refractive index at different positions within the film all seem to collapse about the bulk value. These results for P2VP films are distinctly different from the strong positive refractive index gradients observed for PMMA and PS thin films. To first order, these results would suggest that the refractive index is likely more homogeneous within P2VP films. Thus, the greater sample-to-sample variability observed for P2VP thin films could simply reflect the greater difficulty in fitting very thin films, with their correspondingly larger fitting errors, especially for weak or near-zero gradients.

It is worth recalling that our model enforces a *linear* gradient to the refractive index, chosen to minimize the number of fitting parameters, and as such any *nonlinear* change to the depth-dependence of the refractive index in reality is being approximated by a linear slope in $A(z)$. Specific to P2VP, one might consider that the weak or near-zero gradient observed in very thin films could reflect some non-monotonic gradient in refractive index. For example, a parabolic-shaped $A(z)$ profile would sim-

ply average to a roughly zero slope when fit by the linear gradient model. To assess this possibility, we have attempted fitting the data to a parabolic $A(z)$ function. This parabolic model still has the same number of fitting parameters as the linear gradient or homogeneous Cauchy layer model. Besides the film thickness h, two fit parameters are used to describe the refractive index profile $A(z)$ with depth, a parameter corresponding to the value of A at the center of the film and a term describing the strength of the curvature. We find that fits of the parabolic model to the P2VP data do not give consistent trends with decreasing film thickness. This suggests that the weak or near-zero gradient observed for the P2VP thin films when fit to the linear gradient model is not the result of a nonlinear parabolic-type trend in $A(z)$ with depth. We have also tried various other nonlinear functional forms for $A(z)$ such as asymmetric parabolas and higher order polynomials, but none of these more complex models, which necessitate an additional nonlinearity parameter, gave any more meaningful results than the simple linear gradient model already presented.

It is also worth recognizing that the linear gradient model is unable to distinguish between a continuous change in refractive index with depth and a refractive index change that occurs primarily near the interfaces, leaving the interior of the film mostly bulk-like. Even though we cannot exactly determine the form of the refractive index change with depth, the results from the linear gradient model still demonstrate the presence of a strong positive gradient in refractive index for PMMA and PS thin films, while P2VP films appear to be more homogeneous.

We find that one of the distinguishing features of the linear gradient model is that for a given polymer, the film average refractive index values A_{average} remain closer to the bulk value for thinner films. Note that as the relationship between refractive index and density depends on the specific molecular polarizability of the polymer units, therefore, it is not possible to infer that a larger magnitude in the deviation of the average refractive index from one polymer to the next implies a larger density

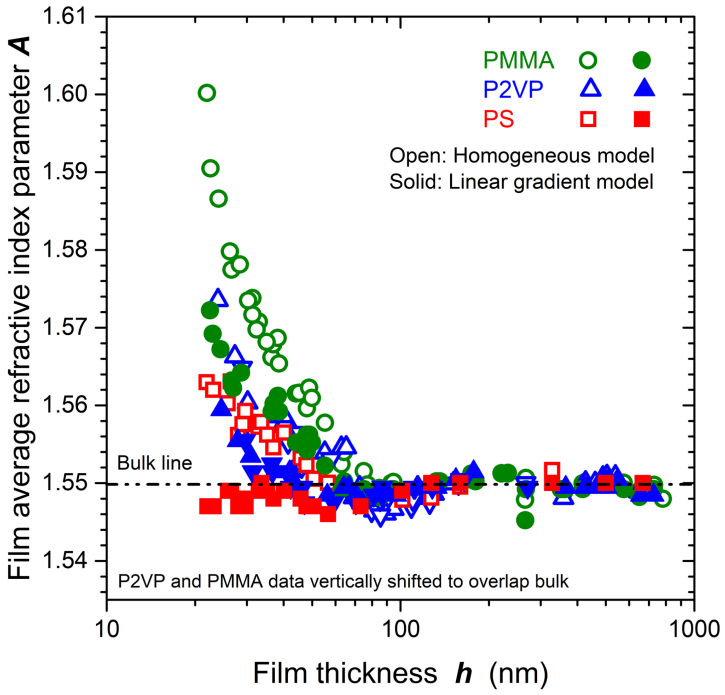

Figure 4.5: Comparison of the film average refractive index trends with decreasing film thickness from fits to the linear gradient model (parameter A_{Midpoint}, solid symbols) and fits to the homogeneous Cauchy layer model (parameter A, open symbols) for data measured in the liquid regime at $T = T_g^{\text{bulk}} + 15$ K: PMMA ($M_w = 815$ kg/mol, green circles), PS ($M_w = 650$ kg/mol, red squares), and P2VP ($M_w = 650$ kg/mol, blue upward pointing triangles; $M_w = 643$ kg/mol, blue downward pointing triangles). Data for P2VP and PMMA have been shifted vertically to align the bulk data with that for PS.

deviation in thin films. In the linear gradient model, the film average refractive index value is characterized by the fit parameter A_{Midpoint} corresponding to the value of A at $z = h/2$, while in the homogeneous Cauchy layer model the film average refractive index value is characterized by the fit parameter A. In Figure 4.5, we compare these measures of the film average refractive index value A_{average} as a function of decreasing film thickness h. For comparison, the P2VP and PMMA data have been vertically shifted by -0.00455 and $+0.0872$, respectively, to overlap the bulk data with PS. When fit with the homogeneous Cauchy layer model, the anomalous and unphysical increase in $n(h)$ occurred in PMMA thin films for $h \lesssim 65$ nm, P2VP thin films for $h \lesssim 50$ nm, and PS thin films for $h \lesssim 40$ nm.[16] In contrast, the data in Figure 4.5 show

that the film average refractive index value A_{average} as determined by the parameter A_{Midpoint} in the linear gradient model remains close to the bulk value for PS films of all thicknesses, and increases less with decreasing film thickness for P2VP thin films for $h \lesssim 30$ nm and PMMA thin films for $h \lesssim 50$ nm. For the thinnest PMMA and P2VP films ($h \approx 23$ nm), the deviation in the film average value A_{average} from the bulk is less than a half for A_{Midpoint} from the linear gradient model fit than for the parameter A from the homogeneous Cauchy layer model fit. This suggests that the linear gradient model provides a more physically realistic description of the refractive index changes occurring in thin films than the larger physically unrealistic increases in $n(h)$ observed in thin polymer films when fit with the simple homogeneous Cauchy layer model.

All the data shown are for a temperature of $T = T_{\text{g}}^{\text{bulk}} + 15$ K in the supercooled equilibrium liquid state. However, we have also fit and examined the gradient in refractive index at a temperature in the nonequilibrium glassy state ($T = T_{\text{g}}^{\text{bulk}} - 45$ K). Following the same fitting procedure of applying the linear gradient model and comparing the results to the corresponding bulk refractive index in the glassy state, we find that the %grade and changes in the local magnitude of the refractive index values A_{Top}, A_{Midpoint}, and A_{Bottom} with decreasing film thickness are within experimental error the same for all three polymers, as are shown in Figures 4.2−4.5. The same gradients in refractive index present in the equilibrium liquid state above T_{g} persist into the nonequilibrium glassy state. This demonstrates that the structural gradient in refractive index is not due to some nonequilibrium glassy behavior, but is reflective of sustained depth-dependent interfacial perturbations that exist in the supercooled equilibrium liquid state above T_{g}. We next discuss how this structural gradient may relate to the dynamical gradient known to be present in these thin films.

4.3.4 Comparison of linear gradient model results with known dynamical gradients

In this section, we compare the results of the linear gradient model in refractive index applied to PMMA, PS, amd P2VP films, and discuss these results within the context of what is known about the gradient in dynamics of these films from the literature. Figure 4.6 directly compares the magnitude of the gradients in refractive index for the three polymers by plotting the film thickness dependence of the %grade(h) on the same axes. Graphed in this manner, we can clearly see that PMMA and PS have similar trends where %grade(h) stays near-zero for bulk and thick films until a significant increase is observed for films $h \lesssim 45$ nm for PMMA and $h \lesssim 35$ nm for PS. The magnitude in the %grade(h) increase is approximately three times larger for PMMA thin films than for PS thin films. In contrast, the value of %grade for P2VP films fluctuates near zero for all film thicknesses without presenting a well-defined trend. These results are surprising given that in our previous study that fit the homogeneous Cauchy layer model a large increase in refractive index with decreasing film thickness $n(h)$ was observed for all three polymers, with P2VP and PS behaving very similarly.[16]

Numerous reports in the literature have described gradients in local dynamics in thin films of PS, PMMA, and P2VP.[4,6,7,19,21,32,33,48–50] Most commonly, this is observed as some measure of enhanced (faster) mobility near the free surface, although results for PMMA and P2VP films on silica have also reported reduced mobility near the substrate interface attributed to hydrogen bonding.[17,18,21,33,48,51–53] Can we rationalize the presence of a refractive index gradient in these thin films from the existence of a gradient in dynamics that has already been established for these polymers in thin films?

The most heavily studied system is that for PS thin films where the reduction in film-average glass transition temperature $T_g(h)$ with decreasing film thickness h

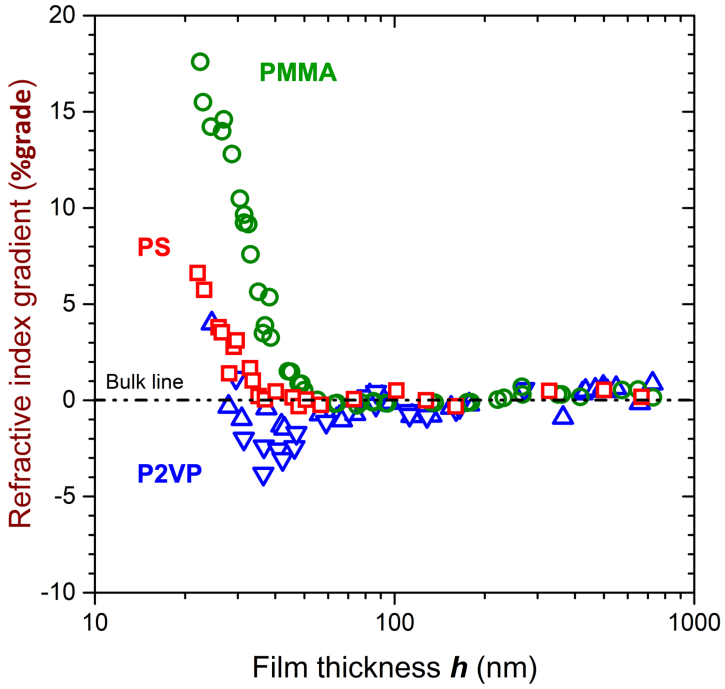

Figure 4.6: Comparison of film thickness dependent trends in the magnitude of the refractive index gradient %grade measured in the liquid regime ($T = T_g^{bulk} + 15$ K) for PMMA ($M_w = 815$ kg/mol, green circles), PS ($M_w = 650$ kg/mol, red squares), and P2VP ($M_w = 650$ kg/mol, blue upward pointing triangles; $M_w = 643$ kg/mol, blue downward pointing triangles) films. PMMA films show strong positive %grade values in thin films that are nearly three times larger than the modest positive %grade values observed in PS films, while P2VP films do not appear to present a well-defined gradient.

below ≈ 60 nm has long been attributed to a gradient in dynamics resulting from local perturbations at the polymer-air free surface.[4,7,17,19,20] The strongest support confirming this dynamical gradient in local T_g values comes from the fluorescence measurements by Ellison and Torkelson who used a 12-14 nm thick pyrene-labeled PS probe layers localized at either the free surface or silica substrate interface to determine the local T_g at these positions.[19] For film thicknesses $h \gtrsim 60$ nm, the probe layer positioned at the top of the film (free surface) showed a T_g reduction of 32 K below the bulk value T_g^{bulk}, while a similar probe layer positioned at the polymer-silica substrate interface showed a bulk-like local T_g. The free surface being the source of the $T_g(h)$ reduction was also confirmed by Sharp and Forrest who demonstrated that thin

PS films capped with neutral substrate interfaces (gold and aluminum) showed no deviation from T_g^{bulk} down to $h = 7$ nm, and that the $T_g(h)$ decrease could be recovered when the aluminum capping layer was removed.[20] Other studies have also observed neutral interactions between PS and silica substrates.[54,55] In addition, many studies have confirmed faster dynamics near the free surface by directly measuring relaxations of surface features and probes.[4,56–58] This dynamical gradient picture has been used to interpret numerous other types of measurements such as physical aging[59–61] and dye rotational relaxation[50,62] in thin films, as well as form the foundation for theoretical models.[6] Thus, for PS thin films, the dynamical gradient originating from the free surface propagating deeper into the film is well established.

Dynamical gradients in PMMA thin films are also relatively well characterized. Early work observing opposing trends in film-average glass transition temperature $T_g(h)$ with decreasing film thickness h for PMMA films supported on different substrates, were able to attribute the effects to competing dynamical perturbations occurring at the free surface and substrate interface when attractive polymer-substrate interactions were present.[18,51] This inference was later confirmed using local T_g measurements via fluorescence by Torkelson et al. who identified a 7 K reduction in local T_g relative to T_g^{bulk} near the free surface and a 10 K increase in local T_g near the substrate interface,[21] which was able to reconcile the varying $T_g(h)$ tends.[53] Local physical aging measurements on identical supported PMMA films also observed a strong gradient in dynamics with depth consistent with these local T_g shifts.[33] In comparison to PS, numerous studies have reported that the strength of the free surface effect causing the local T_g reduction in PMMA is roughly 1/3 the strength of the T_g reduction typically observed for PS.[49,50,63,64] The strength of the attractive interactions at the PMMA–substrate interface can vary across studies, especially for PMMA with different tacticities.[65–67] In general, the role of attractive interactions between PMMA and the silica substrate is viewed as inhibiting dynamics locally, which may

impact molecular packing near this interface.

In contrast, the dynamical gradient in P2VP thin films is less well understood. From pyridine's chemical structure, it is known that favorable interactions are present allowing for hydrogen bonding between P2VP's nitrogen unit and the hydroxyl groups naturally present on the silica substrate.[68] The extent to which this interaction hinders the dynamics of the polymer near the substrate is less clear. Perhaps the strongest experimental evidence for slower P2VP dynamics near the silica substrate interface comes from dielectric spectroscopy measurements on the nanocomposite system of P2VP mixed with silica nanoparticles, where the segmental relaxation time of the interfacial polymer layer was found to be ∼2 orders of magnitude slower than bulk dynamics.[69] Recent local fluorescence measurements on P2VP–silica nanoparticle systems also report large increases in local T_g next to the nanoparticle interface, especially for low molecular weights.[70] However, how much this slower local dynamics near the substrate then translates into a gradient in dynamics in the rest of the film is unclear. Early measurements of the film average glass transition temperature $T_g(h)$ for P2VP thin films supported on silica substrates have reported strong increases in T_g with decreasing film thickness h, up to ≈ 35 K above T_g^{bulk} for a ≈ 15 nm thick film.[52,71,72] However, more recent studies have not observed such a dramatic increase in $T_g(h)$,[48,50] where one study observed a slight reduction in the average $T_g(h)$ with decreasing film thickness in P2VP thin films on similar substrates that varied with cooling rate, but also reported a broadening of the transition suggesting a splitting of fast dynamics at the free surface with slow dynamics at the substrate interface.[48] We also do not observe a large $T_g(h)$ increase in P2VP thin films based on the data collected in this study. Dye rotational relaxation measurements on free-standing P2VP thin films by Paeng and Ediger have found that P2VP exhibits a nearly identical free surface mobile layer thickness to that measured for PS thin films.[49] This suggests that P2VP could have as strong a free surface effect as PS. Collectively these ex-

perimental results indicate that P2VP thin films supported on silica substrates have a very strong dynamical gradient with slower mobility near the substrate interface and faster mobility near the free surface, where perhaps the conflicting reports of film average $T_g(h)$ behavior in thin P2VP films partially reflect how different experimental techniques sample this gradient or variations in molecular weight.

Given this summary of dynamical gradients in PS, PMMA, and P2VP films, how do we reconcile the observed refractive index gradients presented in Figure 4.6. All literature studies of dynamical gradients always point to the free surface having faster local mobility, regardless of polymer. This faster mobility is frequently associated with the presumption that the local density is reduced near the free surface. In fact, numerous theories associated with the glass transition have long been constructed around this correlation between density and dynamics.[73] Such a simple correlation between dynamics and density, would imply a lower density near the free surface for all three polymers, and a higher density near the substrate interface for PMMA and P2VP where attractive interactions slow local dynamics. In contrast, we find the structural gradient in refractive index suggests that the near free surface region appears denser, while the region near the substrate interface appears less dense, for both PMMA and PS, with the effect being more pronounced in PMMA. Other studies have also reported density variations with depth in thin polymer films.[74–76] Bollinne et al. found a similar reduction in density near the substrate interface for PMMA and PS films,[74] and recently Beena Unni et al. observed a similar direction in the density gradient for thin films of poly(4-chloro styrene) (P4ClS), while P2VP density profiles were flatter.[75]

The well-known Lorentz-Lorenz equation relating refractive index to density is only the first term in a series expansion. Higher order terms involve integrals over two- and three-body density correlation functions to correctly account for the local electric field.[44,45] The Lorentz-Lorenz form assumes that the material has a homoge-

neous and isotropic distribution of dipoles. Certainly for a thin polymer film with a depth-dependent gradient in density this is no longer true. The density correlations near the free surface and substrate interfaces will be different, and likely anisotropic. Unfortunately an evaluation of such local density correlations to infer a quantitative density gradient from our measured refractive index gradients would be nontrivial to calculate.[44,45,77] Thus, our refractive index measurements provide only a relative magnitude and direction for the depth-dependent gradient in density in thin films of PMMA, PS, and P2VP.

To understand the cause of the observed direction in the structural gradient and estimate a magnitude for the density increase near the free surface, we can look at the density increases observed from the formation of stable glasses. Glasses with exceptional kinetic stability can be formed by sufficiently slow physical vapor deposition (PVD) onto substrates held at a temperature just below the glass transition temperature of the glass former.[78,79] This process leverages the enhanced mobility at the free surface to allow molecular units to pack more efficiently into a higher density state prior to being covered by the next surface layer of molecules.[79,80] The glass states formed from this process have exceptional kinetic stability, requiring temperatures well above the conventional temperature-cooled T_g to transform back into an equilibrium liquid state, equivalent to glasses that have been aged for millions of years.[79] Under optimal PVD conditions, the amorphous molecular packing of the stable glass state formed has densities that are ≈1.5% higher than the ordinary temperature-cooled glass state,[78,79,81] reaching densities that are considered to be close to the 'ideal glass' state with the highest packing density possible for an amorphous state.[82] Although the density increases are small, these small changes in molecular packing can have profound impact on other material properties, where stable glasses can show increases in modulus that are almost 20% higher than the ordinary temperature-cooled glass.[79,83] Even though most stable glasses formed to

date are with small molecule glass formers, recent studies have shown that similar high density stable glasses (≈1.5% denser) can be formed with polymers, including PS and PMMA.[84,85]

Simmons et al. have reasoned that the ability to form such stable glasses with higher density implies not only that the free surface has enhanced mobility, but that a "nanoscale 'facilitated' region" (of order 10 nm) must be present near the free surface.[80] On cooling below T_g^{bulk}, this near-surface 'facilitated' layer will continue to densify, following the thermal expansion of the equilibrium supercooled liquid. From computer simulations, Simmons et al. have shown that this results in a local increase in density of the near-surface region of order 1.5%,[80] consistent with the stable glass formation process. Most relevant for the present results is that Simmons et al. argues this denser near-surface region should also be present near the free surface of ordinary temperature-cooled polymer films.[80] Thus, we believe our gradient in refractive index measurements are indicative of such a higher density near free surface region (likely of order 1–1.5% denser than bulk) associated with improved local molecular packing arising from the facilitated enhanced mobility present near the free surface. Similarly, we reason that local reductions in mobility near the substrate interface for PMMA and P2VP, correlated with the observed local increases in T_g near silica interfaces for these polymers,[21,69,70] can result in locally less dense regions with poorer molecular packing as the material will locally vitrify at a temperature higher than T_g^{bulk}. The more pronounced gradient in refractive index (3 times larger %grade values) observed for PMMA films compared to PS films is likely reflective of this additional local packing constraint near the silica substrate interface of PMMA films. The more muted gradient observed for P2VP films may be associated with a decoupling of the near free surface and substrate dynamics, as has been suggested for systems with strong interfacial effects like P2VP.[48,86,87]

Since the original submission of this manuscript, a new study investigating the

density of vapor deposited thin films of the molecular glass N,N'-bis(3-methylphenyl)-N,N'-diphenylbenzidine (TPD) has observed the existence of a high density supercooled liquid state that is only present in thin films <60 nm thick.[88] The highest film densities occur at film thicknesses of 30–40 nm where the gradient in dynamics of the liquid cooled glass is the most pronounced. This study suggests that the thin film geometry with its inherent interfaces may facilitate the formation of higher density amorphous states that are not accessible in the bulk.

4.4 Conclusions

In this study, we have explored the use of an ellipsometric optical layer model with a depth-dependent refractive index gradient to model thin polymer films of PMMA, PS and P2VP. Specifically we proposed a gradient linear in the magnitude of the refractive index, Cauchy parameter $A(z)$, with depth. Keeping the wavelength-dependent dispersion relation equivalent to bulk, $n(\lambda) \sim \frac{B}{\lambda^2}$, this adds no additional fitting parameters, but results in more realistic refractive index values for thin films compared to the commonly used homogeneous layer model that leads to large physically unrealistic density and refractive index increases.[8–12,15,16,47] Compared to the results from the homogeneous layer model that showed deviations from bulk for film thicknesses $h \lesssim 40 - 65$ nm,[16] the refractive index values from the linear gradient model remain more bulk-like down to thinner films $h \lesssim 45$ nm for PMMA and $h \lesssim 35$ nm for PS, while P2VP films remain bulk-like for nearly all film thicknesses.

From the ellipsometric fits to the linear gradient model, we demonstrate the presence of a strong positive gradient in the magnitude of refractive index (%grade) for PMMA and PS thin films. At an equivalent film thickness, the gradient for PMMA is found to be three times larger than that for PS, which is likely caused by the additional attractive interactions present between PMMA and the silica substrate.

P2VP films, in contrast, show a refractive index gradient that primarily fluctuates about zero for all film thicknesses, which may reflect a decoupling of free surface and substrate dynamics previously observed for systems with strong interfacial interactions.[48,86,87] Although all data shown are for temperatures $T = T_g^{bulk} + 15$ K in the supercooled equilibrium liquid state, we observe the same gradient in refractive index at temperatures $T = T_g^{bulk} - 45$ K in the nonequilibrium glassy state. This indicates that the structural gradient in refractive index is not the result of some nonequilibrium glassy behavior, but caused by interfacial perturbations to the supercooled equilibrium liquid state and present as a precursor to the glass transition.

Counter to common expectations of a reduced density near the more mobile free surface, we always observe positive %grade values implying a higher refractive index near the free surface and lower refractive index near the substrate interface. Although converting this gradient in refractive index into a density gradient is problematic for inhomogeneous films, the %grade values describing the refractive index gradient are representative of the relative magnitude and direction of a structural gradient in density present in these thin films.[44,45] We can rationalize this observation of a denser near free surface mobile layer by comparing to the formation requirements for stable glasses.[79,80,85] The enhanced mobility near the free surface facilitates more optimal packing of the molecular units leading to a locally more dense region of order 1–1.5% higher than the density of the bulk, that has been proposed to also exist in the supercooled equilibrium liquid state of thin films.[80]

Bibliography

[1] J. A. Forrest, K. Dalnoki-Veress. The glass transition in thin polymer films. *Advances in Colloid and Interface Science* **2001**, *94*, 167–195.

[2] C. B. Roth, J. R. Dutcher. Glass transition and chain mobility in thin polymer films. *Journal of Electroanalytical Chemistry* **2005**, *584*, 13–22.

[3] J. Baschnagel, F. Varnik. Computer simulations of supercooled polymer melts in the bulk and in confined geometry. *Journal of Physics: Condensed Matter* **2005**, *17*, R851.

[4] M. D. Ediger, J. A. Forrest. Dynamics near Free Surfaces and the Glass Transition in Thin Polymer Films: A View to the Future. *Macromolecules* **2013**, *47*, 471–478.

[5] D. S. Simmons. An Emerging Unified View of Dynamic Interphases in Polymers. *Macromolecular Chemistry and Physics* **2016**, *217*, 137–148.

[6] K. S. Schweizer, D. S. Simmons. Progress towards a phenomenological picture and theoretical understanding of glassy dynamics and vitrification near interfaces and under nanoconfinement. *The Journal of Chemical Physics* **2019**, *151*, 240901.

[7] C. B. Roth. Polymers under nanoconfinement: Where are we now in understanding local property changes? *Chemical Society Reviews* **2021**, *50*, 8050–8066.

[8] S. Ata, K. Kuboyama, K. Ito, Y. Kobayashi, T. Ougizawa. Anisotropy and densification of polymer ultrathin films as seen by multi-angle ellipsometry and X-ray reflectometry. *Polymer* **2012**, *53*, 1028–1033.

[9] G. Vignaud, M. S. Chebil, J. K. Bal, N. Delorme, T. Beuvier, Y. Grohens,

A. Gibaud. Densification and Depression in Glass Transition Temperature in Polystyrene Thin Films. *Langmuir* **2014**, *30*, 11599–11608.

[10] A. Beena Unni, G. Vignaud, J. P. Chapel, J. Giermanska, J. K. Bal, N. Delorme, T. Beuvier, S. Thomas, Y. Grohens, A. Gibaud. Probing the Density Variation of Confined Polymer Thin Films via Simple Model-Independent Nanoparticle Adsorption. *Macromolecules* **2017**, *50*, 1027 – 1036.

[11] J. Giermanska, S. B. Jabrallah, N. Delorme, G. Vignaud, J.-P. Chapel. Direct experimental evidences of the density variation of ultrathin polymer films with thickness. *Polymer* **2021**, *228*, 123934.

[12] Y. Li, J. Q. Pham, K. P. Johnston, P. F. Green. Contact Angle of Water on Polystyrene Thin Films: Effects of CO2 Environment and Film Thickness. *Langmuir* **2007**, *23*, 9785–9793.

[13] J. Brandrup, E. H. Immergut, E. A. Grulke, A. Abe, D. H. Bloch (Eds.), *Polymer Handbook 4th ed.*, Wiley: New York, **1999**.

[14] J. N. Hay. Crystallization kinetics of high polymers: Isotactic polystyrene. *Journal of Polymer Science Part A: General Papers* **1965**, *3*, 433–447.

[15] X. Huang, C. B. Roth. Changes in the temperature-dependent specific volume of supported polystyrene films with film thickness. *The Journal of Chemical Physics* **2016**, *144*, 234903.

[16] Y. Han, X. Huang, A. C. W. Rohrbach, C. B. Roth. Comparing refractive index and density changes with decreasing film thickness in thin supported films across different polymers. *The Journal of Chemical Physics* **2020**, *153*, 044902.

[17] J. L. Keddie, R. A. L. Jones, R. A. Cory. Size-Dependent Depression of the Glass Transition Temperature in Polymer Films. *Europhysics Letters* **1994**, *27*, 59–64.

[18] J. L. Keddie, R. A. L. Jones, R. A. Cory. Interface and surface effects on the glass-transition temperature in thin polymer films. *Faraday Discussions* **1994**, *98*, 219.

[19] C. J. Ellison, J. M. Torkelson. The distribution of glass-transition temperatures in nanoscopically confined glass formers. *Nature Materials* **2003**, *2*, 695 – 700.

[20] J. S. Sharp, J. A. Forrest. Free Surfaces Cause Reductions in the Glass Transition Temperature of Thin Polystyrene Films. *Physical Review Letters* **2003**, *91*, 235701.

[21] R. D. Priestley, M. K. Mundra, N. J. Barnett, L. J. Broadbelt, J. M. Torkelson. Effects of Nanoscale Confinement and Interfaces on the Glass Transition Temperatures of a Series of Poly(n-methacrylate) Films. *Australian Journal of Chemistry* **2007**, *60*, 765–771.

[22] R. P. White, J. E. G. Lipson. Dynamics across a Free Surface Reflect Interplay between Density and Cooperative Length: Application to Polystyrene. *Macromolecules* **2021**, *54*, 4136–4144.

[23] J. A. Forrest, K. Dalnoki-Veress, J. R. Dutcher. Brillouin light scattering studies of the mechanical properties of thin freely standing polystyrene films. *Physical Review E* **1998**, *58*, 6109–6114.

[24] R. P. White, J. E. G. Lipson. Thermodynamic treatment of polymer thin-film glasses. *Physical Review E* **2011**, *84*, 041801.

[25] R. P. White, C. C. Price, J. E. G. Lipson. Effect of Interfaces on the Glass Transition of Supported and Freestanding Polymer Thin Films. *Macromolecules* **2015**, *48*, 4132 – 4141.

[26] P. Z. Hanakata, J. F. Douglas, F. W. Starr. Local variation of fragility and glass transition temperature of ultra-thin supported polymer films. *The Journal of Chemical Physics* **2012**, *137*, 244901.

[27] P. Z. Hanakata, B. A. P. Betancourt, J. F. Douglas, F. W. Starr. A unifying framework to quantify the effects of substrate interactions, stiffness, and roughness on the dynamics of thin supported polymer films. *The Journal of Chemical Physics* **2015**, *142*, 234907.

[28] D. M. Sussman, S. S. Schoenholz, E. D. Cubuk, A. J. Liu. Disconnecting structure and dynamics in glassy thin films. *Proceedings of the National Academy of Sciences* **2017**, *114*, 10601 – 10605.

[29] Y. Zhou, S. T. Milner. Short-Time Dynamics Reveals Tg Suppression in Simulated Polystyrene Thin Films. *Macromolecules* **2017**, *50*, 5599–5610.

[30] W. Zhang, F. W. Starr, J. F. Douglas. Reconciling computational and experimental trends in the temperature dependence of the interfacial mobility of polymer films. *The Journal of Chemical Physics* **2020**, *152*, 124703.

[31] D. Hudzinskyy, A. V. Lyulin, A. R. C. Baljon, N. K. Balabaev, M. A. J. Michels. Effects of Strong Confinement on the Glass-Transition Temperature in Simulated Atactic Polystyrene Films. *Macromolecules* **2011**, *44*, 2299–2310.

[32] J. Lipson, S. T. Milner. Percolation model of interfacial effects in polymeric glasses. *The European Physical Journal B* **2009**, *72*, 133.

[33] R. D. Priestley, C. J. Ellison, L. J. Broadbelt, J. M. Torkelson. Structural Relaxation of Polymer Glasses at Surfaces, Interfaces, and In Between. *Science* **2005**, *309*, 456–459.

[34] F. A. Jenkins, H. E. White, *Fundamentals of Optics 2nd ed.*, McGraw-Hill Book Company, New York, **1950**.

[35] H. Fujiwara, *Spectroscopic Ellipsometry: Principles and Applications*, John Wiley & Sons, West Sussex, England, **2007**.

[36] M. Schubert, *Theory and Application of Generalized Ellipsometry* in *Handbook of Ellipsometry*, H. G. Tompkins, E. A. Irene (Eds.), William Andrew Publishing, Springer, Norwich, NY, **2005**, pp. 637 – 717.

[37] R. M. A. Azzam, N. M. Bashara, *Ellipsometry and Polarized Light*, Elsevier Science Publishers, Amsterdam, **1987**.

[38] F. Abelès, *Optical Properties of Inhomogeneous Films* in *Ellipsometry in the Measurement of Surfaces and Thin Films*, E. Passaglia, R. R. Stromberg, J. Kruger (Eds.), National Bureau of Standards Miscellaneous Publication 256, U.S. Government Printing Office, Washington, DC, **1964**, pp. 41 – 58.

[39] D. W. Berreman. Optics in Stratified and Anisotropic Media: 4×4-Matrix Formulation. *Journal of the Optical Society of America* **1972**, *62*, 502.

[40] P. C. S. Hayfield, G. W. T. White, *An Assessment of the Suitability of the Drude-Tronstad Polarised Light Method for the Study of Film Growth on Polycrystalline Metals* in *Ellipsometry in the Measurement of Surfaces and Thin Films*, E. Passaglia, R. R. Stromberg, J. Kruger (Eds.), National Bureau of Standards Miscellaneous Publication 256, U.S. Government Printing Office, Washington, DC, **1964**, pp. 157 – 199.

[41] I. Hughes, T. Hase, *Measurements and their Uncertainties: A practical guide to modern error analysis*, Oxford University Press, New York, **2010**.

[42] M. Born, E. Wolf, *Principles of Optics*, Cambridge University Press, New York, **2006**.

[43] N. W. Ashcroft, N. D. Mermin, *Solid State Physics*, Saunders College Publishing, Philadelphia, **1976**.

[44] S. Y. Larsen, R. D. Mountain, R. Zwanzig. On the Validity of the Lorentz–Lorenz Equation Near the Critical Point. *The Journal of Chemical Physics* **1965**, *42*, 2187–2190.

[45] D. Beysens, P. Calmettes. Temperature dependence of the refractive indices of liquids: Deviation from the Lorentz–Lorenz formula. *The Journal of Chemical Physics* **1977**, *66*, 766–771.

[46] C. M. Herzinger, B. Johs, W. A. McGahan, J. A. Woollam, W. Paulson. Ellipsometric determination of optical constants for silicon and thermally grown silicon dioxide via a multi-sample, multi-wavelength, multi-angle investigation. *Journal of Applied Physics* **1998**, *83*, 3323–3336.

[47] S. E. Root, R. Gao, C. K. Abrahamsson, M. S. Kodaimati, S. Ge, G. M. Whitesides. Estimating the Density of Thin Polymeric Films Using Magnetic Levitation. *ACS Nano* **2021**, 15676–15686.

[48] E. C. Glor, G. V. Angrand, Z. Fakhraai. Exploring the broadening and the existence of two glass transitions due to competing interfacial effects in thin, supported polymer films. *The Journal of Chemical Physics* **2017**, *146*, 203330.

[49] K. Paeng, M. D. Ediger. Molecular Motion in Free-Standing Thin Films of Poly(methyl methacrylate), Poly(4-tert-butyl styrene), Poly(α-methyl styrene), and Poly(2-vinyl pyridine). *Macromolecules* **2011**, *44*, 7034–7042.

[50] K. Paeng, R. Richert, M. D. Ediger. Molecular mobility in supported thin films of polystyrene, poly(methyl methacrylate), and poly(2-vinyl pyridine) probed by dye reorientation. *Soft Matter* **2012**, *8*, 819 – 826.

[51] D. S. Fryer, P. F. Nealey, J. J. de Pablo. Thermal Probe Measurements of the Glass Transition Temperature for Ultrathin Polymer Films as a Function of Thickness. *Macromolecules* **2000**, *33*, 6439–6447.

[52] C. B. Roth, K. L. McNerny, W. F. Jager, J. M. Torkelson. Eliminating the Enhanced Mobility at the Free Surface of Polystyrene: Fluorescence Studies of the Glass Transition Temperature in Thin Bilayer Films of Immiscible Polymers. *Macromolecules* **2007**, *40*, 2568–2574.

[53] M. K. Mundra, S. K. Donthu, V. P. Dravid, J. M. Torkelson. Effect of spatial confinement on the glass-transition temperature of patterned polymer nanostructures. *Nano Letters* **2007**, *7*, 713 – 718.

[54] X. Huang, C. B. Roth. Optimizing the Grafting Density of Tethered Chains to Alter the Local Glass Transition Temperature of Polystyrene near Silica Substrates: The Advantage of Mushrooms over Brushes. *ACS Macro Letters* **2018**, *7*, 269 – 274.

[55] X. Huang, M. F. Thees, W. B. Size, C. B. Roth. Experimental study of substrate roughness on the local glass transition of polystyrene. *The Journal of Chemical Physics* **2020**, *152*, 244901.

[56] T. Kerle, Z. Lin, H.-C. Kim, T. P. Russell. Mobility of Polymers at the Air/Polymer Interface. *Macromolecules* **2001**, *34*, 3484–3492.

[57] Z. Fakhraai, J. A. Forrest. Measuring the Surface Dynamics of Glassy Polymers. *Science* **2008**, *319*, 600–604.

[58] D. Qi, C. R. Daley, Y. Chai, J. A. Forrest. Molecular weight dependence of near surface dynamical mechanical properties of polymers. *Soft Matter* **2013**, *9*, 8958 – 8964.

[59] J. E. Pye, K. A. Rohald, E. A. Baker, C. B. Roth. Physical aging in ultrathin polystyrene films: Evidence of a gradient in dynamics at the free surface and its connection to the glass transition temperature reductions. *Macromolecules* **2010**, *43*, 8296 – 8303.

[60] M. F. Thees, C. B. Roth. Unexpected Molecular Weight Dependence to the Physical Aging of Thin Polystyrene Films Present at Ultra-High Molecular Weights. *Journal of Polymer Science Part B: Polymer Physics* **2019**, *57*, 1224–1238.

[61] B. Frieberg, E. Glynos, P. F. Green. Structural Relaxations of Thin Polymer Films. *Physical Review Letters* **2011**, *108*, 268304.

[62] K. Paeng, S. F. Swallen, M. D. Ediger. Direct Measurement of Molecular Motion in Freestanding Polystyrene Thin Films. *Journal of the American Chemical Society* **2011**, *133*, 8444–8447.

[63] C. B. Roth, J. R. Dutcher. Glass transition temperature of freely-standing films of atactic poly(methyl methacrylate). *The European Physical Journal E* **2003**, *12*, 103–107.

[64] C. B. Roth, A. Pound, S. W. Kamp, C. A. Murray, J. R. Dutcher. Molecular-weight dependence of the glass transition temperature of freely-standing poly(methyl methacrylate) films. *The European Physical Journal E* **2006**, *20*, 441–448.

[65] K. Geng, O. K. C. Tsui. Effects of Polymer Tacticity and Molecular Weight on the Glass Transition Temperature of Poly(methyl methacrylate) Films on Silica. *Macromolecules* **2016**, *49*, 2671–2678.

[66] Y. Grohens, M. Brogly, C. Labbe, M.-O. David, J. Schultz. Glass Transition of Stereoregular Poly(methyl methacrylate) at Interfaces. *Langmuir* **1998**, *14*, 2929–2932.

[67] Y. Grohens, L. Hamon, G. Reiter, A. Soldera, Y. Holl. Some relevant parameters affecting the glass transition of supported ultra-thin polymer films. *The European Physical Journal E* **2002**, *8*, 217–224.

[68] S. E. Harton, S. K. Kumar, H. Yang, T. Koga, K. Hicks, H. Lee, J. Mijovic, M. Liu, R. S. Vallery, D. W. Gidley. Immobilized Polymer Layers on Spherical Nanoparticles. *Macromolecules* **2010**, *43*, 3415–3421.

[69] A. P. Holt, P. J. Griffin, V. Bocharova, A. L. Agapov, A. E. Imel, M. D. Dadmun, J. R. Sangoro, A. P. Sokolov. Dynamics at the Polymer/Nanoparticle Interface in Poly(2-vinylpyridine)/Silica Nanocomposites. *Macromolecules* **2014**, *47*, 1837–1843.

[70] T. Wei, J. M. Torkelson. Molecular Weight Dependence of the Glass Transition Temperature (Tg)-Confinement Effect in Well-Dispersed Poly(2-vinyl pyridine)–Silica Nanocomposites: Comparison of Interfacial Layer Tg and Matrix Tg. *Macromolecules* **2020**, *53*, 8725–8736.

[71] C. H. Park, J. H. Kim, M. Ree, B.-H. Sohn, J. C. Jung, W.-C. Zin. Thickness and composition dependence of the glass transition temperature in thin random copolymer films. *Polymer* **2004**, *45*, 4507–4513.

[72] J. H. van Zanten, W. E. Wallace, W.-L. Wu. Effect of strongly favorable substrate interactions on the thermal properties of ultrathin polymer films. *Physical Review E* **1996**, *53*, R2053–R2056.

[73] R. P. White, J. E. G. Lipson. Polymer Free Volume and Its Connection to the Glass Transition. *Macromolecules* **2016**, *49*, 3987–4007.

[74] C. Bollinne, V. W. Stone, V. Carlier, A. M. Jonas. Density Perturbations in Polymers Near a Solid Substrate: An X-ray Reflectivity Study. *Macromolecules* **1999**, *32*, 4719–4724.

[75] A. Beena Unni, K. Chat, K. Balin, K. Adrjanowicz. Connecting the density distribution and segmental dynamics of confined polymer films. *Nano-Structures & Nano-Objects* **2020**, *23*, 100519.

[76] A. van der Lee, L. Hamon, Y. Holl, Y. Grohens. Density Profiles in Thin PMMA Supported Films Investigated by X-ray Reflectometry. *Langmuir* **2001**, *17*, 7664–7669.

[77] F. Hynne, R. K. Bullough. The Scattering of Light II. The Complex Refractive Index of a Molecular Fluid. *Philosophical Transactions of the Royal Society of London. Series A, Mathematical and Physical Sciences* **1987**, *321*, 305–360.

[78] S. F. Swallen, K. L. Kearns, M. K. Mapes, Y. S. Kim, R. J. McMahon, M. D. Ediger, T. Wu, L. Yu, S. Satija. Organic Glasses with Exceptional Thermodynamic and Kinetic Stability. *Science* **2007**, *315*, 353–356.

[79] M. D. Ediger. Perspective: Highly stable vapor-deposited glasses. *The Journal of Chemical Physics* **2017**, *147*, 210901.

[80] J. H. Mangalara, M. D. Marvin, D. S. Simmons. Three-Layer Model for the Emergence of Ultrastable Glasses from the Surfaces of Supercooled Liquids. *The Journal of Physical Chemistry B* **2016**, *120*, 4861–4865.

[81] S. S. Dalal, M. D. Ediger. Molecular Orientation in Stable Glasses of Indomethacin. *The Journal of Physical Chemistry Letters* **2012**, *3*, 1229–1233.

[82] M. S. Beasley, C. Bishop, B. J. Kasting, M. D. Ediger. Vapor-Deposited Ethyl-

benzene Glasses Approach "Ideal Glass" Density. *The Journal of Physical Chemistry Letters* **2019**, *10*, 4069–4075.

[83] K. L. Kearns, T. Still, G. Fytas, M. D. Ediger. High-Modulus Organic Glasses Prepared by Physical Vapor Deposition. *Advanced Materials* **2010**, *22*, 39–42.

[84] H. Yoon, Y. P. Koh, S. L. Simon, G. B. McKenna. An Ultrastable Polymeric Glass: Amorphous Fluoropolymer with Extreme Fictive Temperature Reduction by Vacuum Pyrolysis. *Macromolecules* **2017**, *50*, 4562–4574.

[85] A. N. Raegen, J. Yin, Q. Zhou, J. A. Forrest. Ultrastable monodisperse polymer glass formed by physical vapour deposition. *Nature Materials* **2020**, *19*, 1110–1113.

[86] R. J. S. Ivancic, R. A. Riggleman. Dynamic phase transitions in freestanding polymer thin films. *Proceedings of the National Academy of Sciences* **2020**, *117*, 25407–25413.

[87] W. Zhang, J. F. Douglas, F. W. Starr. Effects of a "bound" substrate layer on the dynamics of supported polymer films. *The Journal of Chemical Physics* **2017**, *147*, 044901.

[88] Y. Jin, A. Zhang, S. E. Wolf, S. Govind, A. R. Moore, M. Zhernenkov, G. Freychet, A. A. Shamsabadi, Z. Fakhraai. Glasses denser than the supercooled liquid. *Proceedings of the National Academy of Sciences* **2021**, *118*, e2100738118.

Chapter 5

Characterizing the Temperature Dependence of Perylene Doped in Various Polymer Matrices

5.1 Introduction

The nature of the glass transition remains an unresolved problem, in particular the mechanisms behind the drastic slowing down of the dynamics over a relative short temperature range in the supercooled regime approaching the glass transition.[1–4] To study the glass transition in the homogeneous and bulk state, efforts have been made to correlate physical properties of the material such as viscosity, modulus and density, to the growing size of cooperative motion that is required for rearrangements to occur as the temperature decreases.[5] For the past two and half decades, polymer thin films have been extensively studied to enlighten the underlying mechanisms of the glass transition in bulk system, due to the profound alteration of the dynamics in the presence of interfaces.[6,7] The major open question in the polymer thin film field is the nature of the spatial gradients in dynamical and material properties near

the interfaces.[8] Such spatially distributed dynamical gradients have been observed in various polymers by different experimental methods.[6,7] Nevertheless, the mechanisms and the key lengthscales of the interfacial perturbations propagating into the film are yet not well understood. To characterize how different material properties change in nanoconfined systems, there is a need to develop new methods to measure local properties to construct a picture of the spatial variations in material properties of polymer thin films under nanoconfinement. In particular, a probe for local mobility at the molecular or segmental level would contribute to the understanding of shifts in dynamics in polymer thin films.

Fluorescence probes have been used to characterize changes in polymeric properties due to the probe's sensitivity to various parameters of its local environment (e.g. temperature, viscosity, polarity and pressure),[9] via changes in the fluorescence emission. One group of fluorescence probes exhibits changes in the emission spectrum reflecting changes in the vibronic band structure due to the probe's local environment. Pyrene has been widely used as an indicator of polarity (py-scale) in solutions.[9] The most well-known example of the use of pyrene to characterize polymer thin films is using pyrene covalently attached to the polymer backbone to measure the local glass transition temperature T_{g}.[10] The different temperature dependence of the emission intensity of pyrene's first peak can be attributed to the changes in the local density and polarity that alter the rate of nonradiative decay.[11] Similar sensitivity to local molecular caging around pyrene molecules has been employed to probe changes in local stiffness in polymer thin films.[12,13] The relative intensities between the first and third vibronic bands increases in a more caged environment (stiffer) as the higher energy transition is more preferential through the dipole-dipole coupling between pyrene and surrounding molecules.[14] The other group of probes exploits the rotational or translational motion of the dye to interpret the local mobility of polymer matrices. Reorientation of the fluorophore measured by fluorescence anisotropy has been used

to probe the mobility and the lengthscale of the more mobile surface region in polymer thin films.[15–17] Similarly, the segmental dynamics of the polymer near polymer interface has been characterized by the rotational motion of the probe tethered to the polymer chains.[18,19] Translational diffusion perpendicular to the substrate[20] and parallel to the substrate[21–23] have also been studied.

Perylene, as one of the polycyclic aromatic hydrocarbon fluorophores, has been reported to have good thermal stability at high temperature, as well as a high quantum yield in fluorescence emission,[24]making it an ideal choice as a molecular probe of polymer thin films. Perylene incorporated in polymer binders has been used as temperature-sensitive paints (TSP) for real-time monitoring of the surface temperature distribution in the aerodynamics community.[25,26] A dual-component molecular thermometer consisting of perylene and another non-emissive molecule was reported to show ratiometric variation upon changes in temperature, due to the change in the shape of the emission spectrum via the exciplex formation between the two components.[27] Bur et al. have measured emission spectra at different temperatures for perylene doped in polycarbonate (PC), where they found that the intensity ratio of the second peak to the first trough shows a linear dependence on temperature.[24] Due to this linear temperature dependence, perylene has been used as a molecular thermometer, as reported in a later study where perylene was doped in poly(acrylonitrile) (PAN) to monitor temperature perturbations from embedded metal nanoparticles.[28] Nevertheless, the mechanism of the temperature dependence of perylene and how the temperature dependence of perylene is influenced by the embedded polymer matrices is little studied.

Temperature is an important intensive parameter that strongly impacts the dynamics of polymers, as well as the emission of fluorophore embedded in the polymer matrices. When the electrons of a fluorophore at the higher energy excited states return to the ground state, the excess energy will be dissipated either through a ra-

diative transition (fluorescence) or a nonradiative transition (e.g. vibration relaxation and collision with surrounding molecules).[9] The rate of nonradiative decay increases with increasing temperature, leading to a suppression of fluorescence emission and a decrease in the emission intensity. Therefore, monitoring the emission intensity as a function of temperature can provide an indirect probe of the nonradiative decay rate which can then be correlated with the dynamics of the surrounding polymer matrices.

In the present work, we investigate the temperature dependence of perylene doped in various polymer matrices and assess the impact of the physical properties of the surrounding polymers. We find a temperature-invariant region in the emission spectrum collected at different temperatures, which we name as the self-referencing region (SRR). Normalizing to this self-referencing region provides an internal correcction for fluctuations in the excitation intensity when characterizing the temperature dependence of the emission spectrum. The temperature dependence of the intensity ratio between the first peak I_{Peak} and SRR I_{SRR} is reproducible for a given polymer. We find that the temperature dependence of this intensity ratio $I_{\mathrm{Ratio}}(T)$ reflects the temperature dependent dynamics of the surrounding polymer matrix. The temperature dependent nonradiative decay process can be viewed as an activated process, and we define a fluorescence intensity "shift factor" a_T for the emission intensity ratio $I_{\mathrm{Ratio}}(T)$ with respect to that at the reference temperature T_{ref}, in analogy to the shift factor a_T in the Williams-Landel-Ferry (WLF) equation. We find that the trend of $\log(a_T)$ vs $1000(1/T - 1/T_{\mathrm{ref}})$ shows a non-Arrhenius behavior in the supercooled liquid regime above $T_{\mathrm{g}}^{\mathrm{bulk}}$, suggesting that the nonradiative decay process is influenced by the cooperative α-relaxations of the surrounding polymer segments. In contrast, in the glassy regime below $T_{\mathrm{g}}^{\mathrm{bulk}}$ when cooperative motion arrests, the nonradiative decay follows a simple Arrhenius trend with a constant activation energy, consistent with the local β-relaxation.

5.2 Experimental methods

Polystyrene (PS) with molecular weight $M_w = 650$ kg/mol, $M_w/M_n = 1.06$ from Pressure Chemical, poly(methyl methacrylate) (PMMA) with $M_w = 815$ kg/mol, $M_w/M_n = 1.09$, poly(2-vinyl pyridine) (P2VP) with $M_w = 650$ kg/mol, $M_w/M_n = 1.08$ and polycarbonate (PC) with $M_w = 28$ kg/mol, $M_w/M_n = 1.66$ from Scientific Polymer Products were used as received. Polymer solutions were prepared by dissolving PS or PMMA in toluene, P2VP in butanol and PC in 1,1,2-trichloroethane. Perylene (Aldrich) was doped into polymer solutions at trace levels (0.15 wt%) to prevent the formation of excimer at high concentrations. Polymer films were made by spin-coating polymer solutions onto 25 mm × 25 mm × 3.7 mm fused silica (SCHOTT) for fluorescence measurements and 20 mm × 20 mm silicon wafers (Wafernet) for film thickness measurements.

Film thicknesses of the polymer films were measured by spectroscopic ellipsometry (Woollam M-2000). Raw $\Psi(\lambda)$ and $\Delta(\lambda)$ data for $\lambda = 400 - 1000$ nm were fit to an optical layer model to obtain the film thickness. The optical layer model consisted of a transparent Cauchy layer, $n(\lambda) = A + B/\lambda^2$ for the polymer film and a 1.25-nm-thick native oxide layer atop a semi-infinite silicon substrate. Film thicknesses of the films spin-coated on fused silica were assumed to be the same as that spin-coated on silicon wafers at identical spin speeds and solution concentrations. Bulk T_g values were determined by ellipsometry measurements of the temperature dependent film thickness $h(T)$ on cooling at 1 K/min, where values of T_g^{bulk} are 96 °C for PS, 115 °C for PMMA, 94 °C for P2VP and 145 °C for PC.

Steady state fluorescence spectra were acquired by a Photon Technology International QuantaMaster spectrometer. Samples were covered by a clear quartz piece with the same dimension as the fused silica substrate to limit oxygen quenching and sublimation of the fluorophore. The doped perylene was excited at 390 nm for PMMA and 394 nm for PS, P2VP and PC via a xenon arc lamp with an excitation bandpass

of 3 nm and an emission bandpass of 5 nm. All films were annealed on the fluorometer heater (Instec HCS402) at T_g^{bulk} + 35 K for 20 min to remove thermal history and facilitate relaxation. Emission spectra at different temperatures were collected on cooling at different temperatures. Full emission spectra (425-525 nm) were collected at T_g^{bulk} + 35 K, T_g^{bulk}- 5 K and T_g^{bulk} − 45 K with respect to T_g^{bulk} of each polymer. Shorter spectra focused on the first peak and the self-referencing region (SRR) were collected between T_g^{bulk} + 35 K and T_g^{bulk} − 45 K in increments of 2 K and 10 K. The span of this shorter spectrum was 15 nm where the specific wavelength range varied slightly depending on the polymer matrix. The system was always cooled at 2 K/min between temperature settings. All samples were reheated to the initial temperature to guarantee the initial emission intensity was recovered, verifying no photobleaching occurred during the course of the experiment.

5.3 Results and discussion

We start by comparing the emission spectrum of perylene doped into various polymer matrices in the glassy state at a consistent temperature that is 45 K below the bulk glass transition temperature T_g^{bulk}. Figure 5.1 demonstrates the normalized emission intensity as a function of wavelength for four bulk polymer films: PS (h = 360 nm), PMMA (h = 282 nm), P2VP (h = 262 nm) and PC (h = 541 nm). The emission spectra were normalized to the interval of [0,1] based on the intensity of the first peak for comparison. Comparison of the emission spectra across different polymers shows similar emission spectra in general with small variations in peak locations and relative intensity of the peaks. PS and PC show similar spectral structure with the first, second and third peak located at $\sim$ 445, 475 and 507 nm, respectively. In contrast, the spectrum of PMMA exhibits a blue shift of $\sim$4 nm with respect to PS and PC, while the spectrum of P2VP exhibits a red shift of $\sim$2 nm. Such blue

and red shifts result from differences in polarity of the polymer matrices. With the intensity of the first peak normalized to 1, we observe small varaitions in the relative intensities of the rest of the peaks. PMMA and PS share similar magnitude of the peaks, which is slightly lower than the strength of the peaks that are similar between P2VP and PC. The difference in the relative strength between the peaks suggest small changes are occurring in the vibronic bands of perylene, reflecting perturbations to the intramolecular vibrations by the surrounding polymers.

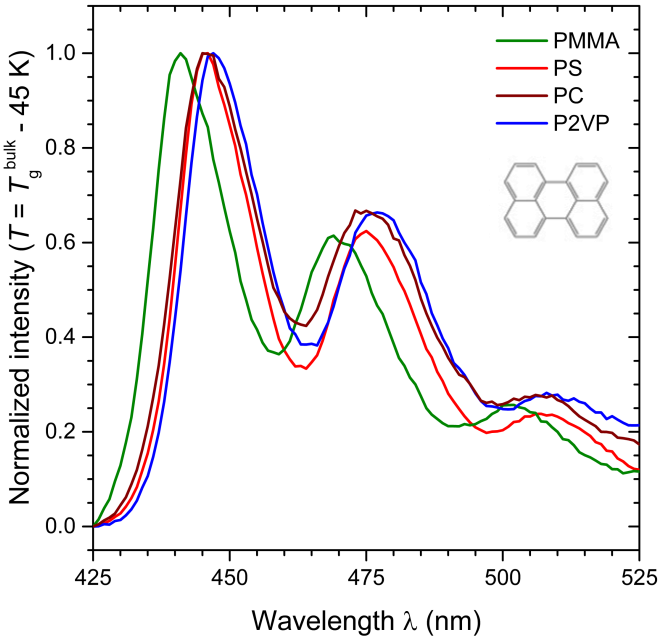

Figure 5.1: Normalized emission intensity as a function of wavelength for perylene doped (0.15 wt%) bulk polymer films: PS (red), PMMA (green), P2VP (blue) and PC (brown) in the glassy state ($T = T_g^{bulk} - 45$ K). The perylene probe is excited at 390 nm for PMMA and 394 nm for PS, P2VP and PC. Emission intensities are normalized to between [0,1]. Inset shows the chemical structure of perylene.

To investigate the temperature dependence of perylene doped in polymer matrices, emission spectra were collected at three different temperatures in distinct regimes with respect to T_g^{bulk}: high temperature at $T_g^{bulk} + 35$ K deep in the equilibrium liquid regime, medium temperature at $T_g^{bulk} - 5$ K near the glass transition and low temperature at $T_g^{bulk} - 45$ K deep in the glassy regime. Figure 5.2 shows the emission intensity as a function of wavelength for perylene doped in bulk polymer

films (same samples as in Fig. 5.1) at different temperatures. The trend in shifts with temperature to the spectra is similar for all four polymers, where the magnitude of the first and second peak increases with decreasing temperature and the magnitude of the first trough decreases with decreasing temperature. The increase in overall emission intensity with decreasing temperature can be explained by the decrease in nonradiative decay rate at lower temperatures.

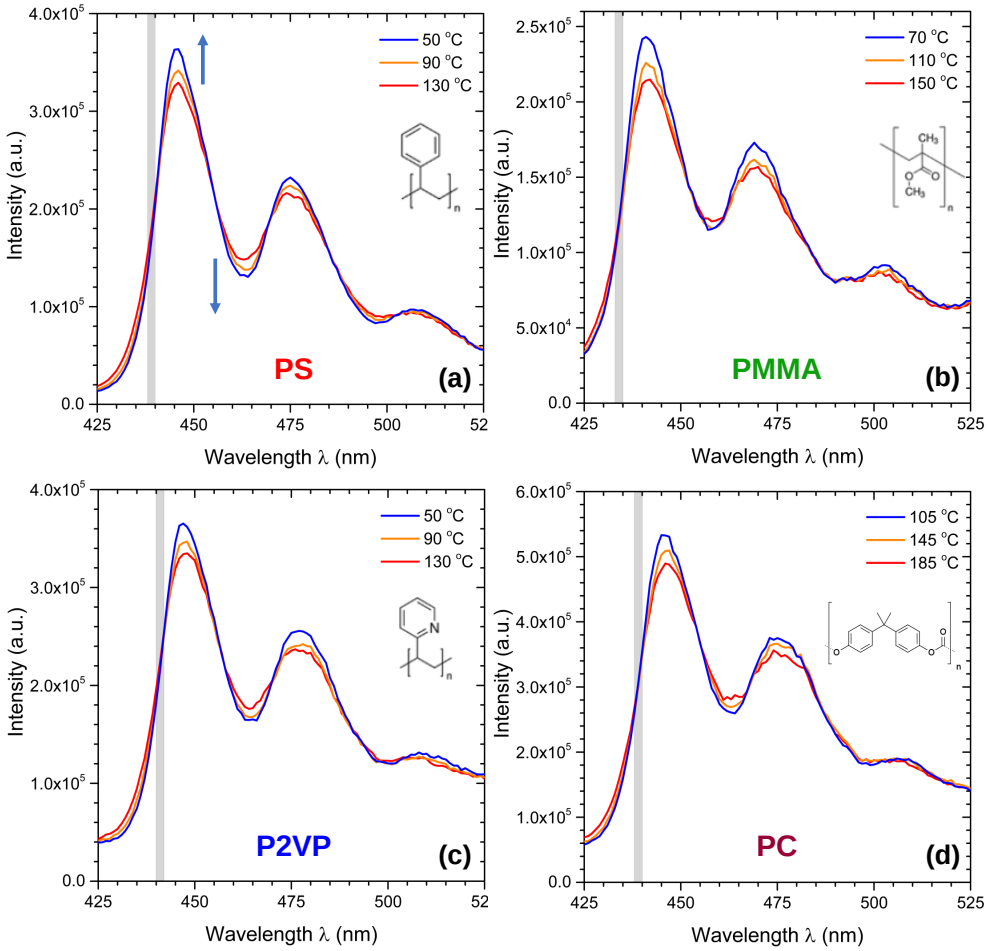

Figure 5.2: Emission intensity as a function of wavelength at different temperatures (high temperature: red lines / T_g^{bulk} + 35 K, medium temperature: orange lines / T_g^{bulk}- 5 K and low temperature: blue lines / T_g^{bulk} − 45 K) for perylene doped in bulk polymer films: (a) PS, (b) PMMA, (c) P2VP and (d) PC. Self-referencing region (SRR) is represented by the light gray bar, indicating the part of the spectrum that is invariant at different temperatures. Blue arrows represent the shifts in the spectra with decreasing temperature. Inset shows the corresponding chemical structures of the polymers.

One interesting feature of the temperature dependent spectra is that the spectrum does not shift uniformly as the temperature changes. Instead, some locations of the spectrum move in the opposite direction to that of the peaks, resulting in regions where the intensity is invariant as temperature changes. We named the temperature invariant region to the left of the first peak as the self-referencing region (SRR) and use it to account for the overall magnitude of the spectrum which can be subject to perturbations (e.g. fluctuations in excitation light intensity), not reflective of changes in temperature. Therefore, the intensity ratio between the intensity of the first peak I_{Peak} and the intensity of SRR I_{SRR},

$$I_{\text{ratio}} = \frac{I_{\text{Peak}}}{I_{\text{SRR}}} \ , \tag{5.1}$$

would be less influenced by the fluctuations in excitation light intensity, compared to solely measuring the peak intensity I_{Peak}. In practice, we find that for bulk films with different film thicknesses, the SRR for a given polymer consistently falls within a span of 2 nm on the wavelength axis, which we defined as the width of the SRR, confirming that the existence of the SRR is a characteristic feature of perylene doped in the polymer matrices. The locations of the SRR are represented by gray bars in the figure. In contrast to the uniform width of the SRR, the location of the SRR depends on the specific polymer matrix that perylene is doped into. Specifically, SRR is located at 438-400 nm for PS, 433-435 nm for PMMA, 440-442 nm for P2VP and 438-440 nm for PC. The relative locations of the SRRs for the different polymers agree with the red and blue shifts of the emission spectrum, suggesting that the SRR is a fundamental feature of the perylene emission spectrum while the location of the SRR is altered by the polarity of the surrounding polymer matrices that shift the emission spectrum.

Now we examine more closely how the spectrum of perylene doped in polymer ma-

trices changes relative to the SRR at various temperatures. To minimize the amount exposure to the excitation light and reduce photobleaching, a short wavelength range (span = 15 nm) that includes the SRR and the first peak is selected instead of the full spectrum scan (span = 100 nm). The exact range of the short emission scan varies with the specific positions of the first peak and SRR of the polymer, with a fixed span of 15 nm. With this reduced range of emission scan, the temperature dependence can be characterized at a finer resolution (e.g. every 10 K) than the high / medium / low temperature settings shown in Fig. 5.2. The short wavelength range emission spectra were acquired every 10 K during cooling from T_g^{bulk} + 35 K to T_g^{bulk} − 45 K at a cooling rate of 2 K/min. No noticeable photobleaching was observed after the reheat to the initial temperature for samples measured following this procedure. Figure 5.3 demonstrates the emission spectra (431 - 446 nm) of a 444-nm-thick PMMA film measured at different temperatures upon cooling. The emission spectra collected from high temperature (T_g^{bulk} + 35 K) to low temperature (T_g^{bulk} − 45 K) are graphed in varying colors from red to green, with the SRR at 434 nm and the peak at 441 nm. With decreasing temperature, the intensity at SRR I_{SRR} remains invariant, while the intensity at the peak I_{Peak} increases monotonically. We are interested in the temperature dependence of the peak to SRR ratio for different polymers. Such intensity ratio I_{Peak}/I_{SRR} could be informative of the physical properties of the polymer matrices around the perylene probe dye. For instance, ratiometric measurements have been reported that the intensity ratio between the second peak and the first trough of the perylene spectrum changes linearly with temperature.[24,28] Due to our selection of the first peak and the SRR, the temperature dependence of the ratio I_{Peak}/I_{SRR} could be different than those reported in the literature, revealing different local properties than simply a temperature dependence.

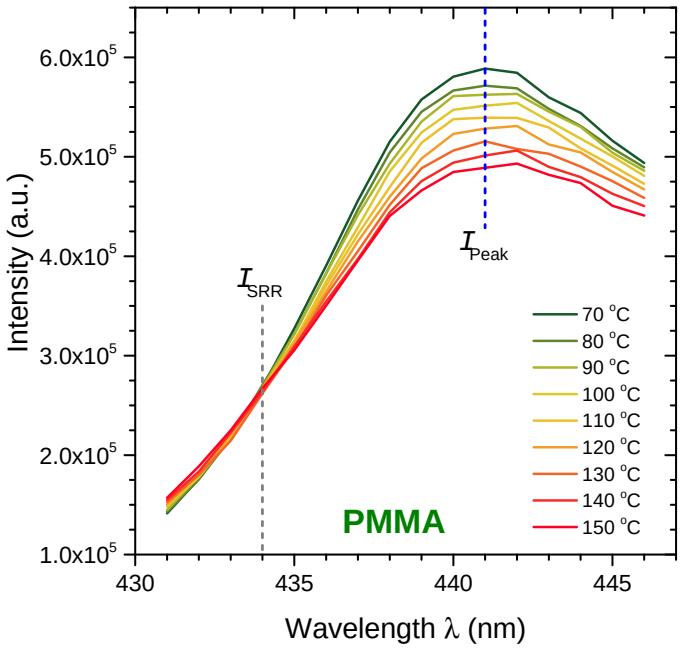

Figure 5.3: Emission spectra at different temperatures for perylene doped in a bulk PMMA film ($h = 444$ nm). The emission spectra were collected at every 10 K from T_g^{bulk} +35 K to T_g^{bulk} − 45 K on cooling at 2 K/min. The locations of the SRR and the first peak are 434 nm and 441 nm, respectively.

To further characterize the temperature dependence of the I_{Peak}/I_{SRR} intensity ratio, we reduce the step size of the temperature ramp from 10 K to 2 K to increase the number of data points. Following this procedure, the short emission spectrum (span = 15 nm) that includes the first peak and the SRR were measured every 2 K on cooling from T_g^{bulk} + 35 K to T_g^{bulk} − 45 K with 2 K/min cooling rate between temperature steps. The intensity ratio I_{Ratio} (Eqn.5.1) is calculated as the peak intensity (averaged over ±1 nm range) divided by the intensity at SRR. Figure 5.4 graphs the intensity ratio I_{Ratio} as a function of temperature for bulk films of different polymers. Representative datasets are shown as solid symbols while the shaded area demonstrates the sample-to-sample variability for nominally identical samples. For all four polymers, the intensity ratio of the perylene probe shows similar trend with temperature, where I_{Ratio} decreases with increasing temperature monotonically. The intensity ratio trends are reproducible for bulk films of the same polymer, where the

reference to I_{SRR} can account for any fluctuations in the emission intensity of I_{Peak}. Such good reproducibility of I_{Ratio} suggests that the temperature dependence of the perylene probe results from the perturbation by the surrounding polymer matrix. To quantify the differences in the temperature dependent trends between polymers, we apply linear fits to the trends as a first order approximation. We find that the slopes and the intercepts of the linear fits vary depending on the polymer matrix. The values of the slopes of the linear trends are -0.00477 for PS, -0.00310 for PMMA, -0.00153 for P2VP and -0.00171 for PC. Comparing the slopes of the temperature dependence between different polymers, the slopes for P2VP and PC are similar and the slope of PMMA is roughly twice of that for P2VP, while the slope of PS is roughly three times of that for P2VP. To compare the intercepts of the linear fits without extrapolation, we compare the magnitude of I_{Ratio} at the same temperature ($T = 120\ ^{\circ}\mathrm{C}$) for different polymers. The values of $I_{\mathrm{Ratio}}(T = 120\ ^{\circ}\mathrm{C})$ are 1.895 for PS, 1.797 for PMMA, 1.680 for PC, and 1.366 for P2VP. It is interesting that polymers with larger slopes tend to have a larger magnitude of I_{Ratio} at a given temperature.

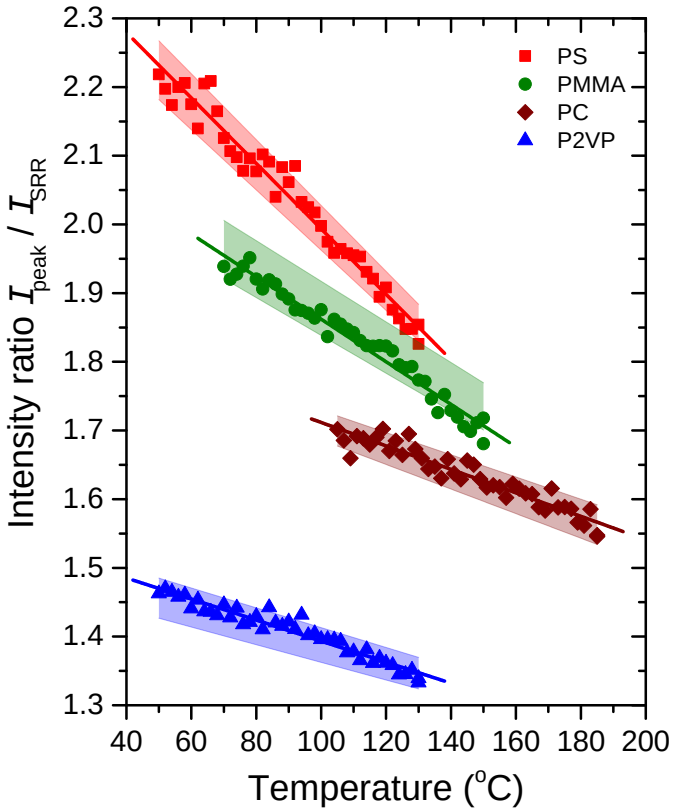

Figure 5.4: Temperature dependence of intensity ratio $I_{\mathrm{Ratio}} = I_{\mathrm{Peak}}/I_{\mathrm{SRR}}$ for bulk films of different polymers: PS (red), PMMA (green), PC (brown), and P2VP (blue). Representative datasets are shown as solid symbols with corresponding linear fits. Shaded areas demonstrate the sample-to-sample variability of nominally identical samples.

Now we investigate the mechanism behind the different temperature dependences of the intensity ratio I_{Ratio} in different polymers. Fundamentally, the decrease in the emission intensity at high temperature results from the more preferential nonradiative pathway via intramolecular vibrations and intermolecular collisions with the neighbouring polymer matrices. Therefore, the temperature dependence of the emission intensity ratio can be described by the temperature dependence of the rate of nonradiative decay. Such rate parameters represent the probability of a certain electronic transition occurring under a given condition. The efficiency of the fluorophore, quantum yield Φ, is defined as the ratio of the emission light intensity I_{F} to the excitation light intensity I_{E}, $\Phi = \frac{I_{\mathrm{F}}}{I_{\mathrm{E}}}$.[9] The quantum yield Φ can also be written as

the ratio of the rate parameters $\Phi = \frac{k_R}{k_R + k_{NR}}$, where k_R is the rate of radiative decay (fluorescence emission) and k_{NR} is the rate of nonradiative decay.[9] Previous studies have shown that the temperature dependence of the nonradiative decay rate k_{NR} can be treated as a sum of a temperature invariant part k_0 and a temperature dependent part k_1, where k_1 has often been shown to follow an Arrhenius activated process, $k_1 = A\ \exp(-E/kT)$,[25,29,30] where A a prefactor, E is the activation energy of the nonradiative decay, k is Boltzmann's constant and T is the absolute temperature,

$$k_{NR} = k_0 + k_1 = k_0 + A\ \exp(-E/kT)\ . \tag{5.2}$$

By incorporating the temperature dependent nonradiative decay rate k_{NR}, the I_E to $I_F(T)$ can be written as

$$\frac{I_E}{I_F(T)} = \frac{k_R + \left[k_0 + A\ \exp(-\frac{E}{kT})\right]}{k_R}\ . \tag{5.3}$$

Subtracting $\frac{I_E}{I_F(0)}$ at $T = 0$ to cancel the temperature invariant parts, a pure temperature dependent term $\Omega(T)$ can be obtained:[25,26]

$$\Omega(T) = I_E\ \frac{I_F(0) - I_F(T)}{I_F(0) I_F(T)} = \frac{A}{k_R}\ \exp(-\frac{E}{kT})\ . \tag{5.4}$$

The ratio $\Omega(T_{ref})/\Omega(T)$ is expressed by:

$$\frac{\Omega(T_{ref})}{\Omega(T)} = \frac{I_F(0) - I_F(T_{ref})}{I_F(0) - I_F(T)} \cdot \frac{I(T)}{I(T_{ref})} = \exp\left[\frac{E}{k}\left(\frac{1}{T} - \frac{1}{T_{ref}}\right)\right]\ , \tag{5.5}$$

where the term $\frac{I_F(0) - I_F(T_{ref})}{I_F(0) - I_F(T)}$ can be approximated as 1 when T does not deviate too far from the reference temperature T_{ref}.[25,26] Therefore, the fluorescence intensity relative

to that at a reference temperature can be written in an Arrhenius form,[25,26]

$$\log\left[\frac{I(T)}{I(T_{\mathrm{ref}})}\right] = \frac{E}{k}\left(\frac{1}{T} - \frac{1}{T_{\mathrm{ref}}}\right) \ . \tag{5.6}$$

When we graph the temperature dependence of $I_{\mathrm{Ratio}}(T)$ in this form, we find that the activation energy E of the nonradiative decay is not simply a temperature invariant constant, but instead it is modified by the mobility of the neighbouring polymer segments which change with temperature. In analogy with WLF equation that treats the non-Arrhenius behavior in the supercooled liquid regime as a temperature dependent activation energy $E(T)$,[31] we define a fluorescence intensity "shift factor" a_T similar to the WLF equation with respect to a reference temperature T_{ref}, based on the intensity ratio I_{Ratio},

$$\log(a_T) = \log\left[\frac{I_{\mathrm{Ratio}}(T)}{I_{\mathrm{Ratio}}(T_{\mathrm{ref}})}\right] = \frac{E}{k}\left(\frac{1}{T} - \frac{1}{T_{\mathrm{ref}}}\right) \ . \tag{5.7}$$

To compare with literature parameters for the bulk WLF dependence, we select T_{ref} as the bulk T_{g} of each of the polymers. For the temperature range in the present work, T does not deviate too far from $T_{\mathrm{g}}^{\mathrm{bulk}}$, so that the approximation $\frac{I_{\mathrm{F}}(0)-I_{\mathrm{F}}(T_{\mathrm{ref}})}{I_{\mathrm{F}}(0)-I_{\mathrm{F}}(T)} = 1$ is still valid. The temperature dependent $\log(a_T)$ for bulk PMMA films is graphed as a function of $1/T - 1/T_{\mathrm{ref}}$ in Figure 5.5, where a representative dataset is shown in green circles and grey circles demonstrate the sample-to-sample variability of nominally identical samples. The temperature dependence of $\log(a_T)$ does not follow a simple Arrhenius trend which is a linear trend vs $1/T$. Instead, it follows the bulk WLF dependence in the region above $T_{\mathrm{g}}^{\mathrm{bulk}}$ and transitions into a simple Arrhenius trend in the region below $T_{\mathrm{g}}^{\mathrm{bulk}}$. The bulk WLF parameters for PMMA we used in this study were $T_{\mathrm{ref}} = 393$ K, $C_1 = 34$, and $C_2 = 80$, obtained from Reference 32. We note here that the slope of $\log(a_T)$ versus $\left(\frac{1}{T} - \frac{1}{T_{\mathrm{ref}}}\right)$ is proportional to the activation energy of the nonradiative decay process according to the definition of a_T (Eqn.5.7).

We observed that the transition from a curve following bulk the WLF dependence to a linear trend occurs at $T = T_{\mathrm{g}}^{\mathrm{bulk}}$. This transition point is independent of the choice of T_{ref}, where we have tested various choices of T_{ref} and found no changes to the transition point that always occurs at T_{g}. Given that the nonradiative decay process can reflect dynamics of the surrounding polymer matrix, we will next investigate the correlation between nonradiative decay rate and the local polymer dynamics by comparing $\log(a_T)$ vs $1/T - 1/T_{\mathrm{ref}}$ for different polymers.

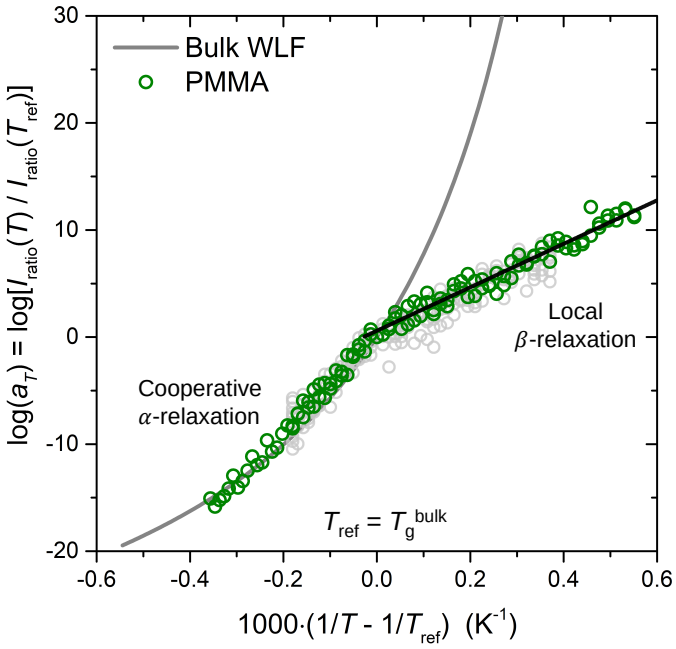

Figure 5.5: Temperature dependence of fluorescence intensity shift factor $\log(a_T)$ for bulk PMMA films. Representative dataset is shown as green circles where grey circles demonstrate the sample-to-sample variability of nominally identical samples. The data for tempperature greater than $T_{\mathrm{ref}} = T_{\mathrm{g}}^{\mathrm{bulk}}$ follow the bulk WLF dependence for PMMA (gray curve) where WLF parameters were obtained from Ref. 32. The data below $T_{\mathrm{g}}^{\mathrm{bulk}}$ follow a simple Arrhenius trend. A linear fit to this region is shown by the black line.

Figure 5.6 plots the fluorescence intensity shift factor $\log(a_T)$ as a function of $1/T - 1/T_{\mathrm{ref}}$ for different polymer matrices. The temperature dependent trends in $\log(a_T)$ are similar for all polymers, following the bulk WLF dependence in the region above $T_{\mathrm{g}}^{\mathrm{bulk}}$ and then transitioning into a linear trend below $T_{\mathrm{g}}^{\mathrm{bulk}}$. The bulk WLF

parameters for PS and PC we used in this study were $T_{\mathrm{ref}} = 375$ K, $C_1 = 12$, and $C_2 = 49$ for PS, $T_{\mathrm{ref}} = 425.7$ K, $C_1 = 10.4$, and $C_2 = 52.2$ for PC, obtained from Reference 32. We apply the same WLF parameters of PS to P2VP due to their similar T_{g} and chemical structure as well as the lack of existing values for P2VP in the literature. The similarity between the temperature trends of perylene doped in the various polymer matrices confirms that the nonradiative decay process of perylene reflects changes in the local polymer dynamics. For a given number of the electrons at the excited state, they will return to the ground state via either the radiative transition or the nonradiative transition. The radiative transition leads to fluorescence where the population of the electrons going through this pathway are characterized by the emission intensity. In contrast, the rate of nonradiative transition can be inferred from the emission intensity since an increase in the nonradiative decay rate would suppress the emission intensity. Due to the intermolecular collision with the surrounding polymer segments, more energy would be dissipated when the polymer segments have a higher mobility. In analogy to the WLF equation that describes the non-Arrhenius relaxation behavior of supercooled liquid regime with a temperature dependent activation energy $E(T)$, the activation energy $E(T)$ in Eqn. 5.7 shares a similar non-Arrhenius behavior that leads to the WLF dependence in the regime above $T_{\mathrm{g}}^{\mathrm{bulk}}$. It appears that the nonradiative decay process in the supercooled liquid regime is impacted by the cooperative α-relaxation of the polymer segments that slows down near the glass transition, which in turn reduces the nonradiative decay and facilitates the fluorescence emission. For the region below T_{g} in the glassy state, the cooperative α-relaxation is frozen out, leaving the nonradiative decay process solely affected by the local β-relaxation of the polymer with a temperature independent activation energy, resulting in a simple Arrhenius trend. The deflection point in the $\log(a_T)$ curve that agrees with the $T_{\mathrm{g}}^{\mathrm{bulk}}$ for each of the polymers can be explained by the transition of local polymer dynamics from liquid to glassy regime. The temperature

that the transition from the non-Arrhenius behavior to Arrhenius behavior occurs at is defined as T_{Trans}. The values of T_{Trans} for different polymers are $T_{\mathrm{Trans}} = 373$ K for PS, $T_{\mathrm{Trans}} = 391$ K for PMMA, $T_{\mathrm{Trans}} = 372$ K for P2VP, and $T_{\mathrm{Trans}} = 425$ K for PC. For all polymers used in this study, the values of T_{Trans} are consistent with the values of the polymers' bulk T_{g}.

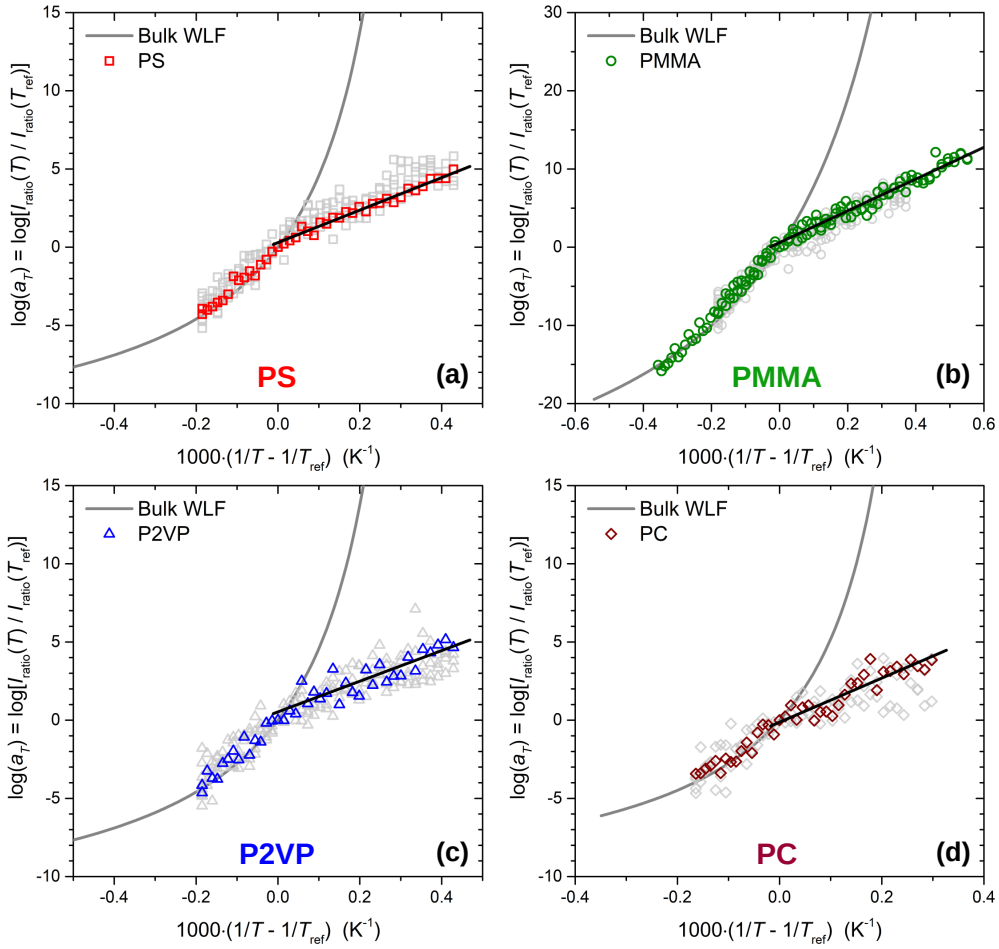

Figure 5.6: Temperature dependence of fluorescence intensity shift factor $\log(a_T)$ for bulk (a) PS, (b) PMMA, (c) P2VP, and (d) PC films. Representative datasets are shown as colored symbols (PS: red squares, PMMA: green circles, P2VP: blue triangles, and PC: brown diamonds) where grey symbols demonstrate the sample-to-sample variability of nominally identical samples. The part above $T_{\mathrm{ref}} = T_{\mathrm{g}}^{\mathrm{bulk}}$ follows the bulk WLF dependence for different polymers (gray curve) where WLF parameters were obtained from Ref. 32. The part below $T_{\mathrm{g}}^{\mathrm{bulk}}$ follows a simple Arrhenius trend. A linear fit to this region is shown in black line.

5.4 Conclusion

In this study, we have explored the potential of using perylene doped in bulk PS, PMMA, P2VP, and PC films as a probe for the polymer's local dynamics surrounding the perylene dye. We characterized the the temperature dependence of perylene doped in various polymer matrices. We defined a self-referencing region (SRR) as the temperature invariant region to the left of the first peak. This SRR can be used to correct for fluctuations in excitation intensity. We found that the intensity ratio I_{Ratio} between the peak intensity and the intensity at SRR decreases monotonically with increasing temperature for all polymers. Similar to the shift factor a_T in the WLF equation, We defined a fluorescence intensity "shift factor" a_T for the emission intensity ratio $I_{\mathrm{Ratio}}(T)$ relative to the referent temperature T_{ref}. The fluroescence intensity "shift factor" $\log(a_T)$ shows distinct behaviors in the supercooled liquid regime and the glassy regime. In the supercooled liquid regime, $\log(a_T)$ follows the bulk WLF dependence, suggesting that the nonradiative decay process is influenced by cooperative α-relaxation of the local polymer segments. With the cooperative α-relaxation arresting at T_{g}, the nonradiative decay process is only influenced by the the local β-relaxation below T_{g}, following a simple Arrhenius trend with a constant activation energy. The temperature dependent nonradiative decay rate for perylene doped in polymer matrices reflects the changes in the local polymer dynamics transitioning from liquid to glassy regime. Future efforts will address its application in polymer thin films and as a localized probe when covalently attached to polymer backbones.

Bibliography

[1] A. Cavagna. Supercooled liquids for pedestrians. *Physics Reports* **2009**, *476*, 51–124.

[2] M. D. Ediger, C. A. Angell, S. R. Nagel. Supercooled liquids and glasses. *The Journal of Physical Chemistry* **1996**, *100*, 13200–13212.

[3] M. D. Ediger, P. Harrowell. Perspective: Supercooled liquids and glasses. *The Journal of Chemical Physics* **2012**, *137*, 080901.

[4] C. B. Roth, R. R. Baglay. Fundamentals of polymers and glasses. *Polymer Glasses* **2016**, 3–22.

[5] G. B. McKenna, S. L. Simon. 50th anniversary perspective: Challenges in the dynamics and kinetics of glass-forming polymers. *Macromolecules* **2017**, *50*, 6333–6361.

[6] M. D. Ediger, J. A. Forrest. Dynamics near free surfaces and the glass transition in thin polymer films: a view to the future. *Macromolecules* **2014**, *47*, 471–478.

[7] C. B. Roth. Polymers under nanoconfinement: Where are we now in understanding local property changes? *Chemical Society Reviews* **2021**, *50*, 8050–8066.

[8] K. S. Schweizer, D. S. Simmons. Progress towards a phenomenological picture and theoretical understanding of glassy dynamics and vitrification near interfaces and under nanoconfinement. *The Journal of Chemical Physics* **2019**, *151*, 240901.

[9] B. Valeur, M. N. Berberan-Santos, *Molecular fluorescence: principles and applications*, John Wiley & Sons, **2012**.

[10] C. J. Ellison, J. M. Torkelson. The distribution of glass-transition temperatures in nanoscopically confined glass formers. *Nature Materials* **2003**, *2*, 695 – 700.

[11] P. M. Rauscher, J. E. Pye, R. R. Baglay, C. B. Roth. Effect of adjacent rubbery layers on the physical aging of glassy polymers. *Macromolecules* **2013**, *46*, 9806–9817.

[12] S. Askar, C. M. Evans, J. M. Torkelson. Residual stress relaxation and stiffness in spin-coated polymer films: Characterization by ellipsometry and fluorescence. *Polymer* **2015**, *76*, 113–122.

[13] S. Askar, J. M. Torkelson. Stiffness of thin, supported polystyrene films: Free-surface, substrate, and confinement effects characterized via self-referencing fluorescence. *Polymer* **2016**, *99*, 417–426.

[14] K. Kalyanasundaram, J. K. Thomas. Environmental effects on vibronic band intensities in pyrene monomer fluorescence and their application in studies of micellar systems. *Journal of the American Chemical Society* **1977**, *99*, 2039–2044.

[15] K. Paeng, S. F. Swallen, M. D. Ediger. Direct Measurement of Molecular Motion in Freestanding Polystyrene Thin Films. *Journal of the American Chemical Society* **2011**, *133*, 8444–8447.

[16] K. Paeng, M. D. Ediger. Molecular Motion in Free-Standing Thin Films of Poly(methyl methacrylate), Poly(4-tert-butyl styrene), Poly(α-methyl styrene), and Poly(2-vinyl pyridine). *Macromolecules* **2011**, *44*, 7034–7042.

[17] K. Paeng, R. Richert, M. D. Ediger. Molecular mobility in supported thin films of polystyrene, poly(methyl methacrylate), and poly(2-vinyl pyridine) probed by dye reorientation. *Soft Matter* **2012**, *8*, 819 – 826.

[18] J. Choi, S. Lee, J. Choe, Y. Chung, Y. E. Lee, J. Kim, M. Kim, K. Paeng. How Tethered Probes Report the Dynamics of a Polymer near the Glass Transition. *ACS Macro Letters* **2019**, *8*, 1181–1186.

[19] Y. Chung, J. Nam, D. Son, H. Lee, M. Kim, K. Paeng. Direct Observations of Segmental Dynamics at the Polymer–Substrate Interface Enabled by Localizing Fluorescent Probes with Polymer Brushes. *Macromolecules* **2021**, *54*, 4546–4556.

[20] D. B. Hall, J. M. Torkelson. Small molecule probe diffusion in thin and ultrathin supported polymer films. *Macromolecules* **1998**, *31*, 8817–8825.

[21] B. Frank, A. P. Gast, T. P. Russell, H. R. Brown, C. Hawker. Polymer mobility in thin films. *Macromolecules* **1996**, *29*, 6531–6534.

[22] J. M. Katzenstein, D. W. Janes, H. E. Hocker, J. K. Chandler, C. J. Ellison. Nanoconfined self-diffusion of poly (isobutyl methacrylate) in films with a thickness-independent glass transition. *Macromolecules* **2012**, *45*, 1544–1552.

[23] R. Katsumata, A. R. Dulaney, C. B. Kim, C. J. Ellison. Glass transition and self-diffusion of unentangled polymer melts nanoconfined by different interfaces. *Macromolecules* **2018**, *51*, 7509–7517.

[24] A. J. Bur, M. G. Vangel, S. Roth. Temperature dependence of fluorescent probes for applications to polymer materials processing. *Applied Spectroscopy* **2002**, *56*, 174–181.

[25] B. Campbell, T. Liu, J. Sullivan, *Temperature sensitive fluorescent paint systems* in *25th Plasmadynamics and Lasers Conference*, pp. 2483–2503.

[26] T. Liu, B. T. Campbell, S. P. Burns, J. P. Sullivan, et al.. Temperature-and pressure-sensitive luminescent paints in aerodynamics. *Applied Mechanics Reviews* **1997**, *50*, 227–246.

[27] N. Chandrasekharan, L. A. Kelly. A dual fluorescence temperature sensor based on perylene/exciplex interconversion. *Journal of the American Chemical Society* **2001**, *123*, 9898–9899.

[28] S. Maity, J. R. Bochinski, L. I. Clarke. Metal Nanoparticles Acting as Light-Activated Heating Elements within Composite Materials. *Advanced Functional Materials* **2012**, *22*, 5259–5270.

[29] R. G. Bennett, P. J. McCartin. Radiationless deactivation of the fluorescent state of substituted anthracenes. *The Journal of Chemical Physics* **1966**, *44*, 1969–1972.

[30] L. Song, M. Fayer. Temperature dependent intersystem crossing and triplet-triplet absorption of rubrene in solid solution. *Journal of Luminescence* **1991**, *50*, 75–81.

[31] M. L. Williams, R. F. Landel, J. D. Ferry. Mechanical properties of substances of high molecular weight. 19. The temperature dependence of relaxation mechanisms in amorphous polymers and other glass-forming liquids. *Journal of the American Chemical Society* **1955**, *77*, 3701–3707.

[32] K. L. Ngai, D. J. Plazek, *Temperature dependences of the viscoelastic response of polymer systems* in *Physical Properties of Polymers Handbook 2nd ed.*, J. E. Mark (Ed.), Springer, New York, **2007**, chapter 26, pp. 455–478.

Chapter 6

Summary and Conclusions

In this dissertation, I presented experimental results on how density changes in polymer thin films, and developed a new fluorescence technique using perylene to probe dynamics of the surrounding polymers. In this chapter, I will put my results in the context of the current literature and discuss my contributions to the literature.

Density, as a fundamental property of the material, has been extensively studied to understand the glass transition. It is well known that even a tiny change in density can have a strong impact on dynamics.[1–5] An open question in the field of confinement is how local density is correlated to local dynamics in thin films. Within the free volume framework, a simple correlation that lower density would lead to faster dynamics has been adopted by many theories studying the glass transition.[3] This simple correlation between density and dynamics has been shown to work reasonably well for some bulk systems.[2] However, computer simulation results have suggested that the local mobility and density are not simply correlated,[6–11] where the density profile of polymer thin films are not directly correlated to the dynamical gradients.[8,12–15] To reconcile the discrepancy between the free volume theory and computer simulation results, there is the need to experimentally measure density and dynamics in polymer thin films in the context of perturbations from the interfaces.

Prior to my work published in 2020 *Journal of Chemical Physics*[16] and a later follow-up work published in 2021 *Journal of Chemical Physics.*[17], there have been experimental efforts trying to characterize changes in density in polymer thin films.[18–24] In the late 1990s, studies on both supported and freestanding polystyrene (PS) films using neutron reflectivity[18] and Brillouin light scattering[19] showed no change in the density of PS films to within $\pm 1\%$ experimental error down to film thicknesses of ≈ 20 nm. Some recent works claimed enormous increases in mass density ($\approx 25\%$) with decreasing film thickness for thin PS films ($h < 30 - 40$ nm) based on the results of x-ray reflectivity, ellipsometry, and nanoparticle adsorption.[20,21,23] Huang and Roth also reported similar large increases in refractive index with decreasing film thickness for supported PS films, speculating that the large apparent increase in refractive index could result from a loss of uniform polarizability in thin PS films.[22] Besides experimental work studying density changes in polymer thin films, theoretical works by White and Lipson predicted a decrease in density of thin freestanding PS films with decreasing film thickness due to film expansion at the free surface, based on calculations from their thermodynamic model.[25] A follow-up work by them suggested the film expansion due to the free surface could be countered by attractive substrate interactions, inducing different density changes.[26]

Inspired by these previous efforts, in Chapter 3, I presented an ellipsometric study of density (refractive index) with decreasing film thickness for thin films of PS, poly(methyl methacrylate) (PMMA), and poly(2-vinyl pyridine) (P2VP), which have different substrate interactions with the silica substrate. In contrast to the predictions by White and Lipson,[25,26] I found similar apparent increases in the thickness-dependent refractive index trend $n(h)$ for all polymers in this study, despite the differences in the polymer-silica substrate interactions. The nearly identical trends between PS and P2VP suggest the chemical structure and nature of the molecular dipole orientations may play a role in the observed behavior. To explore the physics

behind these similar trends across different polymers, I tested for possible sources of the non-uniform polarizability. Chain connectivity which could be a potential cause, was rule out by testing varying molecular weights and polydispersities of PS. Non-uniform polarizability caused by chain distortion was excluded by forming films from bilayers to create different extents of chain localization within the film. Molecular dipole orientations near the substrate interface were found to have no impact on the film thickness dependent refractive index $n(h)$ trends by modifying the surface chemistry of the substrate. After the process of elimination, I suspected the use of homogeneous (uniform and isotropic) layer approximations, typical of data analysis in many thin film techniques, can lead to unphysical results when film inhomogeneities associated with non-uniform polarizability are present. The main contributions of my work presented in Chapter 3 are emphasizing that the large apparent increases in mass density ($\approx 25\%$) are physically unrealistic which was not fully acknowledged by many people in the field, and proposing that film inhomogeneities asscociated with dynamical gradients often observed in polymer thin films as being the underlying cause of the large apparent increase in refractive index.

Most studies in the literature treat the polymer film as homogeneous and isotropic during data analysis, including those reporting large density changes that are physically unrealistic.[18,20–24,27] The fact that similar large apparent increases in density are observed by different experimental techniques might indicate that the homogeneous film assumption may not be correct for film thicknesses ≤ 100 nm, as many studies have suggested property changes in nanoconfined geometries.[6,28–33] Inspired by the fact that deviations from bulk dynamics are reported at similar film thicknesses where the large increases in $n(h)$ take place, I modeled a depth-dependent refractive index gradient in polymer thin films and studied the correlations between the refractive index gradients, implying density gradients, and known dynamical gradients. In Chapter 4, I presented the use of an ellipsometric optical layer model with a depth-

dependent refractive index gradient $n(z)$ applied to thin polymer films of PMMA, PS, and P2VP. I proposed a gradient linear in the magnitude of the refractive index, Cauchy parameter $A(z)$, with depth. Keeping the wavelength-dependent dispersion relation equivalent to bulk, $n(\lambda) \sim \frac{B}{\lambda^2}$, this adds no additional fitting parameters, but results in more realistic refractive index values for thin films compared to the commonly used homogeneous layer model that leads to large physically unrealistic density and refractive index increases.[16,20–24,34,35]

From the ellipsometric fits to the linear gradient model, I demonstrated the presence of a strong positive gradient in the magnitude of the refractive index (%grade) for PMMA and PS thin films. The magnitude of the gradient in the refractive index increases with decreasing film thickness. At an equivalent film thickness, the gradient for PMMA is found to be three times larger than that for PS, which is likely caused by the additional attractive interactions present between PMMA and the silica substrate. In contrast, P2VP films, show a refractive index gradient that primarily fluctuates about zero for all film thicknesses, which may reflect a decoupling of free surface and substrate dynamics previously observed for systems with strong interfacial interactions.[36–38] Counter to common expectations of a simple free volume correlation between density and dynamics, we find that the direction of the refractive index (density) gradient indicates a higher density near the free surface. Such a high density near-free surface region agrees well with the recent results on stable glasses, both experiments[39–41] and computer simulation.[42] The enhanced mobility near the free surface facilitates more optimal packing of the molecular units leading to a locally more dense region of order 1–1.5% higher than the density of the bulk, that has been proposed to also exist in the supercooled equilibrium liquid state of thin films.[42]

The main contributions of my work presented in Chapter 4 to the literature are suggesting a depth-dependent gradient in the refractive index is present in thin films, reflecting strong presence of film inhomogeneities, and the finding of a denser near-

surface region due to better molecular packing with enhanced mobility, which contradicts the simple free volume correlation between density and dynamics frequently assumed. Since the publication of the first work in 2020, several studies on density changes were published, including a magnetic levitation technique[35] and some QCM dissolution experiments.[34] However, the underlying physics behind the physically unrealistic large apparent increase in mass density were not well appreciated. In contrast, a recent study that was published in 2021 on the density of vapor deposited thin films of a molecular glass (TPD) has observed the existence of a high density supercooled liquid state that is only present in thin films <60 nm thick.[43] The highest film densities occur at film thicknesses of 30–40 nm where the gradient in dynamics of the liquid cooled glass is the most pronounced. This study suggests that the thin film geometry with its inherent interfaces may facilitate the formation of higher density amorphous states that are not accessible in the bulk. Their most up-to-date work seems to pursue a density distribution (anisotropy) in TPD thin films. Stable glasses formed with polymers, including PS and PMMA, have been reported recently.[44,45] Whether similar density gradients can be observed in such polymeric stable glasses would be an interesting question.

My works on the density changes in polymer thin films have left a number of open questions regarding the true mechanism of the density gradient, as well as the key lengthscale of the density gradient. What is the exact functional form of the density gradient and how far does it extend from the interface? How do the interfacial perturbations lead to the density gradient? How is the density gradient qualitatively comparable to the density profile observed in computer simulation? How is the density gradient influenced by the finite size effect that modifies long range dynamical gradients?[46]

Fluorescence probes have been widely used in characterizing property changes in materials due to their sensitivity to the local environment. A number of such meth-

ods have been instrumental in probing local property changes in polymer thin films, addressing how interfacial effects cause perturbations.[47–59] To answer open questions about how different material properties change in nanoconfined systems, there is the need to develop new methods (fluorophores) to measure different local properties. Hence, in Chapter 5, I developed a new method using perylene to probe dynamics of the surrounding polymer matrices. Perylene has been used as a molecular thermometer due to its linear response in intensity ratio to temperature.[60,61] It has also been used as a component in temperature-sensitive-paint to display different colors at various temperatures.[62–64] We characterized the temperature dependence of perylene doped in various polymer matrices. I defined a self-referencing region (SRR) as the temperature invariant region to the left of the first peak, which can be used to correct for fluctuations in excitation intensity. Inspired by the work of Campbell et al.[62] and Liu et al.[63], I defined a fluorescence intensity "shift factor" a_T for the emission intensity ratio $I_{\text{Ratio}}(T)$, similar to the shift factor a_T in the Williams-Landel-Ferry (WLF) equation. The fluroescence intensity "shift factor" $\log(a_T)$ follows the bulk WLF dependence in the supercooled liquid regime, suggesting that the nonradiative decay process is influenced by cooperative α-relaxation of the local polymer segments. With the cooperative α-relaxation arresting at T_{g}, the nonradiative decay process is only influenced by the the local β-relaxation below T_{g}, following a simple Arrhenius trend with a constant activation energy. The temperature dependent nonradiative decay rate for perylene doped in polymer matrices reflects these changes in the local polymer dynamics transitioning from the liquid to glassy regime.

This new fluorescence method could provide a new approach to characterize T_{g} since the dynamical transition from the liquid to glassy regime takes place at T_{g}. Future efforts would apply this fluorophore to polymer thin films and measure the film thickness dependence of the transition point in the $\log(a_T)$ curve. In addition, the activation energy of the linear trend in the glassy regime could be compared with

the activation energy of the local β-relaxation measured by dielectric spectroscopy. Perylene could be turned into a localized probe if it is covalently bonded to the polymer backbone. In addition to the temperature dependent dynamics, perylene has been reported to undergo spectral shifts at high pressure,[65] which may make perylene sensitive to changes in local stress and modulus. A fluorescence compatible pressure heater has been built and some preliminary tests have been done. Unfortunately, details about the design and simulation of this pressure heater was not included in this dissertation.

Bibliography

[1] C. M. Roland, S. Hensel-Bielowka, M. Paluch, R. Casalini. Supercooled dynamics of glass-forming liquids and polymers under hydrostatic pressure. *Reports on Progress in Physics* **2005**, *68*, 1405 – 1478.

[2] R. P. White, J. E. G. Lipson. Free Volume in the Melt and How It Correlates with Experimental Glass Transition Temperatures: Results for a Large Set of Polymers. *ACS Macro Letters* **2015**, *4*, 588–592.

[3] R. P. White, J. E. G. Lipson. Polymer Free Volume and Its Connection to the Glass Transition. *Macromolecules* **2016**, *49*, 3987–4007.

[4] S. F. Swallen, K. L. Kearns, M. K. Mapes, Y. S. Kim, R. J. McMahon, M. D. Ediger, T. Wu, L. Yu, S. Satija. Organic glasses with exceptional thermodynamic and kinetic stability. *Science* **2007**, *315*, 353–356.

[5] S. S. Dalal, M. D. Ediger. Molecular Orientation in Stable Glasses of Indomethacin. *The Journal of Physical Chemistry Letters* **2012**, *3*, 1229 – 1233.

[6] J. Baschnagel, F. Varnik. Computer simulations of supercooled polymer melts in the bulk and in confined geometry. *Journal of Physics: Condensed Matter* **2005**, *17*, R851.

[7] P. Z. Hanakata, J. F. Douglas, F. W. Starr. Local variation of fragility and glass transition temperature of ultra-thin supported polymer films. *The Journal of Chemical Physics* **2012**, *137*, 244901.

[8] P. Z. Hanakata, B. A. P. Betancourt, J. F. Douglas, F. W. Starr. A unifying framework to quantify the effects of substrate interactions, stiffness, and roughness on the dynamics of thin supported polymer films. *The Journal of Chemical Physics* **2015**, *142*, 234907.

[9] F. Varnik, J. Baschnagel, K. Binder. Reduction of the glass transition temperature in polymer films: A molecular-dynamics study. *Physical Review E* **2002**, *65*, 021507.

[10] A. Shavit, R. A. Riggleman. Influence of backbone rigidity on nanoscale confinement effects in model glass-forming polymers. *Macromolecules* **2013**, *46*, 5044–5052.

[11] A. Shavit, R. A. Riggleman. Physical aging, the local dynamics of glass-forming polymers under nanoscale confinement. *The Journal of Physical Chemistry B* **2014**, *118*, 9096–9103.

[12] Y. Zhou, S. T. Milner. Short-Time Dynamics Reveals Tg Suppression in Simulated Polystyrene Thin Films. *Macromolecules* **2017**, *50*, 5599–5610.

[13] P. Z. Hanakata, J. F. Douglas, F. W. Starr. Local variation of fragility and glass transition temperature of ultra-thin supported polymer films. *The Journal of Chemical Physics* **2012**, *137*, 244901.

[14] W. Zhang, F. W. Starr, J. F. Douglas. Reconciling computational and experimental trends in the temperature dependence of the interfacial mobility of polymer films. *The Journal of Chemical Physics* **2020**, *152*, 124703.

[15] D. M. Sussman, S. S. Schoenholz, E. D. Cubuk, A. J. Liu. Disconnecting structure and dynamics in glassy thin films. *Proceedings of the National Academy of Sciences* **2017**, *114*, 10601 – 10605.

[16] Y. Han, X. Huang, A. C. W. Rohrbach, C. B. Roth. Comparing refractive index and density changes with decreasing film thickness in thin supported films across different polymers. *The Journal of Chemical Physics* **2020**, *153*, 044902.

[17] Y. Han, C. B. Roth. Gradient in refractive index reveals denser near free surface region in thin polymer films. *The Journal of Chemical Physics* **2021**, *155*, 144901.

[18] W. E. Wallace, N. C. Beck Tan, W. L. Wu, S. Satija. Mass density of polystyrene thin films measured by twin neutron reflectivity. *The Journal of Chemical Physics* **1998**, *108*, 3798–3804.

[19] J. A. Forrest, K. Dalnoki-Veress, J. R. Dutcher. Brillouin light scattering studies of the mechanical properties of thin freely standing polystyrene films. *Physical Review E* **1998**, *58*, 6109.

[20] S. Ata, K. Kuboyama, K. Ito, Y. Kobayashi, T. Ougizawa. Anisotropy and densification of polymer ultrathin films as seen by multi-angle ellipsometry and X-ray reflectometry. *Polymer* **2012**, *53*, 1028–1033.

[21] G. Vignaud, M. S. Chebil, J. K. Bal, N. Delorme, T. Beuvier, Y. Grohens, A. Gibaud. Densification and Depression in Glass Transition Temperature in Polystyrene Thin Films. *Langmuir* **2014**, *30*, 11599–11608.

[22] X. Huang, C. B. Roth. Changes in the temperature-dependent specific volume of supported polystyrene films with film thickness. *The Journal of Chemical Physics* **2016**, *144*, 234903.

[23] A. Beena Unni, G. Vignaud, J. P. Chapel, J. Giermanska, J. K. Bal, N. Delorme, T. Beuvier, S. Thomas, Y. Grohens, A. Gibaud. Probing the Density Variation of Confined Polymer Thin Films via Simple Model-Independent Nanoparticle Adsorption. *Macromolecules* **2017**, *50*, 1027 – 1036.

[24] Y. Li, J. Q. Pham, K. P. Johnston, P. F. Green. Contact Angle of Water on Polystyrene Thin Films: Effects of CO2 Environment and Film Thickness. *Langmuir* **2007**, *23*, 9785–9793.

[25] R. P. White, J. E. G. Lipson. Thermodynamic treatment of polymer thin-film glasses. *Physical Review E* **2011**, *84*, 041801.

[26] R. P. White, C. C. Price, J. E. G. Lipson. Effect of Interfaces on the Glass Transition of Supported and Freestanding Polymer Thin Films. *Macromolecules* **2015**, *48*, 4132 – 4141.

[27] G. Reiter. Mobility of Polymers in Films Thinner than Their Unperturbed Size. *Europhysics Letters* **1993**, *23*, 579–584.

[28] M. D. Ediger, J. A. Forrest. Dynamics near free surfaces and the glass transition in thin polymer films: a view to the future. *Macromolecules* **2014**, *47*, 471–478.

[29] J. A. Forrest, K. Dalnoki-Veress. The glass transition in thin polymer films. *Advances in Colloid and Interface Science* **2001**, *94*, 167–195.

[30] C. B. Roth, J. R. Dutcher. Glass transition and chain mobility in thin polymer films. *Journal of Electroanalytical Chemistry* **2005**, *584*, 13–22.

[31] D. S. Simmons. An emerging unified view of dynamic interphases in polymers. *Macromolecular Chemistry and Physics* **2016**, *217*, 137–148.

[32] K. S. Schweizer, D. S. Simmons. Progress towards a phenomenological picture and theoretical understanding of glassy dynamics and vitrification near interfaces and under nanoconfinement. *The Journal of Chemical Physics* **2019**, *151*, 240901.

[33] C. B. Roth. Polymers under nanoconfinement: Where are we now in understanding local property changes? *Chemical Society Reviews* **2021**, *50*, 8050–8066.

[34] J. Giermanska, S. B. Jabrallah, N. Delorme, G. Vignaud, J.-P. Chapel. Direct experimental evidences of the density variation of ultrathin polymer films with thickness. *Polymer* **2021**, *228*, 123934.

[35] S. E. Root, R. Gao, C. K. Abrahamsson, M. S. Kodaimati, S. Ge, G. M. Whitesides. Estimating the Density of Thin Polymeric Films Using Magnetic Levitation. *ACS Nano* **2021**, 15676–15686.

[36] E. C. Glor, G. V. Angrand, Z. Fakhraai. Exploring the broadening and the existence of two glass transitions due to competing interfacial effects in thin, supported polymer films. *The Journal of Chemical Physics* **2017**, *146*, 203330.

[37] R. J. S. Ivancic, R. A. Riggleman. Dynamic phase transitions in freestanding polymer thin films. *Proceedings of the National Academy of Sciences* **2020**, *117*, 25407–25413.

[38] W. Zhang, J. F. Douglas, F. W. Starr. Effects of a "bound" substrate layer on the dynamics of supported polymer films. *The Journal of Chemical Physics* **2017**, *147*, 044901.

[39] S. F. Swallen, K. L. Kearns, M. K. Mapes, Y. S. Kim, R. J. McMahon, M. D. Ediger, T. Wu, L. Yu, S. Satija. Organic Glasses with Exceptional Thermodynamic and Kinetic Stability. *Science* **2007**, *315*, 353–356.

[40] M. D. Ediger. Perspective: Highly stable vapor-deposited glasses. *The Journal of Chemical Physics* **2017**, *147*, 210901.

[41] S. S. Dalal, M. D. Ediger. Molecular Orientation in Stable Glasses of Indomethacin. *The Journal of Physical Chemistry Letters* **2012**, *3*, 1229–1233.

[42] J. H. Mangalara, M. D. Marvin, D. S. Simmons. Three-Layer Model for the Emergence of Ultrastable Glasses from the Surfaces of Supercooled Liquids. *The Journal of Physical Chemistry B* **2016**, *120*, 4861–4865.

[43] Y. Jin, A. Zhang, S. E. Wolf, S. Govind, A. R. Moore, M. Zhernenkov, G. Frey-

chet, A. A. Shamsabadi, Z. Fakhraai. Glasses denser than the supercooled liquid. *Proceedings of the National Academy of Sciences* **2021**, *118*, e2100738118.

[44] H. Yoon, Y. P. Koh, S. L. Simon, G. B. McKenna. An Ultrastable Polymeric Glass: Amorphous Fluoropolymer with Extreme Fictive Temperature Reduction by Vacuum Pyrolysis. *Macromolecules* **2017**, *50*, 4562–4574.

[45] A. N. Raegen, J. Yin, Q. Zhou, J. A. Forrest. Ultrastable monodisperse polymer glass formed by physical vapour deposition. *Nature Materials* **2020**, *19*, 1110–1113.

[46] R. R. Baglay, C. B. Roth. Local glass transition temperature T g (z) of polystyrene next to different polymers: Hard vs. soft confinement. *The Journal of Chemical Physics* **2017**, *146*, 203307.

[47] C. J. Ellison, J. M. Torkelson. The distribution of glass-transition temperatures in nanoscopically confined glass formers. *Nature Materials* **2003**, *2*, 695 – 700.

[48] P. M. Rauscher, J. E. Pye, R. R. Baglay, C. B. Roth. Effect of adjacent rubbery layers on the physical aging of glassy polymers. *Macromolecules* **2013**, *46*, 9806–9817.

[49] S. Askar, C. M. Evans, J. M. Torkelson. Residual stress relaxation and stiffness in spin-coated polymer films: Characterization by ellipsometry and fluorescence. *Polymer* **2015**, *76*, 113–122.

[50] S. Askar, J. M. Torkelson. Stiffness of thin, supported polystyrene films: Free-surface, substrate, and confinement effects characterized via self-referencing fluorescence. *Polymer* **2016**, *99*, 417–426.

[51] K. Paeng, S. F. Swallen, M. D. Ediger. Direct Measurement of Molecular Mo-

tion in Freestanding Polystyrene Thin Films. *Journal of the American Chemical Society* **2011**, *133*, 8444–8447.

[52] K. Paeng, M. D. Ediger. Molecular Motion in Free-Standing Thin Films of Poly(methyl methacrylate), Poly(4-tert-butyl styrene), Poly(α-methyl styrene), and Poly(2-vinyl pyridine). *Macromolecules* **2011**, *44*, 7034–7042.

[53] K. Paeng, R. Richert, M. D. Ediger. Molecular mobility in supported thin films of polystyrene, poly(methyl methacrylate), and poly(2-vinyl pyridine) probed by dye reorientation. *Soft Matter* **2012**, *8*, 819 – 826.

[54] J. Choi, S. Lee, J. Choe, Y. Chung, Y. E. Lee, J. Kim, M. Kim, K. Paeng. How Tethered Probes Report the Dynamics of a Polymer near the Glass Transition. *ACS Macro Letters* **2019**, *8*, 1181–1186.

[55] Y. Chung, J. Nam, D. Son, H. Lee, M. Kim, K. Paeng. Direct Observations of Segmental Dynamics at the Polymer–Substrate Interface Enabled by Localizing Fluorescent Probes with Polymer Brushes. *Macromolecules* **2021**, *54*, 4546–4556.

[56] D. B. Hall, J. M. Torkelson. Small molecule probe diffusion in thin and ultrathin supported polymer films. *Macromolecules* **1998**, *31*, 8817–8825.

[57] B. Frank, A. P. Gast, T. P. Russell, H. R. Brown, C. Hawker. Polymer mobility in thin films. *Macromolecules* **1996**, *29*, 6531–6534.

[58] J. M. Katzenstein, D. W. Janes, H. E. Hocker, J. K. Chandler, C. J. Ellison. Nanoconfined self-diffusion of poly (isobutyl methacrylate) in films with a thickness-independent glass transition. *Macromolecules* **2012**, *45*, 1544–1552.

[59] R. Katsumata, A. R. Dulaney, C. B. Kim, C. J. Ellison. Glass transition and self-diffusion of unentangled polymer melts nanoconfined by different interfaces. *Macromolecules* **2018**, *51*, 7509–7517.

[60] A. J. Bur, M. G. Vangel, S. Roth. Temperature dependence of fluorescent probes for applications to polymer materials processing. *Applied Spectroscopy* **2002**, *56*, 174–181.

[61] S. Maity, J. R. Bochinski, L. I. Clarke. Metal Nanoparticles Acting as Light-Activated Heating Elements within Composite Materials. *Advanced Functional Materials* **2012**, *22*, 5259–5270.

[62] B. Campbell, T. Liu, J. Sullivan, *Temperature sensitive fluorescent paint systems* in *25th Plasmadynamics and Lasers Conference*, pp. 2483–2503.

[63] T. Liu, B. T. Campbell, S. P. Burns, J. P. Sullivan, et al.. Temperature-and pressure-sensitive luminescent paints in aerodynamics. *Applied Mechanics Reviews* **1997**, *50*, 227–246.

[64] N. Chandrasekharan, L. A. Kelly. A dual fluorescence temperature sensor based on perylene/exciplex interconversion. *Journal of the American Chemical Society* **2001**, *123*, 9898–9899.

[65] H. W. Offen, R. A. Beardslee. Perylene Crystal Spectra under Pressure. *The Journal of Chemical Physics* **1968**, *48*, 3584–3587.

Appendix A

Implementation of transfer matrices in MATLAB

A.1 Synopsis

Appendix 1 demonstrates the implementation of the transfer matrices described in Section 2.2.3 in MATLAB environment. This appendix includes code for five relevant .m files:

```
rp_cal.m    % Reflection coefficient for p-polarization
rs_cal.m    % Reflection coefficient for s-polarization
Transfer_matrix_interface.m     % Transfer matrix of the interface
Transfer_matrix_film.m     % Transfer matrix of the film
Transfer_matrix_calculation.m     % Example of using the transfer matrix
```

A.2 Reflection coefficient for p-polarization

The mathematical form of the Frensel reflection coefficient for p-polarization is shown as Eqn. 2.1, with the input parameters n1, n2 and phi1.

n1 is the refractive index of the material on the side of the interface where reflection occurs. n2 is the refractive index of the material on the side of the interface where refraction occurs. phi1 is the angle of incidence and phi2 (not a output parameter) is the angle of refraction.

The output parameter is rp, which is the reflection coefficient for p-polarization.

```
function [ rp ] = rp_cal( n1,n2,phi1 )
%rp_cal calculates rp
%   Detailed explanation goes here
%n1: refractive index for medium 1
%n2: refractive index for medium 2
%phi1: angle of incidence
%phi2: angle of refraction

%Calculate phi2
phi2 = asin(n1*sin(phi1)/n2);

%Calculate rp
rp = (n2*cos(phi1)-n1*cos(phi2))/(n2*cos(phi1)+n1*cos(phi2));

end
```

A.3 Reflection coefficient for s-polarization

The mathematical form of the reflection coefficient for s-polarization is shown as Eqn. 2.3 with the input parameters n1, n2 and phi1.

n1 is the refractive index of the material on the side of the interface where reflection occurs. n2 is the refractive index of the material on the side of the interface where refraction occurs. phi1 is the angle of incidence and phi2 (not a output parameter)

is the angle of refraction.

The output parameter is rs, which is the reflection coefficient for s-polarization.

```
function [ rs ] = rs_cal( n1,n2,phi1 )
%rs_cal calculates rs
%   Detailed explanation goes here
%n1: refractive index for medium 1
%n2: refractive index for medium 2
%phi1: angle of incidence
%phi2: angle of refraction

%Calculate phi2
phi2 = asin(n1*sin(phi1)/n2);

%Calculate rp
rs = (n1*cos(phi1)-n2*cos(phi2))/(n1*cos(phi1)+n2*cos(phi2));

end
```

A.4 Transfer matrix of the interface

The mathematical form of the transfer matrix of the interface is shown as Eqn. 2.7 with input parameters of PorS, n1, n2, and phi1.

PorS is the conditional switch to determine whether the Fresnel coefficient is calculated as p- or s- polarization. n1 is the refractive index of the material on the side of the interface where reflection occurs. n2 is the refractive index of the material on the side of the interface where refraction occurs. phi1 is the angle of incidence and phi2 is the angle of refraction.

I is the transfer matrix of the interface and phi2 is the angle of refraction that is

exactly the angle of incidence for the next layer.

```
function [ I,phi2 ] = Transfer_matrix_interface( PorS,n1,n2,phi1 )
%Transfer_matrix_interface calculates the transfer matrix at the ...
    interface
%
%PorS is the switch between p-polarized and s-polarized light
%n1: refractive index for medium 1
%n2: refractive index for medium 2
%phi1: angle of incidence
%phi2: angle of refraction
%I: transfer matrix


%Calculate phi2
phi2 = asin(n1*sin(phi1)/n2);   %Snell's law

%Calculate transfer matrix
if PorS=='p'
    I = [1/tp_cal(n1,n2,phi1),...
        rp_cal(n1,n2,phi1)/tp_cal(n1,n2,phi1);...
        rp_cal(n1,n2,phi1)/tp_cal(n1,n2,phi1),...
        1/tp_cal(n1,n2,phi1)];
elseif PorS=='s'
    I = [1/ts_cal(n1,n2,phi1),...
        rs_cal(n1,n2,phi1)/ts_cal(n1,n2,phi1);...
        rs_cal(n1,n2,phi1)/ts_cal(n1,n2,phi1),...
        1/ts_cal(n1,n2,phi1)];
end

end
```

A.5 Transfer matrix of the film

The mathematical form of the transfer matrix of the film shown as Eqn. 2.8 with input parameters of n, phi1, lambda and d.

n is the refractive index of the film. phi1 is the angle of incidence from the output parameter of transfer matrix of the interface. lambda is the wavelength of the light which is related to the phase lag across the film. d is the thickness of the film.

F is the transfer matrix of the interface and phi2 is the angle of refraction which is identical to the angle of incidence phi1 for a homogeneous film.

```
1  function [ F,phi2 ] = Transfer_matrix_film( n,phi1,lambda,d )
2  %Transfer_matrix_film calculates the transfer matrix in the film
3  %
4  %n: refractive index for medium of film
5  %phi1: angle of incidence
6  %lambda: wavelength of light (unit: nm)
7  %d: thickness of film (unit: nm)
8  %phi2: angle of refraction
9  %F: transfer matrix
10
11 phi2 = phi1; %angle of incidence does not change in the film
12
13 %Calculate phase thickness
14 Δ = 2*pi*n*d/lambda*cos(phi1);
15
16 %Calculate transfer matrix
17 F = [exp(1i*Δ),...
18     0;...
19     0,...
20     exp(-1i*Δ)];
21
```

```
22 end
```

A.6 Transfer matrix of a graded polymer film

Here is an example of how to calculate the transfer matrices for a graded polymer film with a gradient in refractive index, as well as simulated $\Psi(\lambda)$ and $\Delta(\lambda)$ for such a film.

The wavelength range is the same as the common wavelength range of ellipsometry measurements, 400-1000 nm. The angle of incidence at the polymer-air interface I_0 is 65°. For a PMMA film with $A_{\text{Midpoint}} = 1.462$, $B = 0.00447$, %grade $= 10$, film thickness $h = 100$ nm, number of slices n = 61, the depth dependent refractive index can be calculated following Eqn. 4.2.

At each wavelength, the p- and s-polarization transfer matrices are calculated for each interface and film. The total transfer matrices of p- and s-polarization are then the product of the individual transfer matrices.

r_p and r_s can be calculated from the elements of the total transfer matrices following Eqn. 2.12. Accounting for the wavelength dependence, $\Psi(\lambda)$ and $\Delta(\lambda)$ can be calculated from r_p and r_s via Eqn.2.5.

```
1 clear
2 clc
3
4 %% Initial conditions
5 %Wavelength range
6 lambda = 400:5:1000;
7 %Angle of incidence
8 phi0 = deg2rad(65);
9 %A midpoint
```

```
10 A_mid = 1.462;
11 %B parameter
12 B = 0.00447;
13 %percent grade
14 grade = 10;
15 %film thickness
16 h = 100;
17 %number of slices
18 n = 61;
19 %thickness of a single slice
20 d = h/n;
21
22 %% Calculation based on initial parameters
23 A_top = A_mid + A_mid*grade/100/2;  %A top
24 A_bot = A_mid - A_mid*grade/100/2;  %A bottom
25
26 A_z_discrete = linspace(A_top,A_bot,n); %Discretized z for each slice
27 %% Allocate memory for storage
28 StoragePsi = zeros(1,length(lambda));
29 StorageDel = zeros(1,length(lambda));
30
31
32 %% multiple interfaces
33
34 for i = 1:length(lambda)
35 %Calculate discretized n for each slice
36 lmd = lambda(i);    %current wavelength
37 n_z_discrete = A_z_discrete + B/(lmd/1000)^2;   %index of ...
      refraction for each slice
38 %Free surface
39 [I0p,phi_p] = Transfer_matrix_interface('p',1,n_z_discrete(1),phi0);
40 [I0s,phi_s] = Transfer_matrix_interface('s',1,n_z_discrete(1),phi0);
41 %Product of transfer matrix for p- and s- polarized light
```

```
42 P = I0p;
43 S = I0s;
44
45 %Calculate transfer matrix
46 for j = 1:n
47 %Assign medium refractive index
48     if j≠n
49         n1 = n_z_discrete(j);
50         n2 = n_z_discrete(j+1);
51     else
52         n1 = n_z_discrete(j);
53         n2 = 1; %last slice
54     end
55 %Calculate transfer matrix
56 [Fp,phi_p] = Transfer_matrix_film(n1,phi_p,lmd,d);
57 [Ip,phi_p] = Transfer_matrix_interface('p',n1,n2,phi_p);
58
59 [Fs,phi_s] = Transfer_matrix_film(n1,phi_s,lmd,d);
60 [Is,phi_s] = Transfer_matrix_interface('s',n1,n2,phi_s);
61 %Multiply transfer matrix
62 P = P*Fp*Ip;
63 S = S*Fs*Is;
64
65 end
66
67 %% Calculate Psi and Del
68 %Calculate rp and rs
69 rp = P(2,1)/P(1,1);
70 rs = S(2,1)/S(1,1);
71 %Calculate rho
72 rho = rp/rs;
73 %Calculate Psi and Del
74 Psi = rad2deg(atan(abs(rho)));
```

```
75 Del = rad2deg(angle(rho));
76
77 StoragePsi(i) = Psi;
78 StorageDel(i) = Del;
79 end
80
81 yyaxis left
82 plot(lambda,StoragePsi);
83 yyaxis right
84 plot(lambda,StorageDel);
```